TECHNISCHE UNIVERSITÄT MÜNCHEN

Lehrstuhl für Analytische Chemie
Institut für Wasserchemie und Chemische Balneologie

Online monitoring of biofilm in microchannels with thermal lens microscopy

Tobias Roßteuscher

Vollständiger Abdruck der von der Fakultät für Chemie der Technischen Universität München zur Erlangung des akademischen Grades eines

Doktors der Naturwissenschaften

genehmigten Dissertation.

Vorsitzender:		Univ.-Prof. Dr. M. Schuster
Prüfer der Dissertation:	1.	Univ.-Prof. Dr. R. Nießner
	2.	Univ.-Prof. Dr. H. Horn

Die Dissertation wurde am 16.04.2009 bei der Technischen Universität München eingereicht und durch die Fakultät für Chemie am 28.05.2009 angenommen.

Parts of this thesis have been published in journals or are in preparation for publication:

T. T. J. Rossteuscher, A. Hibara, K. Mawatari, T. Kitamori, Lateral spatial resolution of thermal lens microscopy during continuous scanning for non-staining biofilm imaging, Journal of Applied Physics, in press (DOI 10.1063/1.3116137)

Acknowledgements

This thesis was financially supported by the Japanese Ministry of Education, Culture, Sports, Science and Technology (MEXT) during the first two years of experimental research and by the Japanese Society for the Promotion of Science (JSPS) from April 2008 until February 2009.

Activated sludge biofilm as well as Sphingomonas paucimobilis biofilm were gratefully supported by Ohgaki-Katayama Laboratory, Department of Urban Engineering, The University of Tokyo. MPC copolymer was provided by Ishihara-lab, Department of Material Engineering, The University of Tokyo. Access to the 3D-reflection microscope used in this thesis was provided by the Center of NanoBio Integration (CNBI), The University of Tokyo.

First of all I would like to thank Professor Dr. Reinhard Niessner for giving me the possibility to conduct the research on this very interesting topic abroad at The University of Tokyo, Japan, and supporting me during my research track through discussions and with helpful information. Also I want to thank him for the fast and helpful action during my application for Monbukagakusho as well as JSPS scholarship.

I also would like to thank my supervising professor, Professor Dr. Takehiko Kitamori, who supported me by providing equipment and access to the instruments in his laboratory, as well as with useful help during discussions about experimental procedure and the direction of laboratory research. Also he helped me with contacting the right people at the right time to get my research going and on the right way.

Professor Dr. Akihide Hibara and Dr. Kazuma Mawatari were the main supervisors regarding the experimental procedure of research and provided numerous informations and help on experimental setups as well as technical problems. Also, proofreading of numerous reports and papers including this thesis is gratefully acknowledged.

Professor Dr. Shinichiro Ohgaki provided useful help during the determination of the direction for biofilm experiments inside the microchannel. He also provided me with access to biofilm for my research.

Professor Dr. Hiroyuki Katayama was a great supporter during the whole research period, either by providing biofilm samples whenever needed on short notice as well as by

manifold useful discussions regarding the next steps in the ongoing biofilm research inside the microchannel.

Dr. Dai Simazaki from the Japanese Institute of Public Health was very helpful in providing information during discussions regarding the setup of the biofilm pumping system and the biofilm experiments in microchannels. He also provided the Japanese pipe materials used as references for the channel modification experiments.

Dr. Christoph Haisch was a helpful contact regarding research and procedures back in Germany apart from Professor Niessner and provided information and useful discussions about experimental progress and the conductance of the thesis.

Dr. Takehiko Tsukahara introduced me to the field of microfluidics and explained to me the problems and ideas for chip connections.

Dr. Kae Sato helped me with a lot of Japanese documents and application forms, especially during my last year as a JSPS scholar.

Dr. Kiyohito Shimura provided a lot of very helpful discussions and suggestions regarding the pressure-driven setup for biofilm experiments in a microchannel.

Dr. Arata Aota helped me during my first days in Tokyo to get used to the new environment and during the application procedures which would have been not at all understandable to me as most documents are still provided in Japanese with a lot of characters I cannot understand even up to today. Also, he provided useful discussions regarding flow in microchannels and pressure drop.

Dr. Yo Tanaka supported me throughout my stay with assistance in ‘difficult Japanese’, especially regarding ordering of new material

Dr. Ki-Hoon Jang introduced me to surface modification with MPC copolymer, helped me a lot with day-to-day problems in a world where Japanese is the predominant language (it is interesting to re-learn how to use an ATM) and provided me with a good time in Tokyo. Also he was the one who kept me doing some sports. I wonder how much weight I would have gained without continued attempts to do sports.

Dr. Adelina Smirnova was also of great help during my first year of continued experiences in a new environment where I was happy to have some European researcher who could relate to my problems.

Asakawa-san introduced me to TLM setup and gave me instructions for aligning the laser beams in English! Oikawa-san was helpful in continued discussions regarding TLM in the beginning and was very helpful to set up the measuring times on the shared instrument. Morikawa-san gave useful information regarding the use of pressure controllers.

Many more laboratory members helped me with Japanese throughout my entire stay that I finally got to a point where I can make myself understandable in this strange yet highly fascinating language on a daily basis, although I have still a long way to go until I actually understand it.

Dr. Antonin Hoel and Takahashi-san provided insight and gave continued support regarding Labview.

Jorg Entzinger arrived at the same time as me and provided numerous support and helpful suggestions regarding MatLab procedures and also made life in Tokyo a lot more interesting during various activities, hikes and trips. Together with my wife he also kept some European/Christian traditions alive during our time in Tokyo, namely a yearly Easter picnic and a yearly interlaboratory Christmas party.

The people at the office, Ogawa-san, Kamata-san and Toyama-san helped me a lot with all documents and all regulations regarding my research in Japan.

My FACE-volunteer Mitsuyo Hasegawa was of great help regarding procedures and living in Japan and provided initial knowledge of biofilm specific language in Japanese.

Tokyo University International Center and Faculty of Engineering (Japanese language education) got me to a level of Japanese where I can communicate in daily life which is of real help and utmost importance as otherwise you would miss just too much out.

Most of the bigger problems came down to understanding Japanese in daily life as well as in the laboratory, be it in phone calls, passing of documents, computer software or during discussions. I would like to thank anybody I did not yet mention with providing support in this regard. がんばります。 (“Ganbarimasu” means something like you keep on trying to improve your best and do the best according to your abilities to make it work)

Last but not least I would like to thank my wife, my parents and my brother for continued and ever fulfilling support during the long stay abroad as well as the time during the writing of this thesis. I guess I was not always easy to handle during writing, but your continued support helped me push through. And my wife made my stay here in Japan a most wonderful one which I will be grateful for forever.

Table of contents

1 Introduction 1

1.1 Biofilm 2

1.1.1 Definition 2
1.1.2 Biofilm development 5
1.1.3 Research fields 10
1.1.4 Experimental approaches 15
1.1.5 Present problems in online biofilm monitoring 29

1.2 Microfluidics/Microdevices 30

1.2.1 Production methods 31
1.2.2 Applications 33

1.3 Thermal lens microscopy 34

2 Aims and scope of the thesis 39

3 Theory 43

3.1 Microfluidics 43

3.1.1 Laminar flow and shear stress 43
3.1.2 Pressure drop 44

3.2 Thermal lens microscopy 45

3.2.1 Definitions 45
3.2.2 Signal generation 46
3.2.3 Resolution 52

4 Materials and methods 55

4.1 Biofilm 55

4.1.1 Bacteria 55
4.1.2 Nutrients 56
4.1.3 Staining 57

4.2 Biofilm growth in flow cells 57

4.3 Biofilm growth in microchannels 58

4.3.1 Microchannel production 59
4.3.2 Microchannel setup 60

4.3.3 Continuous flow system 64
4.3.4 Biofilm adsorption and growth studies 70
4.3.5 Biofilm removal and microchip cleaning 73

4.4 Adaptation of thermal lens microscopy for biofilm observation 74

4.4.1 Laser spot characterization 76
4.4.2 Influence of instrumental parameters 79
4.4.3 Three-dimensional scanning 82
4.4.4 Biofilm observation 84

5 Results and discussion 87

5.1 Biofilms in the microchannel 87

5.1.1 Biofilm adhesion in microchannels 90
5.1.2 Online biofilm staining in microchannels 91
5.1.3 Biofilm growth in microchannel 93
5.1.4 Biofilm removal 97

5.2 Thermal lens microscopy 102

5.2.1 Thermal lens scanning parameters 102
5.2.2 Thermal lens resolution 105
5.2.3 Two-dimensional scanning 110

5.3 Biofilm observation with TLM 117

5.3.1 Biofilm grown on slides 118
5.3.2 Biofilm grown in microchannel 121

6 Summary and outlook 129

7 Appendix 137

7.1 Abbreviations 137

7.2 Letters and symbols 139

7.3 Japanese pipe materials 141

7.4 Design drawings 145

8 References 149

1 Introduction

Biofilm research is a vast and growing field in modern research. While initially, the focus of microbial research was on bacterial cells after the invention of microscopy, bacterial research has met a change with the observation of bacteria in slime matrices and the recognition of bacterial colonies in slime matrix, so-called biofilms, as a form of life different to bacteria, which might have existed already for a long time on earth [1]. The implications of biofilm are most profound in the medical field, where bacterial infections have to be treated with regard to the biofilm rather than with regard to the biofilm species. Another field that has gained from biofilm research is the wastewater treatment process, where the biological treatment process is by now a central part in many wastewater treatment systems. A third field where biofilm research is of growing interest is the cleaning of and biofilm growth prevention on surfaces exposed to water, which include pipes, ship hulls, heaters, tables used during food production, etc. Biofilm research is, however, not limited to those fields, as bacteria are also applied in the chemical production industry as well as basic research in the fields of microbiology, physical chemistry, etc.

In biofilm research, various observation methods and culturing methods presently exist. Every method has some advantages and disadvantage in regard to biofilm research, and the method of culturing and observation has to be chosen carefully in regard to the applied research. For example, biofilms grown under flowing conditions express a different phenotype than bacteria grown in a static culture. For biofilms grown in flown systems it is therefore of importance to observe the structure and environment of the biofilms *in situ* to avoid a disturbance of the biofilm matrix. In situ observation methods are manifold, but the methods are often hampered by the scattering nature of the biofilm, the penetration depth of the method or the need to observe the structure non-invading. Photoacoustic spectroscopy (PAS) was shown as a sufficient method to observe thick biofilm *in situ* with a non-invasive method. However, the resolution of PAS is limited and structural information about the biofilm is not obtained. A method similar to PAS is thermal lens microscopy (TLM), which uses the same measuring principle as PAS, but surpasses PAS in resolution and enables structural resolution in the micrometer range when applied to biological samples like cells.

Another problem of biofilm research is the growth of biofilms in flowing field, as it is often seen in pipes in households and the industry. As those pipes normally are not transparent, online monitoring of biofilm growth is impossible, so model systems have to be constructed for mimicking biofilm growth. However, many existing flow systems are either invasive, too big to be monitored as a whole or compromised by a complex flow field. Microchannels are flow channels with well-defined flow conditions that are easily monitored as a whole with existing microscopical techniques. However, due to their recent development and their small size they have not been considered for biofilm research prior to the start of this thesis.

As biofilm monitoring with TLM and the growth of biofilm in microchannels is a new field, this dissertation is focusing on the applicability of TLM on biofilm research as well as on the adaptation and optimization of microfluidic systems to biofilm research.

1.1 Biofilm

1.1.1 Definition

Biofilms are an aggregate of microorganisms, embedded in a gel-like matrix. The microorganisms can contain bacteria, protozoa, metazoan, yeast, fungi, etc. [2]. The gel-like matrix contains a variety of extracellular polymeric substances (EPS). The EPS can consist of polysaccharides, proteins, lipids, DNA, ions, uronic acids, humic substances, pigments, and other components, depending on the environment [3]. The major components of the EPS are polysaccharides, like alginate and cellulose, and proteins, among them pili and fimbriae in prominent positions [4, 5]. Bacteria produce EPS in different ways. For example, DNA release is different for different species, as some bacteria use cell lysis, whereas others release the DNA from intact bacteria [6]. Even among the same species, differences in EPS composition occurs [3]. Extracellular polysaccharide production is crucial for the development of biofilm, either in regulating attachment or for the formation of the three-dimensional structure, as shown in an *Escherichia coli* (*E. coli*) K-12 biofilm [7] and in biofilm from *Streptococcus gordonii*

[8]. Furthermore, extracellular DNA was required for the biofilm formation in *Pseudomonas aeruginosa* (*P.* aeruginosa) [9]. The EPS form a complex environment of three-dimensional structures, where the organisms are embedded. Structures formed include channels inside the biofilm for water and nutrient distribution as well as mushroom-like structures. Further discussion of the biofilm structure will be presented in the next chapter. A schematic of an example biofilm structure is shown in Figure 1.

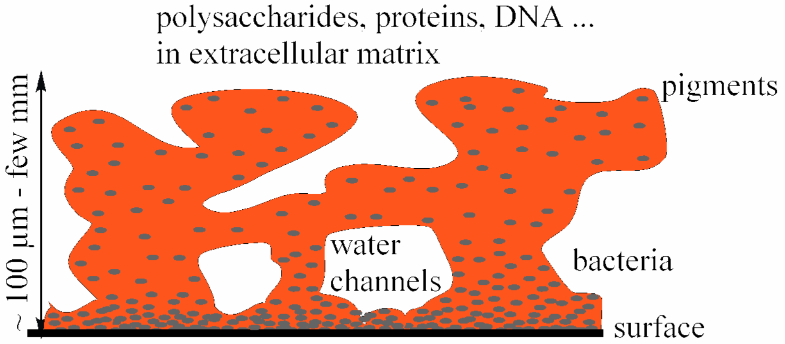

Figure 1 Schematic of a mushroom-shaped biofilm structure with water channels

Different molecules of the EPS are responsible for different functions, e.g. cell attachment or cell-cell connection [10]. The EPS also define the solubility of the biofilm, as they influence the water content of the biofilm. The major component of the matrix is water, though, which is containing up to 90 % of the biofilm wet weight [11]. The water exhibits a fine structure in the biofilm, as water retention can be divided into two regimes. EPS and water comprise the major part of the biofilm structure. For example, they make up between 73 and 98% of the volume of *Pseudomonas* and *Vibrio* biofilms grown on glass slide in flow chambers [12].

Biofilms are divided into biofilms adhering to surfaces, which are biofilms in a narrower sense, and planktonic biofilms, which are suspended in water. In the scope of the thesis, only biofilms adhering to surfaces are considered, so discussion about biofilm behavior will focus on this type of biofilm. Biofilm can be found on every surface that has contact to water, including building facades [13], water distribution systems [8, 14, 15], heating systems [16], mine waters in iron mines [17], plant roots and plant systems [18], or the human body, for example in the oral cavity [19, 20]. Bacteria exist in the soil, where they are responsible for numerous processes, including symbiosis with plant roots in nutrient uptake and protection against opportunistic pathogens, but also fouling of crop can be induced by species like *P. aeruginosa* [18]. Biofilm bacteria from the genus *Ralstonia* were shown to play a role in the biomineralization of gold in soil [21]. Biofilm bacteria found in mine water in Canada also showed the involvement of bacteria in iron precipitation [17]. Biofilms can be also found in extreme environments, for example near underwater hot water volcanoes, so-called ‘black smokers’, where they take part in the sulfur cycle [22].

The biofilm is the normal state of occurrence of bacteria. Biofilm exists as a developed community with community-specific characteristics, in contrast to bacteria. The biofilm matrix offers the bacteria protection against outside forces, for example shear and antibiotics, against predation from other microorganisms like protozoa [10]. In *P. aeruginosa*, a change of only 1 % of gene expression in biofilms compared to bacteria was sufficient for bacterial resistance to the antibiotic tobramycin [23]. The biofilm allows the bacteria to develop special niches with specific labor for bacterial groups. For example, oxygen depletion in thick biofilms leads to the formation of oxic zones, mostly in the surface biofilm, and anoxic zones inside the base biofilm. This way, aerobic bacteria and anaerobic bacteria can work together on degradation of complex molecules in biofilm communities, where oxidation and reduction processes are available to the different species. The bacteria form a community inside the biofilm, share work, specialize and communicate. The intraspecies and interspecies communication is enabled by a system using small molecules as signals and is called quorum sensing (QS).

QS has been observed for many different homologous bacteria [24, 25] and in natural biofilm [26]. In gram-positive bacteria, peptide-based signals are employed, whereas acylated homoserine lactones (AHLs) are mostly employed in gram-negative species [27], but also other factors like the *Pseudomonas* quinolone signal (PQS) [28-30] or the bacterial autoinducers from the AI-2 family [31-34] can be found. For gram-positive bacteria, also DNA seems to play a significant role in biofilm formation, whereas the purpose of extracellular DNA in gram-negative bacteria is unclear [28]. A recent review on QS signals explains in detail about the use of QS for intra- and interspecies communication [35]. A model organism for studying QS mechanisms is the bacterium

Pseudomonas aeruginosa (P. aeruginosa), where the influence of the QS signals on the regulation of gene expression is thoroughly studied [22, 29, 36-40]. In P. aeruginosa both the AHL and PQS system can be found, and they have been shown to interact for regulating each other [29]. *P. aeruginosa* exploits self-built vesicles for trafficking the PQS signals, thereby tacking active control of the group behavior in the biofilm, as mutants lacking vesicle producing capability lost QS availability [39]. Apart from homogeneous species biofilms, QS has been also observed for a mixed-species biofilm. For example, QS signaling is required for interaction between *Pseudomonas putida* and *Acinetobacter sp.* during toluene degradation [41].

Until recently QS was imagined as a process involving a threshold concentration of bacteria, and that QS takes place exclusively in a joined manner within biofilms [35]. However, the common assumption that a threshold level is needed for QS signaling has been proven unjustified. Recent findings suggest that QS signaling can be carried out between single bacteria and extend as far as 78 μm in *Pseudomonas putida* biofilm located on tomato roots [42].

A major influence of QS is on biofilm structural development, which will be discussed in the following chapter.

1.1.2 Biofilm development

The development process of biofilm on surfaces is a complicated process that is difficult to model and still not understood totally. However, at the present state biofilm development on surfaces can be divided 5 steps [22]:

- initial attachment
- production of EPS for irreversible attachment
- growth (lag + log phase) and aggregation
- mature state (new growth and detach in equilibrium), maintenance of colony
- seeding dispersal to form new colonies

Initial adhesion of bacteria is mostly reversible, and bacteria were shown to leave the surface again after initial adhesion [43, 44]. In a first approximation, bacterial adhesion can be described by electrostatic and Van der Waals interaction of the bacteria and the surface using DLVO theory [45]. Therefore, the effect of surface properties on bacterial attachment is evident [46]. Using bacterial tracking experiments, it was speculated that bacteria can adhere in a secondary minimum that is obtained using DLVO theory, and mobile bacteria can leave this minimum after tumbling [43]. However, this assumption could not be verified in follow-up experiments in solutions of different ionic strength where the secondary minimum of the DLVO theory should not exist, as bacteria still moved near to the surface[44]. Newer speculations therefore included hydrodynamic effects in the explanation of bacterial movement near a surface which can extend up to 10 µm away from the surface [47]. The forces described by DLVO theory are only effective during irreversible attachment, which is happening about 20 nm from the surface. However, other factors must influence bacterial adhesion. For example, surface topography plays a role in attachment [48, 49]. Attachment is also depending on bacterial surface morphology, charge, wettability and other factors [50]. The surface characteristics of bacteria, in turn, are dependent on environmental conditions, and a drastic change in those conditions, for example during starvation, can change the bacterial surface to a big extent [51]. Cell surface hydrophobicity seems to be linked to surface nitrogen combined with minor amount of surface oxygen [50]. Measurement of bacteria surface characteristics is tedious, though, and often correlations cannot be made [50, 52]. A generalization of microbial cell surface properties is not possible, and no strain is only hydrophilic or hydrophobic, as seen in a comparative study of the surface characteristics of 142 strains found in literature [52]. Also, bacteria with similar surface properties can show different behavior when they are isolated from different niches [53]. Further influence of cell attachment might also come from the EPS, which are able to penetrate the repulsive layer that is formulated in DLVO theory [10].

During biofilm formation, bacterial population expands either through redistribution of attached cells by surface motility, cell division or incorporation of bacterial cells from the bulk phase [22]. It was furthermore shown that *E. coli* bacteria are forming aggregates via chemotaxis in confined species [54]. Therefore, the incorporation of bacteria into a biofilm could be not only a passive mechanism with adhesion of bacteria to biofilm surface when flown by, but an active approach of bacteria to get incorporated into a biofilm matrix. However, bacterial species can also inhibit the colonization of other bacterial species, for example by release of surfactants [20]. In the growth phase, a biofilm of more or less homogeneous thickness is formed, even on an uneven substrate [55, 56].

Biofilm maturation is described in a biofilm with a quasi-steady state, where biomass accumulation of bacteria is equal to loss of biomaterial from the matrix [55]. In reality, this quasi-steady state, as well as also the growth, is accompanied by cyclic detachment of biomass, so a recurring state of biofilm mass gain followed by biomass loss is seen [57]. During biofilm maturation, complex structures like water channels, pores or mushrooms are formed [22]. The formation of those structures is accompanied by random detachment of biofilm [55]. At this time, also the surface roughness of the biofilm increases. Detachment of parts of a biofilm is necessary for settling new habitats or for finding new nutrient sources during starvation, and a new cycle of biofilm development can follow [22]. Seeding dispersal takes place by detaching a microcolony from the mature biofilm, and a minimum colony diameter of about 80 µm was found for *P. aeruginosa* non-mucoid PAO 1 biofilm [58].

The structure encountered depends on various factors, which include outside influences like shear, topology or nutrients, but also a biofilm species can show different biofilm formation [22]. In general, biofilm structure of mature biofilms can be divided into three general types:

- dense biofilms
- “mushroom” structure
- ciliates

Schematic drawings of the different structures can be found in Figure 2.

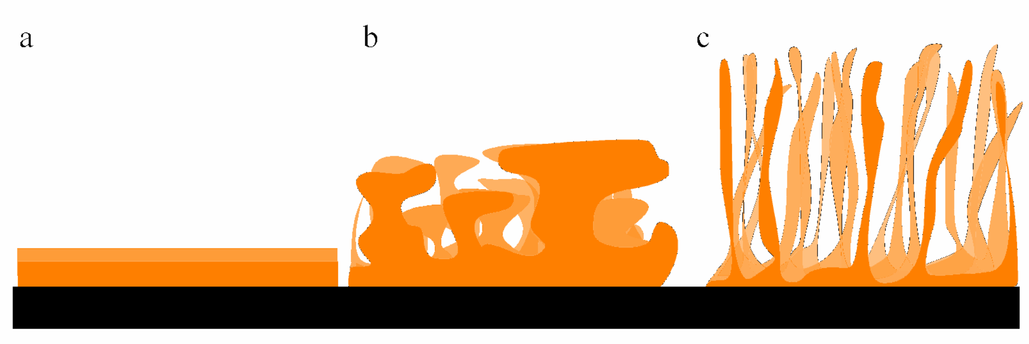

Figure 2 Schematic drawings of biofilm structures occurring in natural environments: dense biofilms (a) thinner agglomerates that form dense and flat networks of EPS; "mushroom" type biofilms (b) form a thick and dense base layer at the adhere to the surface and a more loose surface biofilm with water channels in the structure; ciliates (c) are formed on top of a biofilm and protrude into the surrounding water phase, enhancing surface contact of the biofilm with its environment

A very strong influence on biofilm structure in flown media comes from shear stress. This is exemplified in turbulent biofilm reactors [59]. In most cases, dense biofilms are found in locations with an abundance of nutrients and/or regions of high shear. An example for the occurrence of dense biofilms is on teeth.

Ciliates are formed by the microorganisms in regions where shear is low and nutrients are scarce. The ciliates offer the biofilm microorganisms an enlarged surface for contacting the environment, enhancing nutrient uptake. The interception of micrometer-sized particles by ciliate action was shown to be a major factor for particle intake in biofilms attached on clay marbles embedded in a biofilter [60].

Mushroom-like biofilms are formed in the region between the two extremes of dense biofilms and ciliates. A detailed study of the mushroom formation in *P. aeruginosa* showed that the mushrooms are formed by first constructing the stalks with a non-motile subpopulation, where subsequently motile bacteria climb on top and form the mushroom using type-IV pili mediated movement [61]. An involvement of extracellular DNA in this mechanism is suggested, as extracellular DNA was found mainly on the stalks of a four days old biofilm [6].

The availability of nutrients as an impact factor for biofilm (structural) development can be seen on several occasions. For example, dormant bacteria at the ground of the ocean can be revived after the occurrence of movements of the earth and subsequent generation of black smokers [22]. Also, the nutrient composition can influence the biofilm structure, which is not seen in planktonic bacteria [62]. But also the bacteria themselves influence the biofilm structural development. *P. aeruginosa* was shown to contain a gene coding for a prophage in its genome which, under certain conditions, developed in a prophage that killed individual organisms [63]. This killing is a part of bacterial differentiation. Bacterial control over structural development is furthermore carried out by the quorum sensing system [40]. For example, QS regulates the biofilm structural development during biofilm maturation, although only a part of the genes is affected [22]. QS is applied to control bacterial population [64, 65]. The signal molecules thereby can trigger specific genes in bacteria for cell lysis, effectively killing bacteria [64]. Triggering this “killer gene”, phenotypic change of bacterial appearance were observed [65]. With QS induced bacterial killing, the population can be controlled when environmental influences like nutrient shortage require it. Experimental setups with genetically engineered bacteria can even be controlled to population levels below the natural growth levels [64, 65]. Another way to control biofilm development is by initiating detachment of bacterial cell colonies from mature biofilms, which also may be influenced by QS [22]. Furthermore, *P. aeruginosa* was shown to produce rhamnolipid surfactants which enabled the biofilm to maintain water channels in the late stage of biofilm development [38]. The abundance of genes and regulators enables the bacteria to follow different pathways to develop biofilms. As the biofilm bacteria communicate intra- and interspecies, biofilms can be seen as bacterial communities where bacteria cooperate in nutrient digestion, species can also behave as communities rather than individual bacteria and form structures in a controlled manner, with different species forming different parts of the structure [22]. In their review, Stoodley and coworkers even suggest that bacterial interaction was the first necessary step for developing complex organisms, as share of work provided an evolutionary advantage over single bacteria, which is supported by findings of biofilm development in the oldest existing bacterial lines [22].

1.1.3 Research fields

The fields of biofilm are as vast as the locations of biofilm occurrence. In the chemical industry, bacteria are commonly applied for the production of special chemicals, ranging from the food industry to the production of pharmaceutical products. The usage of bacteria for production of industrial goods can be traced back to years before the existence of bacteria was even known. In the medieval times, *Clostridium* was used for dyeing as a reducing agent [66].

The biggest field of research is probably found in the field of medicine, where efforts are made to control bacteria or kill them as they are a common cause for infections. Approaches are made using antibiotics, surface modification, quorum-sensing inhibitors, enzymes, or combined strategies. For example, the QS inhibitor ribonucleic-acid-III-inhibiting peptide successfully prevented infections of *Staphylococcus aureus* and *Staphylococcus epidermis* by reducing biofilm formation, and showed synergetic effects when used in combination with antibiotics [67]. Another example of a QS inhibitor is garlic extract, which had a synergetic effect with the antibiotic tobramycin in treating infected mice [68]. Sequential application of polysaccharide-degrading enzymes with Pronase, a proteinase, reduced *Pseudomonas fluorescens* biomass by 94% [69]. By encapsulating the Pronase, the enzymes can be administered simultaneously, and the polysaccharide-degrading enzymes are protected from digestion by Pronase for a sufficient time. Also combinations of enzymes with antibiotics can be applied. A combination of dispersin B, which degrades N-acetylglucosamine residues in EPS, and Rifampicin was more effective than any of the compounds alone in removing *Staphylococcus epidermis* biofilm in a microchannel [70]. A further method to control or prevent biofilm growth is the modification of surfaces that get into contact with the human body. For example, intraocular lenses can be modified with 2-methacryloyloxyethyl phosphorylcholine (MPC) copolymer to reduce adhesion and growth of *Staphylococcus epidermis* in laboratory experiments [71]. The effect of MPC copolymer was also shown under dynamic flow conditions, and also bacterial retention was affected by the modification procedure [72, 73]. Surface modification can also be done with a combined strategy. A modification with octadecyl ammonium chloride of titanium, which is applied for example in dental implants, acts by preventing initial adhesion with the long alkyl chain as well as by the antibactericidal activity of the ammonium ion [74]. However, surface modification may be tampered by the adhesion of a conditioning film of proteins, polysaccharides, etc. that is often seen prior to biofilm adhesion [75]. However, also new pharmaceutical products are developed along experiments for biofilm control. An example for this is quorum-quenchers. An acyl-homoserine lactone acylase from *Ralstonia* strain XJ12B successfully quenched the AHL QS system in *P. aeruginosa* PAO 1, and might have a future prospect in the medical field [76]. It is further interesting to notice that also higher organisms produce quorum sensing inhibitors, most likely to mediate biofilm formation. The macroalgae *Delisea pulchra* produces halogenated furanones [77] which inhibit the AHL QS system by interaction with QS regulation proteins [78, 79]. Also, vegetables control QS, and QS inhibition is found even in humans [35].

Another field with wide interest in understanding biological processes in biofilms is urban engineering, and there specifically wastewater treatment. Biofilms are used in aerobic and anaerobic treatment of wastewater, where special care has to be taken of various parameters for biofilm control, for example pH, nutrient inflow, temperature and aeration [80-82]. Furthermore, the solids retention time of the reactor has influence on the biofilm, although to a lesser extent [83], and this influence might be linked to the accumulation of soluble microbial products [84]. The biofilm, on the other hand, also influences the flow inside the system, which has also beneficiary effects in terms of efficiency during loading of the biofilm reactor [85]. In the activated sludge process, biofilms play a big role in the removal of nitrogen and phosphorus sources in wastewater [86]. Furthermore, hazardous chemicals like Cr(VI) can be reduced to non-hazardous species [87]. Also, complex molecules like surfactants [88] or dyes [89-91]are degraded. This may lead to unwanted byproducts, though, which either are hazardous or influence the sludge performance [88, 92]. Therefore, it is of importance to optimize the activated sludge process and understand it better. Recent advances take opportunity of the combination of activated sludge process with membrane separation systems [86, 93]. In aerobic wastewater treatment, methods for optimization of gas-liquid contacting are of interest [94]. Monoliths were applied in model systems and present a way of biofilm growth in microchannels. Also, hyperthermophile bacteria are considered for anaerobic wastewater treatment, which seems especially useful in warmer regions of the world [95]. Biofilms in anaerobic granular and fixed film reactors are implemented in wastewater treatment for a “sustainable, energy-producing approach” [96]. However, the process in the anaerobic digestion is not well understood, as the bacterial matrix is quite complex. Extended research is now focusing on understanding biochemical processes in the reactors at both micro- and macroscopic level. At macroscopic level, modeling of complex processes like biofouling of membrane reactors is of special interest for controlling EPS and soluble microbial products [97]. Modeling is also done for the decay process of nitrifying bacteria to understand kinetics in wastewater treatment plants (WWTPs) [98]. Apart from WWTPs, biofilm sludge is also applied for the remediation of industrial wasteland and other wastewater, for example acid mine drainage, where also nutrient intake and composition is of major interest [99].

Biofilm control is not only of importance in the fields of medicine or wastewater treatment, but also in many other places where biofilms occur. For example, tap water systems, storage tanks, ships, heaters, or places in the food industry repeatedly in contact with water require biofilm control, and if possible inactivation or removal, for several reasons. Biofilm formation has adverse effects to systems in contact with water, most importantly corrosion and bioufouling [13, 15, 16, 100, 101]. Also pathogens might be harbored in biofilm systems in drinking water systems or WWTP, and their release is a potential threat [102-104]. Treatment methods of water systems for biofilm reduction are separated into biofilm inactivation, disinfection and biofilm removal. While biofilm inactivation inhibits biofilm growth in bacteria, disinfection kills the microorganisms. Both methods can leave the biofilm itself in the treated location, and regrowth potential is high, as the treated biofilm can be used as nutrient supply. On the other hand, biofilm removal physically removes biofilm by application of means like mechanical cleaning or cleaning chemicals. The following paragraph will highlight some methods that are applied, and will be divided into subparagraphs about biofilm control and biofilm removal.

- Biofilm control

An example for the inactivation of *Pseudomonas aeruginosa* biofilm is the application of copper, silver, and mixtures thereof, with improved efficiency in the mixture [105]. Furthermore, biofilm can also be controlled by modification of surfaces to hinder bacteria from initial adhesion. An experiment with *E. coli* grown on surfaces with different wettability in a standing dish showed that the initial attachment rate was dependent on contact angle within the first few hours of the experiment, whereas no influence was seen after 16 hours [106]. Surfaces can also be modified in order to inactivate bacteria. Surfaces modified with nanoparticulate titania and titania-silver mixture were efficient in preventing the attachment of large amounts of *Deinococcus geothermalis* biofilm [107]. Surface modification can be carried out to change various parameters of the surface that affect biofilm attachment and retention. A study about the influence of the surface factors roughness, wettability and zeta potential with *P. aeruginosa* biofilm showed that bacteria retention is higher on rougher and hydrophobic surfaces, and a maximum existed for removal in regard to zeta potential [108]. However, hydrophilic surfaces were not tested, and only one bacteria species was studied. Apart from chemical modification, also the topography of the surface can be structured [48, 49]. Topography similar to shark skin thereby seemed very effective in preventing biofilm attachment and growth. As with the surface modification methods mentioned above, the effect of the procedure might be affected by the formation of a conditioning film, which occurs quickly in natural media [109]. Biofilm control can also be sought by means of nutrient limitation. Phosphorus limitation proved to suppress biofilm growth, and inorganic nutrients were shown as limiting factor in Tokyo tap water system for biofilm growth [110]. Pathogen removal is furthermore attempted in sewage sludge, where the alkaline calcium hydroxide was shown to reduce microorganisms [111]. A further possibility to inactivate biofilm bacteria is the application of UV-lamps [104].

- Biofilm removal (shear, chemicals)

The removal process of biofilm can be divided into several types, like abrasion, erosion, or sloughing [10]. During abrasion and erosion, smaller parts are removed from the biofilm surface. Sloughing, in contrast, tears bigger parts of biofilm from the matrix.

The processes can be achieved by application of various methods, but most commonly applied are external shear force and chemicals. For example, increased biofilm removal was observed in copper and polyethylene pipes in a model distribution system immediately upon increase of shear rate [112]. Increased flow velocity resulted in an increase in biofilm growth, yet the release of bacteria into the system did not change. The detachment of bacteria was also observed in bigger pipe reactors [55]. The detachment occurred within the first couple of seconds of the increase of flow rate, and no direct relation was found between shear increase and removal rate. Biofilm detachment seemed to be mainly depending on the initial biofilm size.

Chemical removal of biofilm in water systems can be done in a variety of ways. The most common method as of today is the application of chlorine. However, recent findings show that monochloramine is a better biocide as it is more stable to pH and temperature changes and can penetrate deeper into the biofilm [15]. This effectiveness, on the other hand, might be countered by increased regrowth of the biofilm. In a reactor incubated from water distribution biofilm, monochloramine was depleted faster compared to chlorine, this way enabling a faster regrowth of the remaining bacteria [101]. However, bacterial variety was reduced by the monochloramine treatment. Another chemical recently coming into focus is ozone, which can be easily removed from the system using UV and was shown to be an effective disinfectant in a separated water distribution system [113]. However, as all chemicals, disinfection is limited in dead ends and valves in the system due to limited contact. Hydrogen peroxide is a further chemical that has gained more attention for biofilm removal in recent years. In connection with a catalyst, a 1000 ppm H_2O_2 solution was shown to slough off the biofilm, this way removing big chunks from the biofilm structure [114]. This sloughing originates most likely from the origin of air bubbles that formed due to the reaction of H_2O_2 with biofilm matrix components [115]. The base biofilm is unaffected by this treatment, though, even after a prolonged period of 45 minutes. In contrast to sloughing, biofilm can also be removed chemically by isothiazolinone biocides by abrasion, where the upper layer of the biofilm is removed in smaller pieces [114]. For laboratory cleaning procedures, also sodium hydroxide solution can be applied, which sloughs biofilm off at about pH 11 [116]. In contrast to H_2O_2 solution, this sloughing also affects the base biofilm. An exotic method of removing biofilm is the application of pulsed lasers, which ablate biofilm at peak intensities of 20 MW/cm^2 [117]. With reduced energy costs, the method can be applied for the cleaning of solid surfaces. However, biofilm regrowth still occurs, though to a lesser extent [118].

However, there is no general solution for biofilm prevention, control and removal, and the disinfection procedure has to be established on site, as conditions vary from place to place [100].

1.1.4 Experimental approaches

As whole water systems are difficult to model and monitor, and experimental possibilities are limited due to state regulations, most laboratory biofilm growth systems are applied, with the exception of monitoring experiments and separated systems [14, 113, 119]. Different laboratory experimental growth setups are applied for different purposes of biofilm research. The type of biofilm growing thereby depends on the applied culture method [4]. Biofilms grown in flow cells, or reactors in general, are contrasted by colonies grown on dishes. In standing culture, furthermore “pellicle” biofilm is formed [4]. In the following, some setups and their application fields are described.

- Plates, wells (mostly used in medicine and for water analysis)

In plates and wells, bacteria are put onto nutrient medium and left for growth. By applying serial dilutions, colony forming bacteria can be counted, and the amount of bacteria in a sample can be estimated. Also, bacteria can be easily grown in large number with this method for testing in multiple parallel experiments. Well plates are applied in high-throughput experimental approaches. For example, the effect of antimicrobial coating against various type of bacteria can be assessed statistically in parallel [74]. Also, microtiter plates can be used for screening experiments on the efficacy of antimicrobial substances [120]. The biofilm formed on plates and in wells is stationary and therefore significantly different from biofilm grown under shear conditions, which limits the usage of plates and wells in biofilm research [4].

- Batch reactors (used for experiments in wastewater engineering)

Batch reactors are larger size stationary reactors where biofilm is kept stationary inside the reactor and nutrient supply, and if needed oxygen supply, are provided externally with tubing or pipe systems. A simple example of a batch reactor is shown in Figure 3.

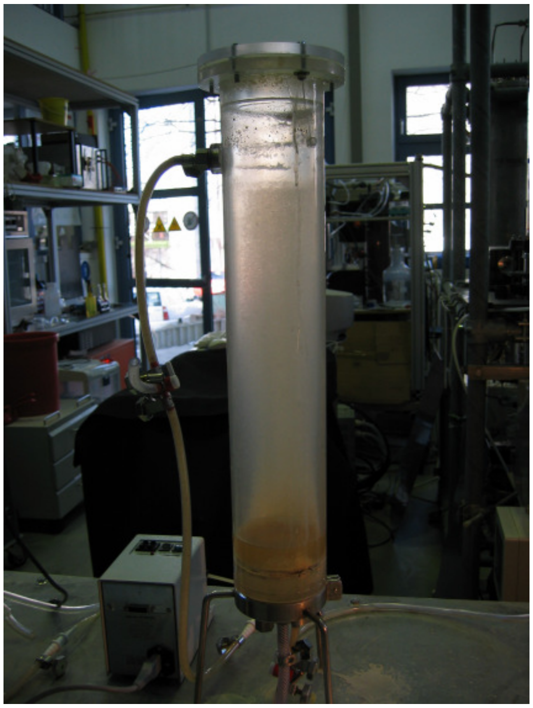

Figure 3 Example of a biofilm batch reactor applied in the IWC of the Technical University of Munich

A statistical assessment of small changes in the factors initialization time, temperature, nutrient concentration and shear stress showed a good repeatability between experiments when growing a *P. aeruginosa* biofilm, making it a reliable device for growing standard biofilm [121]. A sequencing batch reactor with an effective volume of 2 L was applied to study the influence of standard retention time on floc size distribution of biofilm in an experiment lasting longer than one year [83]. But also bigger reactors are applied. An 8-L reactor was used for measuring the long-term effects of starvation on sludge. The bigger batch reactors can mimic wastewater treatment processes easier as they use biofilm in bulk and the observed effects on the mixture are macroscopic. Also, the slow processes in wastewater treatment can be modeled in a more reliable way as factors like solid retention time or aeration volume can be adjusted to the settings of actual plants. However, a complete understanding of the microbiological processes is hard to achieve, and mostly sum parameters are acquired from the experiments.

- Rotating disk reactors (used for wastewater engineering)

In a rotating disk reactor, sample coupons are placed on a magnetically rotated disk at the bottom of a reactor container. By varying the rotation speed, the shear on the biofilm can be set. Rotating disk reactors are applied for example in research of the effect of antifouling surface modification and shear on biofilm formation [72].

- Annular reactors (used for wastewater engineering)

Rotating annular reactors are biofilm reactors with a stationary column as outside wall and a concentric rotating column inside [122]. On the column, various sample slides can be inserted for observation of biofilm adherence and growth. By adjusting the rotational speed of the column, the shear stress on the biofilm can be varied. Annular reactors are useful for growing biofilms under conditions similar to water distribution systems [101]. Samples have to be taken out of the system, though, so biofilm samples are perturbed at this point of the analyzing.

- Modified Robbins device (MRD) (used for monitoring and biofilm growth under defined conditions)

A MRD is a flow reactor, where several samples can be tested simultaneously. Its main advantage is the easy access to the samples without disturbing the flow and the growth to a big extent and the possibility for continued monitoring under defined conditions. For example, a MRD was applied online for monitoring of biofilm growth in a drinking water distribution system [14]. Another example for the application of a MRD is the testing for colocalization of four *Streptococci* with *Aggregatibacter actinomycetemcomitans* [20]. The disadvantages of the MRD include its cost and complexity as well as the invasive action during sample removal, which might damage the biofilm [123].

- Flow cells/flow chambers (used as pipe models and for wastewater engineering)

Flow cells are comparable to pipes. They offer defined flow conditions that can easily be calculated. Examples of flow channels are presented in Figure 4. Flow cell reactors have been applied for numerous studies.

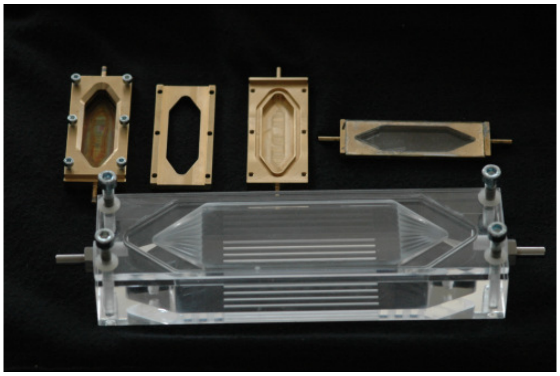

Figure 4 Examples of flow channels where one glass slide can be introduced horizontally (cells on the top) or multiple glass slides can be introduced vertically (cell at the bottom)

A flow cell with millimeter dimensions (1 x 4 x 40 mm) was applied for studying biofilm interactions with CLSM, which facilitates the observation as the biofilm structure could be conserved in its hydrated state [41]. Online observation of the structure was not carried out in this research, though. In another experiment by this group, *P. aeruginosa* cell death was observed [63]. Square channels with 1 x 1 mm were applied for seeding dispersal studies [83]. The advantage of those smaller flow cells is the possibility of direct observation. For the simulation of real tap water systems, often pipes are applied which act like flow cells. For example, biofilm studies with varying water flow velocities were conducted in model water distribution systems of copper and polyethylene with pipe inner diameters of 10 and 12 mm, respectively [112]. Detachment experiments were furthermore conducted in Plexiglas® pipes with an inner diameter of 44 mm [55]. The disadvantage of pipes is that they normally are not easily observable. Open flow chambers offer another possibility for observation of biofilm growth, and monitoring of biofilm can be done either directly [114, 116, 124] or indirectly by placing samples into the channel [123]. In open flow chambers, the biofilm can easily be monitored and samples are readily accessible. The risk of contamination in this setup is higher, though.

- Chemostats (used for bacterial growth under defined conditions)

Chemostats are very sophisticated and experimentally complex systems where many variables of biofilm growth can be controlled at the same time. They are useful for gaining general understanding about bacterial and biofilm behavior. Examples for the application of chemostats are experiments for population control and for gene expression analysis of bacteria [63, 65].

For the different growth forms and growth environments as well as growth setups, manifold analytical techniques are available to get insight into some parameters of the biofilm during growth. Some of the applied methods are presented in the following. However, due to the huge field of biofilm research, no guarantee is given for completeness of the list.

- Bacterial plating

Plating is applied in the medical field for screening of antibiotic efficiency against biofilms [125]. Total bacteria and heterotrophic plate count (HPC) are often applied for studying water quality in larger model systems [112]. Also, HPC is carried out for monitoring of water quality in drinking water distribution systems [14]. Different plate materials resulted in different counts of bacteria, and the data were not correlated, as different media support different bacteria [14]. Many bacterial species are still not cultivable, with estimates ranging in the region of 1 % of existing bacterial species [96].

- Microbiological methods

For complex biofilm systems with manifold bacterial species, microbiological methodologies based on nucleic acid detection are applied. PCR and methods based on DNA analysis are commonly applied means for studying biofilm compositions and population dynamics [20, 80, 96]. The methods are based on sampling of bacterial species and therefore are destructive.

- Microsensors

Microsensors exists for chemical compounds like N_2O, NH_4^+, NO_2^-, NO_3^-, O_2, H_2, H_2S, glucose, and pH value on micrometer scale [126]. With microelectrodes, gradients within the biofilm matrix can be measured in steps of a few micrometers [127]. The major drawback of microsensors, though, is that they are invasive [2]. A noninvasive O_2-sensor for biofilm adhering to surfaces has been introduced recently [128]. A luminescent oxygen indicator dye is spin coated onto cover glass slides that can serve as top / bottom plates in a flow channel setup. The behavior of the sensor is ideal, and only temperature calibration has to be carried out. With the sensor, oxygen depletion could be shown already for thin biofilms (35 µm) of *Pseudomonas putida*. The sensor is limited to the surface, though, and further concentration gradients cannot be detected.

- Transmission light microscopy

Light microscopy offers a possibility for online, *in situ* observation of biofilm. The resolution of the observation is limited by the diffraction limit of light. In the common bright-field microscopy methods, the major disadvantage is the inclusion of out-of-focus light during picture generation, which makes images blurred and renders depth observation difficult. Improvement in observation is possible by the application of phase contrast microscopy, but like most transmission microscopical methods observation is limited to transparent sample surfaces [17]. Hoffmann modulation transmission microscopy also is able to enhance the contrast in light microscopy, and images with a three-dimensional appearance are generated [129]. It can be applied in combination with fluorescence imaging, giving further information about the biofilm structure. Another method with a better contrast for depth observation, differential interference contrast (DIC) microscopy, has been successfully adapted for observation on opaque specimen like rocks [17]. DIC and other transmission microscopical methods are normally limited to biofilm samples with limited depth, though, as scattering and absorption are normally quite high in biofilms.

- Confocal laser-scan microscopy (CLSM)

CLSM was developed by Marvin Minsky in 1955 [130]. It is a fluorescence observation method where sample, objective and ocular lens are positioned at confocal distance to each other [131]. With pinholes, most out-of-focus light is blocked from the detector, this way enabling observation of the biofilm with increased precision [129]. With CLSM, biofilms are scanned as z-stacks, and with image processing tools a three-dimensional image of the biofilm with micrometer resolution is reconstructed from the signal [12]. Quantization of biofilm structure is possible with CLSM [2]. The application of CLSM is limited by the availability of fluorescent stains available for biofilm staining. However, stains are readily available for polysaccharides, DNA, lipids and proteins, the major components of the biofilm matrix [127, 132, 133]. Recently developed stains also are applicable to live staining of biofilm. However, some recent findings showed that the LIVE/DEAD® staining kit as well as cyanoditoryl tetrazolium chloride (CTC) might over- or underestimate viable bacteria [16].

Confocal microscopy has experienced a boost by the development of 16S rRNA-specific markers, which resulted in the method of fluorescence *in situ* hybridization (FISH) [2, 126]. FISH can be easily applied to many bacteria as RNA levels in the organisms normally are high and specific markers can be constructed as a lot of species sequences are stored in databases [121]. With this method, species and abundance of bacteria in a biofilm can be accessed [96]. Even specific bacterial genes can be made visible [41]. Newer fluorescent markers include quantum dots and biarsenic markers that bind selectively to tetra-cysteine (Cys-Cys-Xaa-Xaa-Cys-Cys) regions [133, 134].

Complementary to RNA, also nutrient exchange rates can be monitored using radioactively labeled nutrients in microautoradiography (MAR) [126]. MAR was the best method for measuring viable bacteria in a commercial heating system, in contrast to fluorescent staining methods [16]. Recently, FISH and MAR were combined, this way enabling the observation of the relation between bacterial species and nutrient uptake [96]. Other combinations of FISH include the application of microsensors or other specific stains measuring the membrane potential (rhodamine 123, propidium iodide), esterase activity (fluorescein diacetate) or respiration activity (CTC) [126].

Another way to measure exchange rates, diffusion or molecular structure is the use of ‘advanced’ fluorescent methods [134]. Fluorescent recovery after photo-bleaching (FRAP) measures the diffusion of fluorescent molecules into a region that was intentionally photobleached. Foerster resonance energy transfer (FRET) can measure the proximity of two fluorescent molecules by radiation-less energy transfer. Fluorescence lifetime imaging microscopy (FLIM) can detect changes in the fluorescence intensity of fluorescent markers. As the light intensity of fluorescent markers is also influenced by environmental parameters, FLIM can measure the proximity of molecules that affect the markers. Fluorescence correlation spectroscopy (FCS) optimizes the resolution of CLSM measurements by controlling the illuminated volume inside the sample, but analysis of the recorded data is difficult.

The major drawback of CLSM is the need for stains for observation. Staining might influence the biofilm matrix, and signal quantification is not easily done. Also, nonspecific binding of stains might give wrong signals [135]. Apart from effects directly related to the observation like photobleaching, several other factors, including a need for rigid instrumental control, hamper signal quantification [136, 137]. Furthermore, the penetration depth of the excitation laser into the sample is limited, making observation of thick biofilms or biofilms in complex matrices like sand impossible. A solution for this problem might be the use of an optically transparent matrix of porous fluoropolymers as adhesion matrix [138]. However, the surface characteristics are most likely differing from natural conditions. Last but not least, unstained parts of the biofilm of interest for research, like iron precipitation, cannot be imaged [17].

- SEM (disadvantage biofilm killed, only surface information)

Scanning electron microscopy (SEM) is superior in resolution to light microscopy in its lateral resolution, as a tightly focused electron beam is applied for image generation [17]. It can be applied to observe the initial attachment of bacteria on surfaces, including optical opaque surfaces like gold [21]. However, older biofilms cannot be imaged good, as only biofilm topography is measured with this method [17]. In traditional SEM, biofilm has to be fixed during imaging, and the biofilm structure is damaged during the fixation procedure. Environmental SEM can overcome this problem, but still damage of the sample due to the applied high energy electron beam is likely, making it useless for biofilm monitoring [129].

- PAS (disadvantage: resolution)

Photoacoustic spectroscopy (PAS) is a photothermal method, measuring the generation of an acoustic wave due to absorbance of radiation inside a sample [139]. Thereby, a short excitation laser pulse is absorbed in a sample, and a subsequently generated pressure wave is detected as signal. As PAS only measures radiation absorption, it is insensitive to the scattering matrix of the biofilm. Optically thick samples can be observed online using PAS [140, 141]. With photoacoustic spectroscopy, biofilm reference samples of agar gels with iron(III) oxide particles as well as biofilm have been observed online [116]. Also, the influence of colloidal particles on biofilm growth could be monitored [124]. As radiation absorption is measured, chemical information of the sample is obtained. Using an optical parametric oscillator, biofilm spectra in the visible and near infrared region were recorded, giving information about biofilm structural composition of pigments, carbohydrates and water [142]. Using signal deconvolution, a quantification of samples is possible [143]. This technique can be also theoretically applied to biofilm observation for quantification of the biofilm structure.

The biggest disadvantage of PAS is that only lateral averaging of the sample is conducted, and specific features of the biofilm matrix are unresolved. Also, the depth resolution of the applied measurements was limited to 10 μm [144]. Applying shorter laser pulses for excitation, this depth resolution should be improved though.

- OCT (disadvantage: no chemical information, only scattering image)

Optical coherence tomography (OCT) has only been recently added to the spectrum of applications for biofilm online monitoring [115, 145]. OCT measures backscattered light from the sample and is therefore non-invasive. Resolution in the micrometer range has been achieved, and biofilm densities within the structure could be distinguished [115, 145]. However, the major disadvantage of OCT is that no information about the chemical composition of the biofilm is recorded.

- Raman spectroscopy

Raman spectroscopy allows for the determination of the chemical composition of bacterial cells and biofilms [146, 147]. Bacterial species can be distinguished, and by combination with fluorescent methods measuring can be limited to live bacteria [147]. Using the effect of surface enhancement on Raman scattering by the addition of silver nanoparticles, recording of spectra can be enhanced by a factor of up to two orders of magnitude, and *in situ* imaging inside a biofilm is possible [146]. Due to the lack of a database, band assignment in the biofilm spectra is still difficult. Furthermore, the comparatively long acquisition time of 10 s for one spot limits the possibility to scan across large areas of a biofilm within a day.

- AFM

Atomic force microscopy (AFM) was applied to investigate the attachment and growth of *Aquabacterium commune* on medium density polyethylene and stainless steel, two common pipe materials in Europe [9]. Due to the high resolution of the AFM the effect of the surface structure after polishing on biofilm growth was elucidated, and electropolishing of stainless steel showed no beneficiary effect for bacterial growth prevention. AFM can be applied to samples in the hydrated state, but some dehydration during observation is likely, as AFM imaging is carried out on an open system [129]. In this “live” setup, also the movement of bacteria obstructs the image quality. As with SEM, also AFM only images the topography of the biofilm, and subsurface information is not recorded.

A promising new tool for biofilm surface observation is the combination of AFM with CLSM, which can furthermore be modified with tip-enhanced Raman spectroscopy [135]. Nanostructures can be resolved with this instrument with a resolution of a few nanometers, and the chemical composition can be elucidated. Depth observation of the biofilm, though, suffers from the same obstacles as AFM and CLSM.

- Other techniques

Other techniques that allow imaging at a resolution of a few nanometers are correlative light electron microscopy (CLEM) and stimulated emission depletion (STED) microscopy [133, 134]. In CLEM, recorded CLSM images are correlated with electron microscopic images. This requires tedious work, but gains information of structure on subcellular level. STED microscopy is an advanced fluorescent technique where a part of the illuminated area is photobleached, this way allowing imaging below the diffraction limit [148, 149]. Both techniques require staining, though, which again might influence the structure during imaging. While CLEM has already been applied to biofilms, scientists see STED microscopy as a future method for application to biofilm research.

The simplest method of biofilm observation is probably direct weighing of biomass. It is an easy approach to estimate biofilm thickness in macroscale experiments [55]. Detailed structural information cannot be gained from this measurement, though.

Another simple approach is scanning of biofilms grown on glass slides [150]. Using this method, biofilm can be monitored over a large area of 15 cm^2 in less then 9 minutes. Also, depth observation of biofilm is possible, but is limited to a biofilm thickness of 100 µm. Lateral resolution depends on the pixel size of the scanner, but cellular resolution seems difficult. Another disadvantage is that no further information is gained from scanning but structural information.

Transmission electron microscopy (TEM) offers resolution in the nm range, but sample preparation is needed prior to observation, and for 3-dimensional images the biofilm has to be cut [132]. Therefore, online monitoring cannot be conducted, and the preparation method might also influence the *in situ* structure. As transmission of electrons is recorded, only structural information is gained by this method. Also, only thin samples and small areas can be viewed [17].

Scanning transmission X-ray microscopy (STXM) in combination with near-edge X-ray absorption fine structure spectroscopy (NEXAFS) is another observation method with spatial resolution below 50 nm [132]. In contrast to TEM, chemical information is obtained, as X-ray absorption is measured. The technique is limited though by the low depth penetration (~ 5 µm) of the sample. Also, radiative damage to the sample cannot be excluded. X-ray- absorption fine structure spectroscopy itself also is applied for measuring the chemical element zinc in biofilm sample, although no structural information are obtained this way [151].

Three-dimensional excitation-emission matrix fluorescence spectroscopy is a rapid method for detecting EPS constituents in biofilm matrixes, but no structural information is recorded [152]. It can be applied for screening of wastewater sludge.

Surface plasmon resonance (SPR) was applied to study the attachment of *P. aeruginosa* to gold surfaces in real time [153]. The study is concentration-sensitive and can distinguish different kind of bacteria (wild type vs. knockout mutants), but the penetration depth of SPR is limited to a few hundred nanometers, so only bacteria adhering directly to the surface can be monitored.

A tracking microscope can be applied to track single bacteria in liquid and near a surface for studies on initial attachment [43, 44, 154]. The experiment is only qualitative though, as only selected bacteria are recorded.

Attenuated total internal reflection spectroscopy can be applied to study surface coverage of biofilm [155]. Surface roughness of the biofilm can be assessed with this method, but the lateral resolution of the measurement is limited. Fourier-transform infrared attenuated total internal reflection (FTIR-ATR) spectroscopy allows for the chemical determination of biofilm components, and kinetics like hydrogen-deuterium exchange in the water structure of biofilm can be measured to get insight into the water fine structure of biofilm [11].

Capacitor microsensors which measure impedance spectra of biofilm can distinguish microbial strains by differences in morphology and biological composition [156]. The biofilm observation is limited to the sensor surface, though, and signals are taken from lateral averaging. Also, the channel applied in this research was only 20 µm deep, so the applicability of the sensor to thick biofilms is unclear.

Miniaturized calorimetry can measure the biofilm activity online and non-invasively [157]. Biofilm can be detected from an early biofilm stage, but individual cells are not discriminable.

A summary of the presented methods with instrumental and measuring characteristics regarding biofilm observation is given in Table 1.

Table 1 Comparison of techniques applied for biofilm observation

Technique	online	*in situ*	non-invasive	non-destr.	non-staining	struct. info	quant.	2D res.	depth res.	depth penetration	sensitivity	chem. info	whole biofilm info	biol. info	bacterial environment
HPC	o	x	o	o	o	x	o	x	x	x	low	o	x	o	x
PCR	o	x	o	x	o	x	o	x	x	x	high	o	o	o	x
Microsensors	o	o	x	x	o	o	o	µm	µm	o	high	o	x	x	o
Microscopy Bright field	o	o	o	o	o	o	x	µm	x	x	low	x	o	x	x
Phase contrast	o	o	o	o	o	o	x	µm	Δ	Δ	medium	x	o	x	x
Hoffmann modulation	o	o	o	o	o	o	x	µm	Δ	Δ	high	x	o	x	x
Hoffmann + Fl.	o	o	o	o	o	o	x	µm	Δ	Δ	high	x	o	x	x
DIC	o	o	o	o	o	o	x	µm	Δ	Δ	high	x	o	x	x
CLSM	o	o	o	o	x	o	o	µm	µm	few 100 µm	high	o	o	o	o
FISH	o	o	o	o	x	o	o	µm	µm	few 100 µm	high	o	o	o	o
MAR	o	o	o	Δ	o	o	o	µm	µm	o	high	o	x	x	o
FISH + MAR	o	o	o	Δ	x	o	o	µm	µm	few 100 µm	high	o	o	o	o
FISH + sensors	o	o	x	x	x	o	o	µm	µm	few 100 µm	high	o	o	o	o
FISH + stain	o	o	o	o	x	o	o	µm	µm	few 100 µm	high	o	o	o	o
FRAP	o	o	o	o	x	o	o	µm	µm	few 100 µm	high	o	o	o	o
FRET	o	o	o	o	x	o	o	µm	µm	few 100 µm	high	o	o	o	o
FLIM	o	o	o	o	x	o	o	µm	µm	few 100 µm	high	o	o	o	o
FCS	o	o	o	o	x	o	x	µm	µm	few 100 µm	high	o	o	o	o
SEM	x	x	o	x	x	o	x	nm	x	x	high	x	x	x	o
ESEM	o	o	o	x	x	o	o	nm	x	x	high	x	x	x	o
PAS	o	o	o	o	o	o	x	x	10 µm	o	high	o	o	x	o
OCT	o	o	o	o	o	o	o	µm	µm	few 100 µm	high	x	o	x	x
Raman	o	Δ	o	o	o	o	Δ	µm	µm	few 100 µm	high	o	o	o	o
SERS	o	o	o	o	o	o	Δ	µm	µm	few 100 µm	high	o	o	o	o
AFM	o	o	x	o	o	o	x	nm	x	x	high	x	x	x	x
AFM + CLSM + TERS	o	o	x	o	o	o	o	nm	µm	x	high	o	x	o	o

Table 1 (continued)

Technique	online	*in situ*	non-invasive	non-destr.	non-staining	struct. info	quant.	2D res.	depth res.	depth penetration	sensitivity	chem. info	whole biofilm info	biol. info	bacterial environment
Gravimetry	o	x	o	o	o	x	x	x	x	x	low	x	x	x	x
Scanner	o	x	o	o	o	o	Δ	few µm	x	100 µm	low	x	o	x	x
TEM	x	x	x	x	x	o	x	nm	x	x	high	x	Δ	x	o
STXM + NEXAFS	o	o	o	x	o	o	o	nm	nm	5 µm	high	o	x	x	o
X-ray	o	o	o	x	o	o	o	nm	nm	x	high	o	x	x	o
SPR	o	o	o	o	o	Δ	o	x	x	few 100 nm	high	x	o	o	o
Tracking	o	o	o	o	o	x	x	µm	µm	x	high	x	x	x	x
FTIR-ATR	o	o	o	o	o	o	o	Δ	x	x	high	o	o	o	o
Impedance	o	o	o	o	o	x	o	x	x	x	high	x	o	o	x
Calorimetry	o	o	o	o	o	x	o	x	x	x	high	o	o	x	o

abbreviations: Fl. = fluorescence; stain = application of stains like CTC, etc. for measuring bacterial environment; non-destr. = non-destructive; struct. = structural; quant. = quantitative; res. = resolution, chem. = chemical; boil. = biological

Apart from the mentioned methods, other methods exist to characterize bacteria, and especially bacterial surface properties, which are of big importance in biofilm formation. For measuring the surface characteristics of bacteria, several methods can be applied, including contact angle measurement (CAM), microbial adhesion to hydrocarbons (MATH), X-ray photoelectron spectroscopy (XPS), infrared (IR) spectroscopy and zeta potential measurement [50]. In CAM on biofilm, water and formamide for hydrophilic interaction as well as diiodomethane and α-bromonapthalene for hydrophobic interaction, are commonly applied to determine the surface free energy components of the biofilm [8, 52]. MATH is carried out by extraction in water/hexadecane, and adherence is measured by comparison of light extinction values before and after the extraction [8]. CAM and XPS can also be carried out for testing of surfaces for the formation of conditioning films that facilitate bacterial adhesion [109].

1.1.5 Present problems in online biofilm monitoring

Although biofilm research is extensive, still various difficulties exist. For example, the online observation of thick biofilms is normally hampered by the scattering nature, and micrometer resolved structures can only be viewed up to thicknesses of a few hundred micrometers. On the other hand, existing systems that can measure thicker biofilms, like PAS, lack the resolution to observe processes in the biofilm closely. Another problem with biofilm observation is that in many methods, sample staining or sample preparation is needed, which in turn might influence the biofilm structure itself. This way the results might vary from undisturbed natural biofilm. Also, staining requires the accessibility of stains to all biofilm parts, which might be hampered by the biofilm structure itself.

In order to understand the complex processes in biofilm formation, growth and functionality, like in wastewater treatment systems, a fundamental understanding of the processes at organism level is needed [96]. The same applies also for biofilm formation in pipe-like systems, for example tap-water and wastewater-leading systems. As pipes normally are not easily observable, pipe-like model systems with easy observation and a defined flow are needed to understand the occurrence, growth and removal in those systems.

Model systems with multi-species inoculum in parallel reactors are furthermore needed when studying the effectiveness of chemicals and other water treatment methods on water distribution biofilms [101]. Parallel approaches are applied, for example, when testing materials in wastewater research plants, like biofilm carriers [158]. The observation of those effects should be non-invasive, though, and easy to accomplish. In this regard, the systems also require defined shear stress comparable to real systems to understand the effects of the treatment methods.

1.2 Microfluidics/Microdevices

The application of microfluidic devices is a growing field of interest in scientific research for over 20 years. Microfluidic devices contain microchannels that are on the sub-millimeter level either in width or height or both. Microchannels can be constructed with various designs, making multiple operations on the microfluidic device possible. Those designs are related to macro-operations like mixing, phase separation or blocking and therefore are called micro-unit operations (MUOs). MUOs include combination of flows, mixing, extraction, separation of flows, valves, etc. [159-161]. In microfluidic devices they can be combined in various ways, this way integrating whole processes onto a microchip which are then called micro total analysis systems (µTAS). A simple top-on connected I-type channel, which can be used for cell attachment, is presented in Figure 5.

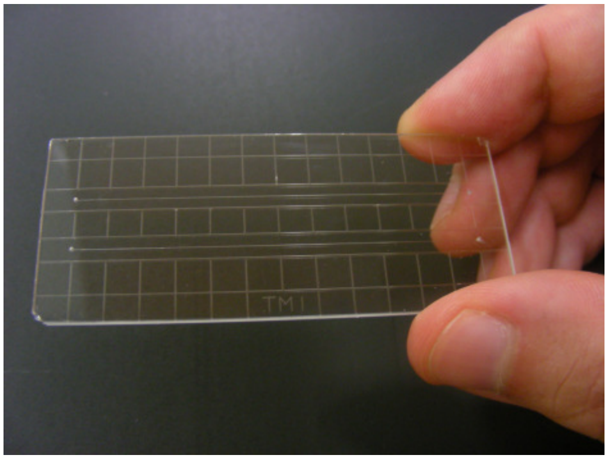

Figure 5 Top-on connected I-channel chip with two channels and connection holes on the right and left side

Microfluidics and μTAS include a wide field of research, including development of new microfabrication methods, integration of analytical devices like , cell handling and cell sorting devices, control devices and analytical applications [162]. Also actuators, including bio-micro actuators, are of interest for flow control as well as for autonomous pumping for microfluidic devices [162, 163]. Integration of analytical devices comprises many research fields. Optical spectroscopy like FTIR-ATR [164], thermal lens spectroscopy or fluorescence spectroscopy [165] is integrated into μTAS systems to include all functions of a chemical laboratory on a chip. This way, sample and reagent amount can be minimized and results quickly obtained.

1.2.1 Production methods

Various production methods exist for the production of microstructures and microdevices.

Mechanical methods include the use of saws, drills and mills. The structures produced this way have a rougher surface though, and the available fineness of the structures is limited.

Electron beam lithography is used for example to make masks for photolithography. In a first step, a metal, the most common chromium, is coated onto a glass slide using evaporation. The coated glass slide is then placed into an electron beam (EB) setup. A desired pattern can be programmed into the EB control software. Afterwards the EB will etch the desired pattern into the metal, this way producing a mask for photolithography.

Photolithography is a common method for producing microstructures. In this method, a photoresist, the most common SU-8, is spin-coated onto a base material, in most cases a silicon wafer or glass slides. The photoresists most commonly are based on epoxy resin. The polymer is then softbaked to remove remaining solvent. A photomask, which can either be printed on special foils or is produced using electron beam lithography, is then placed onto the resist. The resist is exposed to a radiation source, for SU-8 UV light at 365 nm. Following the exposure, a post exposure baking step is applied. After that, another layer of photoresist can be spincoated and treated as before to make thicker patterns, or a different photomask can be applied to fabricate more complicated 3-

dimensional structures. Care has to be taken on the alignment of the structures during the irradiation. After the last layer is processed this way, the photoresist is developed with a polymerization initiator to crosslink the UV-exposed areas. Following this the remaining undeveloped photoresist is washed off and the developed structure is finished. The microstructure produced this way can be either applied to experiments or used as a master for soft lithography methods. Photolithography is also applied in semiconductor fabrication [166].

In soft lithography methods, a micropatterned elastomeric polymer is applied in various techniques to produce microstructures [166]. The elastomer is thereby produced from a micropatterned master, which is taken as negative for the microstructures. A prepolymer is cast onto the master, developed and peeled off afterwards. To facilitate the removal of the patterned elastomer, the master can be modified [167]. The most commonly applied elastomer is poly(dimethylsiloxane) (PDMS). The soft lithography methods where this soft structure is applied then are replica molding, microcontact printing, micromolding in capillaries, microtransfer molding, and the production of microfluidics [166].

In replica molding, a second prepolymer is cast onto the elastomeric master, cured and then peeled away to produce a structure similar to the original master structure. In microcontact printing, the substance that is desired to be patterned is applied onto the elastomer. Afterwards, the elastomer is reversed and stamped onto a substrate, this way printing the pattern onto the substrate. Using this method, cells can be patterned onto gels. Also, self-assembled monolayers can be patterned this way. During micromolding, the elastomer which is open on two sides is placed with the pattern structure onto the substrate, a prepolymer is drawn into the structure by capillary action, and the prepolymer is cured. This way, also a structure similar to the original master is produced. In microtransfer molding, the prepolymer is cast onto the elastomer, and excess prepolymer is removed from the surface, for example by scraping. The stamp is then inverted and put onto the substrate where the prepolymer is cured. For microfluidic production, the elastomer is inverted and put onto the substrate. In the case of PDMS, the contact to the substrate is normally weak and leakage is easy to occur. The hydrophobic surface of PDMS can be oxidized in a plasma-oven, though, and then be bonded covalently to the substrate.

Newer methods for production include fabrication from calcium alginate and “liquid Teflon” as well as a bonding process that works without the requirement for clean room at room temperature [162].

1.2.2 Applications

Microfluidics offer advantages in experiments due to their high surface-to-volume ratio, defined flow conditions and shear stress that can easily be changed, low reagent consumption and high experimental throughput. An example where all these advantages are exploited is an experiment with three microfluidic devices to study fibroblast cell adhesion with varying shear stress, concentration of adhesion molecules modified on the channel surface and external factors, in this case the epidermal growth factor [167]. An adhesion assay was also conducted with human arterial endothelial cells [168].

As microfluidics offer a high surface-to-volume ratio, they are also considered as new tools for the investigation of surface effects on biofilm attachment [106]. A number of papers have been published in the field of bacterial research. A microfluidic device was applied in the research of bacterial persistence, where subpopulations of bacteria with different persistence in a homogeneous culture of *E. coli* were observed [169]. A maze of 100-µm wide channels was constructed to observe the active movement of bacteria due to chemotaxis to aggregate [54]. In a follow-up experiment it was shown that the bacteria move not randomly but in waves during the aggregation process, which shows the tendency of bacteria to stay in bigger colonies [170]. Further research on bacterial movement with *E. coli* cells showed a preferential movement of bacteria depending on surface material [171]. *E. coli* cells were also applied in a microchannel to study their respiratory activity [172]. Another microfluidic device was constructed for rapid detection of microbial viability, with the test finishing within 30 minutes [173]. Microfluidics were also applied in bacterial detection of *Escherichia coli*, *Salmonella typhimurium* and *Legionella pneumophiia* with a microarray system [174]. Microfluidic patterning and the creation of “nanofabricated landscapes” offers even new insights into bacterial research [175]. Bacteria in limited space can be either limited by space or nutrients and a plateau level in bacterial concentration is reached, or they go to extinction, according to common assumptions. In the experiments, bacteria showed the emergence of a metapopulation that is best adapted to the environmental conditions, in this case limited nutrient supply, after other metapopulations with excess nutrient uptake went extinct. The metapopulation spread through separated cells, without a possibility for bacterial movement between cells, which gave rise to the assumption that the whole bacterial colony was coupled through signals. The experiment showed the importance of landscape on bacterial development and the development of the bacterial population.

One of the few applications of microchannels to biofilm research showed the efficiency of treatment procedures against *Staphylococcus epidermis* biofilm in a straight channel [70]. In another experiment, a microchannel with micro-patterned hydrophobicity was used to show that *Streptococcus sobrinus* HG1025 showed no initial preference for attachment on hydrophilic or hydrophobic surfaces, whereas retention of biofilm was higher on hydrophilic surfaces [176]. The orientation of the pattern also seemed to influence the bacterial retention, as bacteria were more readily removed from hydrophobic surfaces oriented parallel to the flow. One further application of microchannels in biofilm research is the development of a miniaturized calorimeter [157]. Calorimetry was carried out on different surface materials which were easily exchanged by application of 50-µm thick foils as surface material.

As the observation area in microchannels is limited, instrumental detection methods have to be adjusted or adapted for observation in confined spaces. Among the detection methods which are easily adapted to the microchannel environment and can be applied for sensitive detection are thermal lens spectroscopy (TLS) and thermal lens microscopy (TLM), respectively [161, 165, 177, 178].

1.3 Thermal lens microscopy

Thermal lens microscopy and thermal lens spectroscopy, respectively, are instrumental methods that measure the photothermal effect inside a sample. The photothermal effect is thereby derived from the absorption of photons inside the sample and the subsequent thermal relaxation of sample molecules which is then imaged. Apart from TLS and TLM, other photothermal methods like photothermal deflection spectroscopy, photothermal interferometry or PAS exist [179].

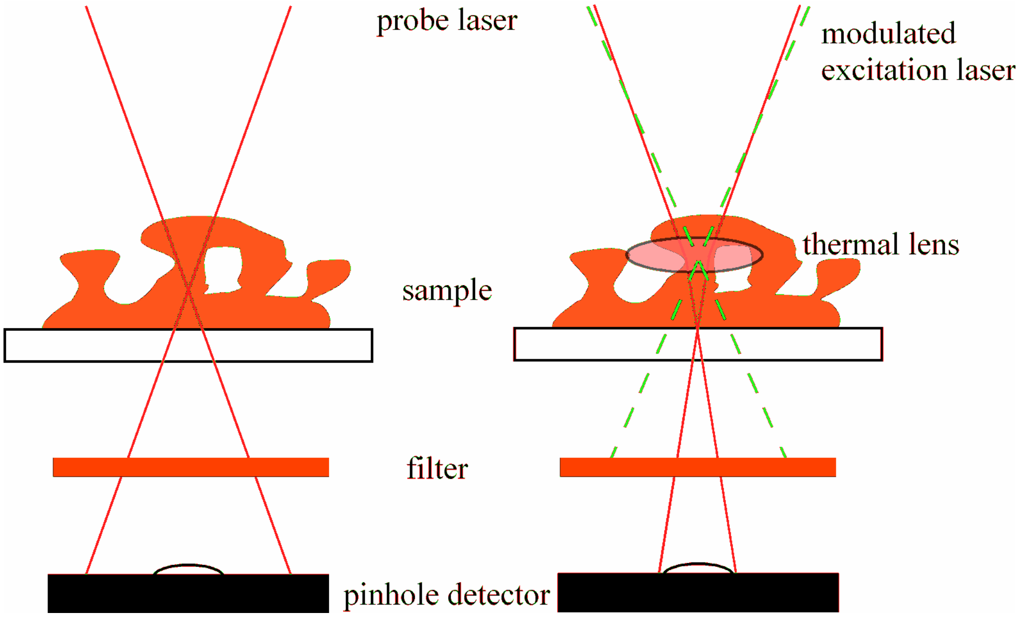

Figure 6 Thermal lens effect: the unaffected probe beam on the right enters the pinhole detector at the bottom (left); after introduction of a modulated excitation laser into the sample which is absorbed by the sample, a thermal lens is generated and diffracts the probe beam which in return leads to a change in the probe beam intensity entering the pinhole detector (right; see text for detailed description)

TLS and TLM are based on the thermal lens effect, which is shown in Figure 6. In TLM, an excitation and a probe beam are applied to a sample. A part of the excitation beam is absorbed by the biofilm sample, and molecules in the matrix are lifted into an excited state. The absorbed energy subsequently is released again from the molecules to return to the ground state, either by radiative or non-radiative relaxation. Non-radiative relaxation results in a local generation of heat. Due to the excitation beam profile and thermal diffusion in the matrix, a temperature gradient around the beam is generated. In water at room temperature, where the temperature coefficient of the refractive index is negative, the temperature gradient acts as a transient concave lens, called thermal lens. The degree of the thermal lens effect depends linearly on generated thermal energy, and therefore on the absorbance of the sample, which in turn depends linearly on the excitation intensity. The lens affects the probe beam by diffracting it. The effect of the lens on the probe beam is directly proportional to absorption of the excitation laser. The diffraction of the probe beam leads to a change of the focus spot of the probe beam, which is recorded by a pinhole detector measuring light intensity. By modulating the excitation beam, the effect of the thermal lens on the probe beam can be extracted from the detected probe beam intensity with a lock-in amplifier. For this purpose, the excitation beam is filtered from the beam path prior to the detector.

Unlike absorbance measurement, thermal lens measurements record the effect of the thermal lens on the probe beam, and are therefore more similar to fluorescence methods. Due to this fact, TLS can be applied to measure absolute quantum yields [180]. Like in fluorescence methods, the thermal lens signal amplitude is directly proportional to the power of the excitation laser.

In thermal lens microscopy, we can probe not only the absorbance of the sample, but also the release of the thermal energy into the sample. This energy release is depending on thermal diffusion within the sample, and therefore the thermal diffusion characteristics of the sample are probed by thermal lens measurements as well. The thermal lens signal does not only contain information about sample absorbance, which is related to the thermal lens signal intensity, but also contains information about the thermal nature of the sample, which is mainly seen in the phase of the signal. The concept of the thermal lens phase will be described in chapter 3.2.2.

The thermal lens effect was reported for the first time in 1964 [181]. At the beginning, thermal lens was exploited for thermal lens spectroscopy (TLS) due to the possibility of highly sensitive measurements. Limitations on optical equipment, especially on objective lenses made imaging difficult. With the development of optics, also TLM was developed. Nevertheless, TLS is still applied due to its high sensitivity, which is also based on the possibility to measure absorption in small observation areas [161, 165, 182, 183]. Integration of other measuring methods into TLS setups like fluorescence detection is of interest as well as miniaturization [165]. In addition, new methods are developed like TLS with total internal reflection for surface observation or photothermal near-field scanning optical microscopy [184-186].

Thermal lens microscopy was first achieved by the use of an achromatic lens. In standard microscopes with apochromatic lenses, chromatic aberrations are minimized and light beams of different wavelength are adjusted to focus in one spot. With this setup, however, the thermal lens of the excitation beam will be formed at the focus of the probe beam and not affect it [187]. Using an achromatic lens, a difference in focus spot of excitation and probe beam is achieved. The thermal lens therefore forms strongest outside the focus of the probe beam, and a thermal lens signal is recorded. Advances in optics now also allow the use of "normal" lenses to be used.

TLM has been applied to biological samples and offers micrometer resolution [177, 188-193]. Proteins were imaged on hemodialysis membranes with immunogold-staining [192]. Differences of protein concentration on the inside and the outside of the membrane were resolved. In renal tubule of fixed kidney, the concentration of tobramycin was imaged two-dimensionally by TLM using gold-modified tobramycin for staining. The sensitivity in this measurement surpassed CLSM by a factor of 10. The sample in this case was fixed, though, and scanning was conducted point-by-point, which led to prolonged imaging time. Applying this method, measurements with a sensitivity corresponding to single blood cell surface antigens can be conducted [190].Adjustments to this scanning scheme can be made by taking into account the spherical shape of the cell surface [189]. Taking it into account, adjustments to the scanning depth inside the sample have to be made, which can be done approximately using the thermal lens signal phase. Live imaging of biological samples can be carried out with TLM inside microchannels [177]. The temporal change of cytochrome C distribution during apoptosis was measured online, enabling the measurement of temporal changes and kinetics. Applying a UV laser, yeast fungus cells were imaged with TLM [193]. Using the TLM microscope in a cross-beam rather than a collinear setup, three-dimensional observation with resolution of 1 μm^3 is possible [191]. This way, stained features of plants as well as bacteria can be imaged. Another method to measure samples in TLM with depth resolution of 1 μm or less is confocal TLM [194]. Phase images give information about the thermal characteristics of a sample and can be applied for comparison of results. In stained *Tilia Americana*, the lignin features inside the plant which are observed in the thermal lens phase image correspond to the absorption images, which is a further prove that stained lignin was imaged with this method [191]. While imaging yeast fungus cells, the phase image showed signals in the vicinity of yeast cells, which were presumably from heat accumulation near the cell walls [193].

Resolution improvements in TLM are introduced recently by introducing new measurement principles, namely photothermal interference contrast (PIC) [195-197] and photothermal heterodyne imaging, termed light induced scattering around a nano-absorber (LISNA) [198-200]. Both methods enable staining-free imaging of samples with a resolution of a few nanometers. In PIC, the probe laser is split into two beams by a Wollaston prism. The excitation laser is only introduced into one of the probe beam, and the second beam serves as a reference beam [196]. With this method, membrane proteins labeled with nanometer-sized gold particles with sizes of a few nanometers can be imaged with an axial resolution about 0.85 µm and a transverse resolution of 200 nm [197]. In LISNA, a “nano-absorbing object” is illuminated with a frequency-modulated excitation beam and produces a modulated change of refractive index around the object [198]. The collinear probe beam interacts with this field and produces a scattering field with a characteristic modulation frequency equal to the modulation of the excitation beam. This scattering field then can interact with a reference field, e. g. from the unmodulated probe beam, and be detected, this way. Using LISNA, live imaging of unstained cell samples and cell structures, including mitochondria, can be carried out, with a resolution similar to CLSM [199]. In this experiment, the LISNA microscope was integrated with transmission and confocal microscopy, making this setup a very powerful tool for correlative experiments.

2 Aims and scope of the thesis

The focus of this thesis is online, *in situ,* staining free observation of biofilm grown under flow conditions similar to flow in pipes. One focus is on the application of microchannels as model flow systems and the other on the application of TLM for biofilm observation, so the aims of the thesis are separated into two parts, before the two parts are reunited by the online observation of biofilm with TLM in microchannels.

Microchannel as pipe model for biofilm growth

Biofilm growth in pipes cannot be easily observed, and monitoring of pipes is normally limited to monitoring of influent and effluent streams or sample taking at defined points. While sampling of influent and effluent cannot inform about adhered biofilm inside the pipes, sampling is invasive and results are limited to the sampling points. Transparent flow cells offer the possibility for noninvasive observation of biofilm under flowing conditions and are therefore good pipe models. Microchannels are miniaturized flow cells that are easy observable. In contrast to bigger flow cells in the millimeter to centimeter range, microchannels offer a smaller observation area and the whole area can be examined easily.

In order to apply microchannels to biofilm research, they have to be tested and optimized for biofilm growth experiments. Also, biofilm growth has to be verified, and their versatility and usefulness for biofilm research needs to be shown. For this purpose, the following points need to be done:

1. Check the hydrodynamic conditions (flow rate, wall shear stress) inside microchannels for their comparability to existing experimental systems.
2. Apply an existing microchannel system to biofilm experiments and verify biofilm adhesion and growth with online, staining-free experiments.
3. Check the system for the occurrence of problems, especially in regards to clogging and dead zones as biofilm structures can develop to the size of microchannel systems.
4. Modify the microchannel system to avoid clogging and minimize dead zones inside the observation area.

5. Develop biofilm removal and cleaning procedures for the channel for reusability of the equipment.
6. Show the versatility of microchannels with parallel experiments inside one microchip under systematically varied growth conditions.
7. Optimize the system for application of a wide range of hydrodynamic conditions and the possibility for multiple parallel experiments.

TLM for online observation of biofilm

While the microchannel is applied as a flow system where online monitoring is possible, also a staining-free observation method to gain further access to chemical and structural information of biofilm grown under flown conditions is needed. An online, staining-free spectroscopic method with resolution in the micrometer range and the possibility for three-dimensional observation therefore needs to be applied. As observation method, the adaptation of TLM to biofilm online research is investigated. For this purpose, several experiments need to be conducted.

Prior TLM measurements on biological samples in Kitamori laboratory were conducted with a step-scan method, in which sample points are taken point-by-point. However, to evaluate biofilm structure, 3-D mapping is required over a height of normally more than 100 µm and an area allowing for spatial averaging in mature biofilms (> 100 µm^2). The step-scan procedure, therefore, cannot be applied for biofilm online observation, as it is too time-consuming. Preferably, the acquisition time of 30-µm-square 2-D scan should be less than 1 min, and, then, 3-D mapping with appropriate scanning time will be realized.

Here, continuous scanning TLM is expected to reduce measurement time. Signal-to-noise (S/N) ratio becomes worse by this procedure, though, and the available resolution (depending on response time of the TLM signal) has to be confirmed for different scanning velocities, to check if biofilm structure is resolved. For homogeneous samples in continuous scanning TLM, resolution has not to be considered as no signal change is observed. At sample edges and inhomogeneities, which are present in biofilm, the response time for the photothermal signal change during scanning has to be considered for lateral resolution. Also, other factors influencing the TLM signal, like the scattering biofilm matrix, should be addressed.

For 3-D observation of a biofilm, the step depth after 2-D scanning of a certain plane has to be evaluated. The minimal step width for samples with equal absorption, and therefore equal photothermal signal, is evaluated.

After the characterization of the TLM setup, biofilm online, *in situ*, staining-free observation experiments are needed to show the applicability of TLM and its usefulness to biofilm research. As an example, the online structure of pigments within the biofilm which has not been recorded before is observed three-dimensionally using TLM. A measurement with a reference method finally needs to be taken to compare the obtained results.

Summarizing the requirements for TLM experiments, the following points have to be undertaken:

1. Apply and characterize a continuous scanning system for TLM measurements.
2. Optimize the system for signal output.
3. Check the existing TLM system for applicability to micrometer-resolved measurements in a heterogeneous matrix.
4. Record biofilm structure with the TLM system.
5. Make online, staining-free observation of a biofilm with the TLM system.
6. Compare the measurement with another observation method.
7. Record biofilm pigment structure for showing the usability of TLM in biofilm experiments.

3 Theory

3.1 Microfluidics

Microfluidics differs from batch experiments or experiments in millimeter sized setups in their high surface-to-volume ratio. This high ratio results in a number of effects that are pronounced in microfluidic research and even more in nanofluidics. From the point of biofilm research, the most prominent factors to be considered in microfluidic research are the flow characteristics, including shear effects, and the pressure drop that are encountered in microfluidic devices. In the following two paragraphs, a brief introduction of the two phenomena and its effect on biofilm research in microchannels will be discussed.

3.1.1 Laminar flow and shear stress

Contradictory reports exist about the transition region from laminar to turbulent flow [201, 202]. The more recent report states that microchannels exhibit similar behavior as bulk systems, but roughness elements are having a bigger effect on the flow [201]. This is also documented in the former report [202]. Therefore, also the effect of biofilm on the flow will be different than in bulk systems in regions of higher Reynolds numbers. The Reynolds number *Re* inside a channel can be calculated as in classical theory with the following formula:

$$Re = \frac{\overline{u} D \rho}{\mu} \qquad 3\text{-}1$$

with $\overline{u}$ the average velocity of the fluid, μ the dynamic viscosity of the fluid, D the equivalent diameter of the channel, and ρ the density of the fluid.

Reynolds shear in the channel behaves similar to pipe flow experiments for larger microchannels with widths and depths of ~ 500 µm, but discrepancies are seen for smaller channels as well as at the wall [203]. The wall shear stress in rectangular microchannels, and in an approximation also in semicircular shaped microchannels, can be calculated as follows [168]:

$$\tau_w = \frac{6\mu\dot{V}}{a^2 b} \qquad 3\text{-}2$$

with τ_w the wall shear stress, a the depth of the microchannel, b the width of the microchannel, and $\dot{V}$ the volume flow inside the channel.

For round channels, or capillaries, the formula changes with the channel geometry:

$$\tau_w = \frac{4\mu\dot{V}}{\pi r^3} \qquad 3\text{-}3$$

r in this case is the radius of the channel. Modeling cells as roughness elements, it was shown that the shear is not spread evenly about the cell surface, but the average shear stress acting on the cell is similar to the wall condition [167]. As a structure gets further away from the microchannel wall, though, the shear rate increases, whereas shear stress is limited in corner regions of the channels [70, 167].

3.1.2 Pressure drop

During the flow of liquids in pipes, a pressure drop between entrance and exit of the pipe is observed. While this pressure loss is almost negligible in large sized pipes, the pressure loss is an important factor to be considered during microchannel construction and operation. In an approximation for laminar flow, it can be calculated from the friction in the channel [204]:

$$\frac{\Delta p}{L} = \frac{2 f \rho \dot{V}^2}{D} \qquad 3\text{-}4$$

For laminar flow, the friction factor f is easy to obtain:

$$f = \frac{16}{Re} \qquad 3\text{-}5$$

Combining equations 3-1, 3-4 and 3-5, we get:

$$\frac{-\Delta p}{L} = \frac{32\mu\bar{u}L}{D^2} \qquad 3\text{-}6$$

The pressure drop is especially of relevance for the construction of pressure-driven flow systems. Not only does it define the pressure that is needed for the system to start working, it is also a way to control the flow and shear inside a system.

3.2 Thermal lens microscopy

Several setup options are available for thermal lens microscopic measurements, and each setup has its own advantages and disadvantages as well as theory for signal generation and signal quantification. Before a theoretical description of the thermal lens microscopic system at Kitamori-laboratory is briefly introduced, the optical setup of the instrument and its components will be discussed briefly.

3.2.1 Definitions

Thermal lens microscopy is based on the photothermal effect. To measure this effect, an excitation light source and a probe light source are needed. The two sources can be the same, in which case the experiment is a single-beam experiment, whereas in a dual-beam experiment excitation beam and probe beam are different.

In photothermal measurements, a change of intensity in a probe beam due to thermal relaxation inside a sample upon sample absorbance is detected. A modulated excitation of the sample is therefore needed to record a temporal change in probe beam intensity. The modulation can be carried out by either applying a pulsed excitation source or modulating a continuous wave excitation source, for example using a mechanical chopper or an acousto-optic modulator (AOM).

Another difference in the setup of the thermal lens instrument is in regard to the beam paths of the excitation and probe laser source. The beams can be either aligned collinear combining the beams before entering the sample or applied inside the sample at an angle to each other, in which case the setup is called cross-beam setup.

The distinction between mode-matched and mode-mismatched is made only for dual-beam setups [205]. For both cases, the excitation and probe beam focus spots are one confocal length z_c apart in z-direction for maximum signal amplitude:

$$z_c = \frac{\pi w_{pr}^{2}}{\lambda_{pr}} \qquad 3\text{-}7$$

The confocal distance depends on the beam width and the wavelength of the probe beam. In the mode-matched case, the beam spot sizes inside the sample are roughly the same and the effect on the probe beam is a diffractive one. The major part of the signal comes from the probe beam focus. At this point, however, the power of the excitation laser is reduced roughly a factor of two compared to the focus point due to the confocal setup. In the mode-mismatched case, the probe beam radius can be larger than the excitation beam radius and signal generation occurs mainly at the excitation beam focus point. This way, a stronger signal is generated, but the signal shows the aberrant nature of the thermal lens, that is the thermal lens acts not like a perfect thin lens.

The last differences in optical setup in thermal lens measurements are the positioning of the detector. In the case of far field detection, the detector is positioned in the optical far field, and the resolution of the instrument is limited by the Rayleigh criterion. In near field thermal lens microscopy, the resulting signal is detected only a few nanometers away from the surface. Therefore, near field optical detection is normally limited to surface characterization. Recently a photothermal near-field scanning optical microscope has been developed [186].

The photothermal setup used in the TLM experiments conducted throughout this thesis is a far-field continuous wave laser induced mode-mismatched dual-beam collinear TLM, so the following brief theoretical introduction will focus on this setup.

3.2.2 Signal generation

Thermal lens microscopy, like all photothermal spectroscopic methods, is based on the thermal lens effect. This effect is based on the absorbance of an excitation beam. In the case of the TLM used in this thesis, the excitation beam is a modulated continuous wave laser in the TEM$_\infty$ mode, whose intensity is:

$$I(r) = \frac{2P_e}{\pi\omega_e^2} \mathrm{e}^{-\frac{2r^2}{\omega_e^2}} \qquad \text{3-8}$$

The intensity *I(r)* depends on the total power of the excitation beam P_e, the radius r and the beam radius of the excitation beam ω_e.

The absorbed energy can then be relaxed by the sample molecules through radiative and non-radiative relaxation, the latter leading to the production of heat in the sample. For non-fluorescing samples, the heat *Q(r)* generated in the sample can be calculated by the following equation, and also depends on the absorption coefficient ε of the sample:

$$Q(r) = 2\pi\varepsilon I(r) r dr \qquad 3\text{-}9$$

For fluorescing samples, a factor regarding fluorescence quantum yield has to be included [179].

In a homogeneous sample, the heat transfer equation with boundary conditions can be applied [205]:

$$Q(r) = c\rho\left[\Delta T(r,t)\right] - k\nabla^2\left[\Delta T(r,t)\right] \qquad 3\text{-}10$$

$$\Delta T(r,0) = 0 \qquad 3\text{-}10a$$

$$\Delta T(\infty,t) = 0 \quad (t > 0) \qquad 3\text{-}10b$$

This equation can be solved in theory by the application of Green’s function [205]. Green’s function describes “the spatial and temporal profile of the temperature rise produced by an impulse of heat along a long, thin path” [206]. The diffusion of heat into the sample medium leads to the generation of a temperature gradient in the sample, which is accompanied by a change of refractive index inside the sample:

$$n(r,t) = n_0 + \frac{dn}{dT}\Delta T(r,t) \qquad 3\text{-}11$$

The equation for the temperature change for homogeneous samples will not be presented here [205], as it does not apply to biofilm, and for heterogeneous samples, no theoretical model exists. However, in the first order approximation the change in refractive index is directly proportional to the temperature change, which in turn is directly proportional to the incident excitation beam power. The degree of the thermal lens is therefore directly proportional to the excitation beam power.

The second part of the thermal lens theory is about the effect of the thermal lens on the probe beam. While in the beginning, the effect of this refractive index gradient was treated like the effect from an ideal thin lens [207, 208], later research acknowledged the aberrant nature of the formed thermal lens element and treated it using diffraction theory [205, 209]. In this later model, the thermal lens causes a phase shift Φ inside the probe beam, which is related to the change in refractive index and the path length *l* [205]:

$$\Phi = \frac{2\pi}{\lambda_{pr}} l[n(r,t) - n(0,t)] \qquad 3\text{-}12$$

This phase shift can be understood easiest as a distortion in the spherical wave front from a punctual beam source [209]. Including this phase shift, the beam can be described just outside the sample with a complex amplitude and phase of its electrical field, which again is given for a homogeneous sample [205]. After exiting the sample, the field propagates freely to the detector. A theoretical approach to the quantification of “continuous wave laser induced mode-mismatched dual-beam thermal lens spectrometry” for a homogeneous sample has been deducted before [205]. However, using TLM in microchannels, the model has to be modified, and numerical solving is necessary for quantification [210]. This model also only applies to homogeneous samples. For heterogeneous samples with inhomogeneities in three dimensions, several factors are thinkable that make a deviation from former solutions necessary. Factors that could lead to a deviation are presented in Figure 7.

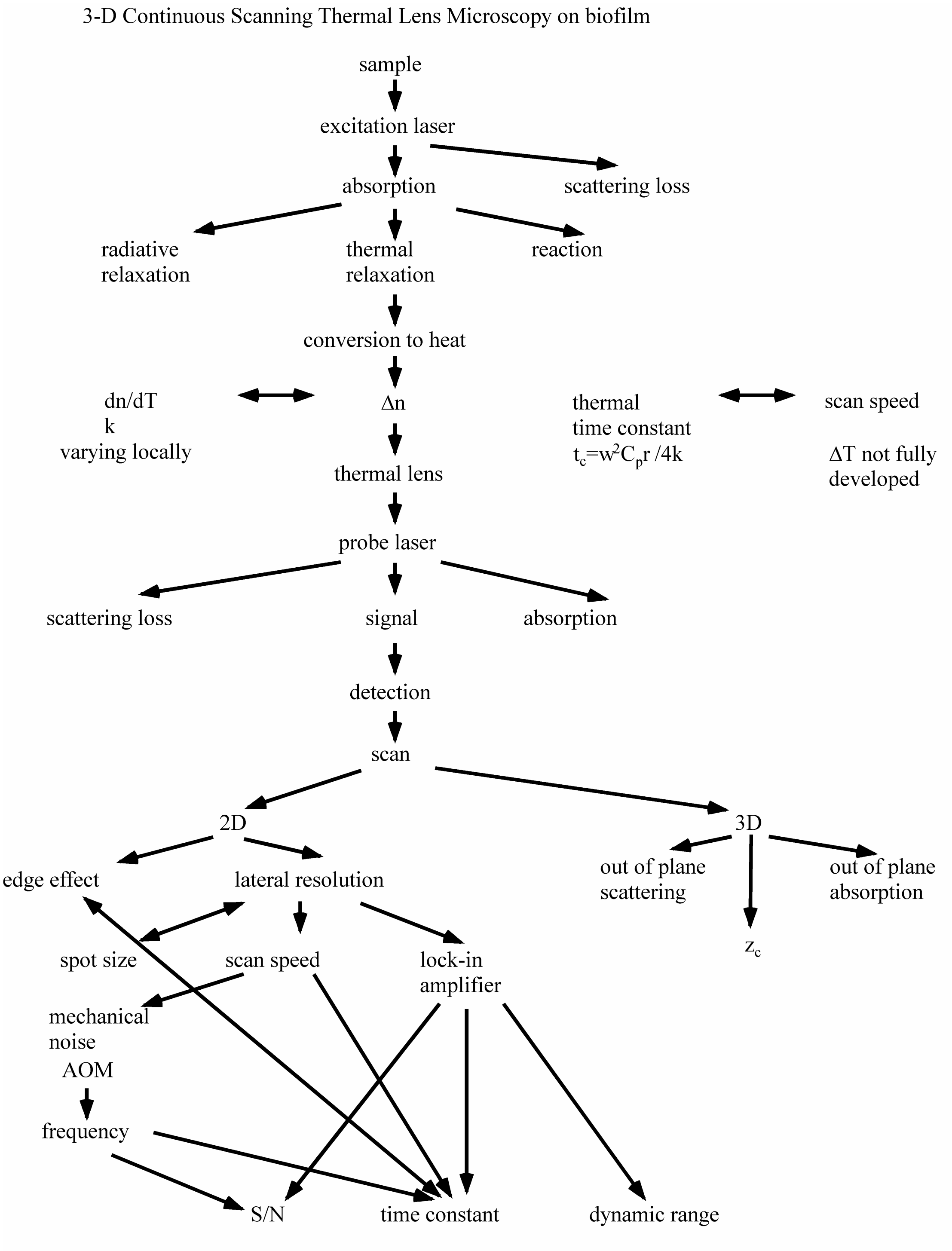
3-D Continuous Scanning Thermal Lens Microscopy on biofilm
sample
excitation laser
absorption
scattering loss
radiative relaxation
thermal relaxation
reaction
conversion to heat
dn/dT
k
varying locally
Δn
thermal lens
thermal time constant
$t_c=w^2C_pr/4k$
scan speed
ΔT not fully developed
probe laser
scattering loss
signal
absorption
detection
scan
2D
3D
edge effect
lateral resolution
out of plane scattering
out of plane absorption
z_c
spot size
scan speed
lock-in amplifier
mechanical noise
AOM
frequency
S/N
time constant
dynamic range

other factors:
- flow -> effect on DT, but not on thermal lens,
  as TL effect is on stationary biofilm structure
- microchannel -> - depth effect negligible, as channel is quite deep
  - channel wall (heat conduction, refraction)

Figure 7 Factors influencing signal quantification of TLM in 3D-heterogeneous samples

A first factor influencing the quantification of TLM signal in scattering three-dimensional is scattering. While samples with high scattering background are immune to scattering over a wide concentration range in liquid samples, scattering influences the thermal lens signal when optical inhomogeneities exist over the range of the probe beam [211]. In addition, scattering of the excitation beam causes loss of initial intensity at points lower in the sample as seen from the objective lens, and TLM signal is therefore reduced.

The next factor influencing the thermal lens signal is the thermal lens itself. While in homogeneous samples, a symmetric lens with defined thermal diffusion is generated, the variation of thermal dn/dT, a molecular constant, and the thermal conductivity k leads to a non-uniform lens, which has to be actually modeled from the results, or the exact composition of the sample has to be known prior to measurement, which would take the measurement ad absurdum. The thermal lens will be always shifted a little towards the direction of scanning, as the beam moves along with the heat diffusion. This shift will most likely depend on the thermal time constant t_c, a characteristic built-up time for the thermal lens:

$$t_c = \frac{\omega_e^2 \rho C_p}{4k} \qquad 3\text{-}13$$

This time constant in turn depends on sample constants like density ρ, thermal conductivity k and specific heat capacity C_p. With a laser spot of a size of 1 µm, the thermal time constant in water would be on the order of 2 µs, so this factor only influences signal generation at very high scanning frequencies which will not be encountered in this thesis.

The probe beam contribution to the thermal lens effect is normally minimized by applying a probe beam with intensity two orders smaller than that of the excitation beam [187]. For absolute quantization, it might be an influence factor, though.

A final factor influencing the thermal lens signal is out-of-plane absorbance of either excitation or probe beam which like scattering will result in a smaller signal.

Other factors influencing the measurement are in regard to resolution of the instrument and will be discussed in the next section. The final limitations on the measurements, however, come from instrumental settings and the setup. In microchannels, for example, the rapid thermal conduction at the channel wall leads to the generation of a high temperature gradient and therefore to a strong thermal lens signal upon light absorption [178]. While this effect can be used to measure TLS assisted by microchannels without the need for the generation of a temperature gradient by the spatial distribution of the laser, the quantification of the thermal lens signal at the channel wall is furthermore made difficult in setups where not the whole channel is irradiated.

Despite all these aspects that are hampering the quantification of TLM signal of biofilm, the thermal lens signal is still directly dependent on the development of the thermal lens, and this in turn is directly dependent on the initial excitation beam power. Therefore, when a biofilm sample is scanned with an excitation beam of constant power, the resulting signal should approximate the absorbance of the beam inside the sample.

The same holds true for another aspect of thermal lens measurements, the phase of the photothermal signal. The phase of the photothermal signal is different to the phase of light that is generated by the diffraction of the probe beam described above. It is a result of the propagation of the thermal wave inside the sample medium. It can be described as an offset between the time the sample is excited, which depends on the modulation frequency, and the time the signal needs to reach its maximum. The phase of the signal is measured inside the lock-in amplifier. Sample heterogeneity or impurities lead to different thermal wave propagation inside the sample medium, which results in the recording of a different phase value inside the lock-in amplifier compared to the homogeneous sample medium. In addition, the phase of the TLM signal is depending on the position of the sample relative to the focus point of the excitation laser [187]. While no TLM signal is generated if the thermal lens is positioned on the focus of the probe laser, the probe beam converges if the thermal lens is positioned above the probe beam for a sample with a negative temperature coefficient of refractive index. If the probe beam focus is positioned above the thermal lens, the probe beam diverges after passing through the thermal lens. Therefore, the effect on the probe beam changes from a converging effect to a diverging effect if a z-scan is taken through a thin sample, and the phase of the thermal lens signal changes by 180°. In non-absorbing regions of a sample, only electrical noise is recorded with TLM measurements, and the phase value of the

TLM signal is changing randomly. In regions with similar thermal properties in the sample, the phase value of the TLM signal is close to a constant value.

The phase of the thermal lens can be measured directly, but quantification is difficult especially for inhomogeneous samples [193]. Another approach for gaining information from the TLM signal phase is an indirect approach that is applied in this thesis. The basis of this approach is that materials of similar thermal properties show a similar TLM signal phase value, whereas materials with different thermal properties (e.g. gold and air, water and proteins/polysaccharides) show different phase values. Considering this, the difference of TLM phase values between adjacent points shows whether or not changes in the thermal properties between those points are observed. Applying this method in two dimensions, regions of different thermal properties can be distinguished.

3.2.3 Resolution

In non-scanning case of homogeneous samples, the lateral resolution of the thermal lens microscope is limited by the spot size of the excitation beam ω_0 [187]:

$$\varpi_0 = 1.22 \frac{\lambda}{N.A.} \tag{3-14}$$

However, during scanning of heterogeneous samples, limitations on lateral resolution (and signal quantification) exist due to restricted heat flow at edges [212]. The heat flow at edges is thereby restricted due to the change of the thermal conductivities between two media. The geometry of the sample has a major influence on the effect of the edge as well as the ratio between excitation beam spot size and detector aperture. In addition, the absorbance and thermal conductivity of the sample influence the effect. The restricted heat flow results in a higher amount of thermal energy being stored at the edges, and therefore a stronger thermal lens signal. For one-dimensional and two-dimensional edges, a theory was developed regarding the restricted heat flow [212]. Subsequently, the influence of scattered light from diffuse reflection was discussed [213]. However, the theoretical considerations are only valid for a thermally isolated edge, and therefore cannot be applied to biofilm. In biofilm, thermal conduction occurs across the edge from biomaterial to the water, making the considerations more complex. Also, the absorbing volumes in the biofilm probably are not only restricted in two dimensions during absorbance, but rather the depth of the absorbance has to be considered as absorbance is in many cases linked to bacterial cells with approximate volumes of 1 μm^3. Theoretical considerations for this case are not developed, and are not the focus of this thesis. However, the influence of the edge on scanning is of interest, as this might compromise the lateral resolution. Measurements across edges were therefore taken during continuous scanning, and the results are shown in section 5.2.2.

4 Materials and methods

Before detailed information is given about the experimental procedures, some explanatory remarks are given at this point about the applied microfluidics for easier comprehensibility:

The microfluidics applied can be divided into top-on and side-on connected channels, where the former are connected with capillaries perpendicular to the channel through drilled entrance holes whereas the latter are connected with holes at the side to lead the capillary flow straight into the channel. Top-on connected channels are commonly applied in Kitamori-laboratory and therefore were applied before the channel setup was modified for the usage of side-on connected channels, as described below.

In addition, the channels can be divided into different channel styles, ranging from straight channels, so-called I-channels, to more complex structures like zigzag, Y-structures, X-structures, etc. In the experiments, I-channels as well as an S-channel, a channel with various curves, were applied.

4.1 Biofilm

4.1.1 Bacteria

Biofilm source for TLM observation experiments grown in flow cells, in the S-type microchannel and I-type channel with top-on connection, adhesion and removal experiments in the I-type channels with top-on connection and growth experiments on differently modified surfaces in I-type channels with side-on connection was provided by Ohgaki-Katayama-laboratory, The University of Tokyo. The samples were transferred from laboratory reactors to glass beakers with a glass pipette, covered for transportation and afterwards introduced into the experimental setup for pumping into the channels. The biofilms in the batch reactors were incubated with microbes from a wastewater treatment plant activated sludge, enabling growth of a mixed species biofilm which is similar to conditions in tap-water and wastewater pipes.

For adhesion and growth in the pressure-driven flow system, a homogeneous biofilm as reference was applied. *Sphingomonas paucimobilis*, a gram-negative bacteria that is observed in the environment as well as nosomical clinical infections, was chosen as source due to its relative low hazard and as a good biofilm builder [214, 215]. Sphingomonas paucimobilis source was cultured and provided by Ohgaki-Katayama-laboratory, The University of Tokyo. Briefly, *Sphingomonas paucimobili*s strain NCTC 11030 (ATCC, USA) was revived according to instruction and then cultured with nutrient Broth BD 234000 at 30 °C for a period between 24 and 48 hours. After aliquoting, glycerol was added and the bacteria were stored in the freezer prior to usage.

Biofilm experiments were conducted at room temperature. All biofilm samples and waste solutions as well as experimental material potentially in contact with biofilm, including unused nutrient and staining solution, were autoclaved after the experiment at 121 °C for 20 min with a high pressure steam sterilizer BS-305 (Tomy Seiko, Japan).

4.1.2 Nutrients

For mixed species biofilms as well as *Sphingomonas paucimobilis* biofilm, a nutrient solution with abundant supply of nutrients was supplied continuously. The solution contained D-glucose (510 mg/L, Dextrose, Anhydrous, Wako Pure Chemical Industries, Ltd., Japan), NH_4Cl (150 mg/L, Kanto Chemical Co., Inc., Japan), KH_2PO_4 (60 mg/L, Kanto Chemical Co., Inc., Japan), Na_2SO_4 (100 mg/L, Kanto Chemical Co., Inc. Japan) and Bacto^{TM} yeast extract (4 mg/L, Becten, Dickinson and Company, USA) and was prepared each time by weighing in the chemicals, adding deionized water (produced by Aquarius Advantec GSR 2000 water purifier) and leave the solution covered for diffusion mixing. During pumping, the container with the solution was covered with aluminium foil to avoid dust from entering when pumped with a peristaltic pump (for description see below). Chemicals were weighed in using AND HM-202 scales (Kabushiki Gaisho, Japan). For *Sphingomonas paucimobilis* biofilm culture, the medium was autoclaved prior to addition to the pumping system.

4.1.3 Staining

Biofilms in the flow cell were stained on the glass slide contained in the flow cell using Acridine Orange in deionized water (0.1 g/L) for 15 minutes. After that, the sample was rinsed with deionized water. Biofilms observed in the I-type channels with top-on connection were stained with a solution containing 2 µL 5.7 mM DAPI (4',6-diamidino-2-phenylindole) and 2 µL 39µM FITC-ConA (Concanavalin A tagged with fluorescein isothiocyanate) in 1 mL PBS-buffer online for 20 minutes with flow applied. In this time, about 1 mL solution was pumped through the channel. *Sphingomonas paucimobilis* was stained with a solution of 1 µL DAPI in 1 mL PBS-buffer.

4.2 Biofilm growth in flow cells

The flow cell system consisted of two copper flow cells produced by the workshop of the Institute of Hydrochemistry, Technical University Munich. They can be seen in Figure 8, and a design drawing is shown in the appendix. A glass slide was placed between the bottom and top holder of the cell and closed with screws with a rubber O-ring included in the bottom holder.

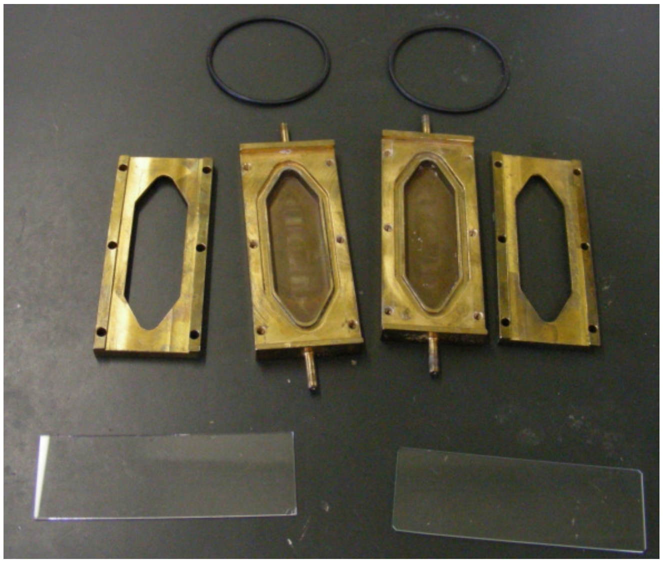

Figure 8 Two unassembled copper flow cells with rubber O-rings which can be inserted into the bottom part (middle); two glass slides (7 x 3 x 0.1 cm, shown at the bottom) can be inserted into the flow cells for biofilm growth

At each side of the flow cell, Tygon® tubes (inner, outer diameter 1.59 mm) were attached to connectors on the flow cells. The nutrients were pumped using a two-channel peristaltic pump (ISO 313T, AS ONE, Japan) in a circular flow from a flask with the nutrient solution.

Biofilm was taken from a storage tube spiked with biofilm taken from a wastewater treatment plant and pumped into the system. After initial adhesion over night, biofilm was grown on a glass objective slide in a flow cell at a flow velocity of 0.23 g/s for 9 days in a circulating flow. Nutrients were provided in excess at the first day of pumping with a mixture of D-glucose (493 mg/L), NH_4Cl (146.1 mg/L), KH_2PO_4 (67.1 mg/L), Na_2SO_4 (102.6 mg/L) and yeast extract (6.5 mg/L) dissolved in tap water.

After the end of the pumping procedure, the overgrown glass slide was taken out of the flow cell and washed with deionized water to remove unadhered cells. Silicon grease was applied to both edges of the glass slide, the biofilm in the central part of the slide was carefully covered with water to avoid destruction of the biofilm matrix, and, then, a cover slide was put on top of the grease. In this way the biofilm structure was not affected by the cover slide and evaporation during measurement was prevented.

The sample was measured with fluorescence microscopy and TLM. A fluorescence microscope IX71 (Olympus) equipped with a mercury lamp, several optical filters and an Imaging Retiga Exi Camera (Imaging) was used for observation of stained biofilm. For better comparability, the measurement conditions for TLM measurement are given in section 4.4.4.

4.3 Biofilm growth in microchannels

Compared to batch reactors or flow cells, reagent consumption inside the microchannel is significantly reduced. In Figure 9, the measures and the resulting reduction in volume of nutrient supply is compared. While a wastewater treatment plant like the Shibaura Water Reclamation Center, which is responsible for water treatment of some wards in Tokyo, is capable of flows of ~ 1 million cubic meters per day, a batch reactor can be pumped with a few liters a day for sustained biofilm growth. In contrast, a microchannel uses up volumes normally not exceeding one liter per day, depending on measurements and volume flow rates.

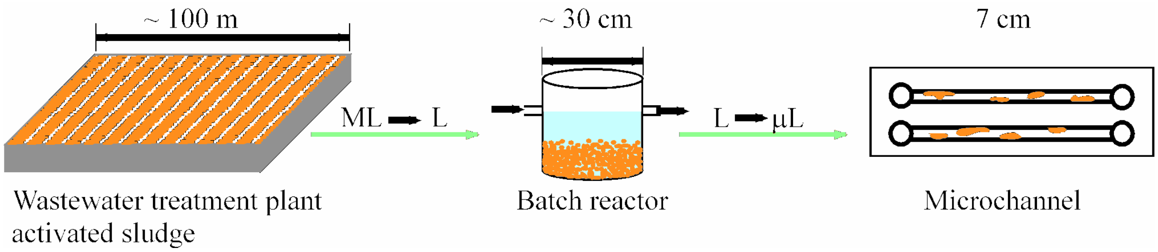

Figure 9 Comparison of dimensions and volumes of a wastewater treatment plant, a batch reactor and a microchip

4.3.1 Microchannel production

For the biofilm experiments in microchannels, different microchannel designs were applied.

For attachment and staining experiments, a commercially available top-on connected Pyrex® glass chip containing two separated, parallel straight microchannels with top-on connection, a width of 200 µm and a depth of 40 µm, produced by wet-etching (Institute of Microchemical Technology Co., Ltd., Japan), was used.

As another top-on connected channel, a Pyrex® glass chip containing an S-type channel (semicircular cross-section, width 200 µm, depth ~100 µm) produced by wet-etching, with two entrance holes and an exit hole on top, (Institute of Microchemical Technology Co., Ltd., Japan) was applied.

For biofilm growth in side-on connected channels, a custom-made Pyrex® glass chip with four 500-µm square channels (Institute of Microchemical Technology Co., Ltd., Japan) was fabricated. Briefly, four channels were cut out with a micro flat end mill inside a Pyrex® glass plate (3x7 cm) with 0.5 mm thickness. No channel were milled at the ends of the chip to provide stability during the production. A top and a bottom plate were laminated and thermally bonded to the glass plate containing the channels. Both ends of the chip were cut off and the chip was divided into two chips.

For biofilm growth in a pressure-pumped system, the side-on connected channel was modified. The channel size was minimized to 400 µm width and depth. After the cutting of the chip, entrance and exit holes were drilled into the channel openings with a length of 2 mm and a diameter of 700 µm. The reason for the change in setup will be described in the following section.

4.3.2 Microchannel setup

The setup for the top-on connected I-channel chip is seen in Figure 10. The top-on connected I-channel chip was placed into an aluminium chip holder containing screwable holes in the upper part. Teflon® screw connectors serve as connectors between capillary and chip. They contain holes in the middle that center a PEEK (polyetheretherketone) capillary into the microchannel openings. The capillary was glued to the connector using an acrylic resin (Araldite® 2021). Leakages between chip and chip holder are prevented by applying a rubber O-ring. The other end of the capillary was connected to a Tygon® tube (inner diameter 0.020 inch, outer diameter 0.092 inch, Cole Palmer) using the same glue. A peristaltic pump (Masterflex 77120-32, Cole Parmer Instrument Co.) was applied to pump the biofilm source microbes into the microchannel and supply nutrient solution afterwards.

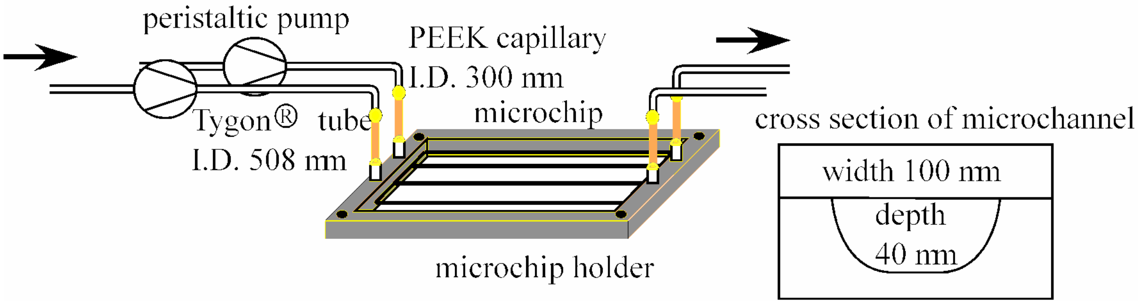

Figure 10 Experimental setup for biofilm adherence and staining experiments in microchannels with top-on connection and microchannel cross section (not to scale; flow in direction of arrows)

The schematic of the chip in the holder is shown in Figure 11. In the case of the S-type channel, the chip was placed into an aluminium holder containing holes in the top for connection to the channel. A rubber O-ring and Teflon® screw connectors with a through-hole were placed into the holes at one microchannel entrance and the exit. The second entrance was blocked with a rubber O-ring and a Teflon® screw without through-hole. A PEEK (polyetheretherketone) capillary (inner diameter 300 µm, outer diameter 500 µm) was placed into the through-hole and glued to the connector as described before. The other ends of the capillaries were glued to Tygon® tubes (inner diameter 508 µm, Cole Parmer, Instrument Co.). Pumping was conducted in the same way as in the top-on connected I-channel chip.

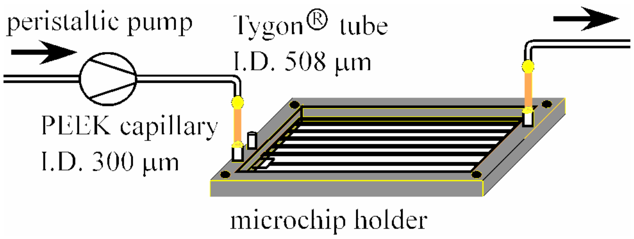

Figure 11 Schematic of S-type channel in aluminium holder

As the PEEK capillaries were amenable to breaking during connection and the PEEK tubing was too rigid, they were exchanged for follow-up experiments to Teflon® capillaries with an inner diameter of 500 µm. A picture of the broken PEEK capillary tip in one entrance hole is seen in Figure 12

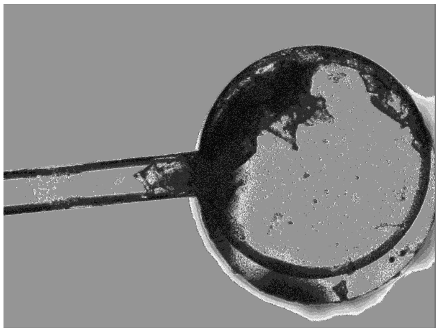

Figure 12 Entrance hole of one top-on connected I-channel where splinters from the PEEK® capillary are seen at the edges and the entrance to the microchannel

Photographs of the top-on connected I-channel chip in the holder with Teflon® capillaries are presented in Figure 13.

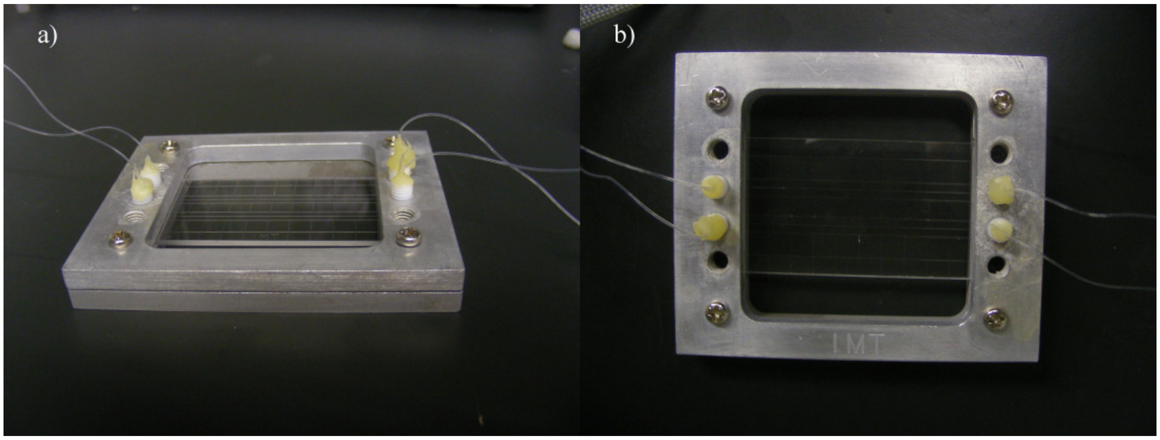

Figure 13 Pictures of the top-on connected I-channels in the aluminium holder with Teflon® capillaries inside the connectors attached

The next problem observed with the top-on connected I-channels is clogging in the connection curves after prolonged culture. And yet another problem with the top-on connected channel became clear during observation. A schematic of the problem is presented in Figure 14.

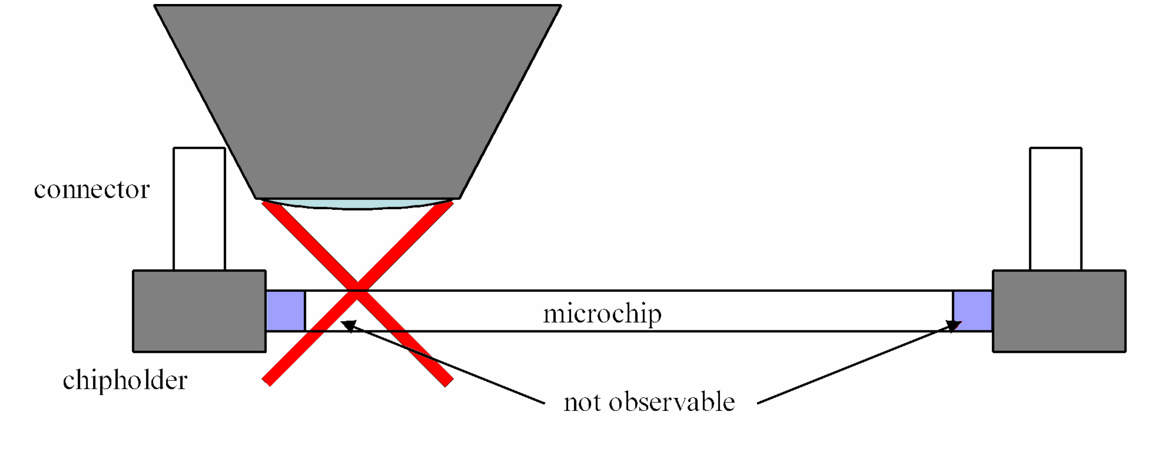

Figure 14 Problem observed during observation of the top-on connected chips, where a small area near the holder is not observable due to the hindrance of the objective lens movement near the connectors

During observation, the connectors of the capillaries limited the observable space due to the clash of the connectors with the objective lens. While this problem could be overcome by cutting the connectors to shorter lengths, the clogging ultimately made it necessary to change the setup to side-on connected channels.

In the side-on connected channels, PTFE (polytetrafluorethylene) capillaries with an inner diameter of 0.3 mm and an outer diameter of 0.5 mm were inserted on both sides and fixed using acrylic adhesive (Araldite® 2021). Capillaries were connected to Tygon® tubes as in experiment 1. A picture of the chip is shown in Figure 15.

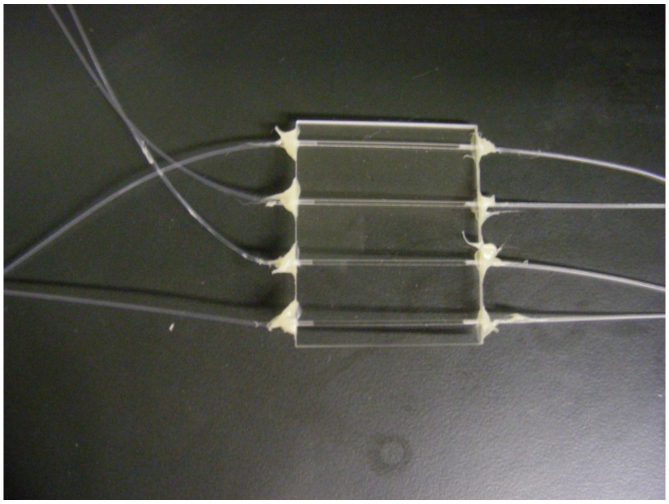

Figure 15 Chip with square microchannels (width, depth 500 µm) with capillaries (PTFE, inner diameter 300 µm) connected on both sides; chip size 30 x 30 mm

A further improvement of the chip was finally accomplished by adding round entrance and exit holes for the capillary to the channel on both sides. Also, the channel size was modified to a width and depth of 400 µm. A schematic of this changed setup is shown in Figure 16. This way, pressure and flow fluctuations in the area near the capillary entrance were minimized as well as the dead volume near the capillary entrance and exit. Furthermore, this way the length of introduction of the capillary inside the channel is standardized, and the probability of leakage along the capillary minimized.

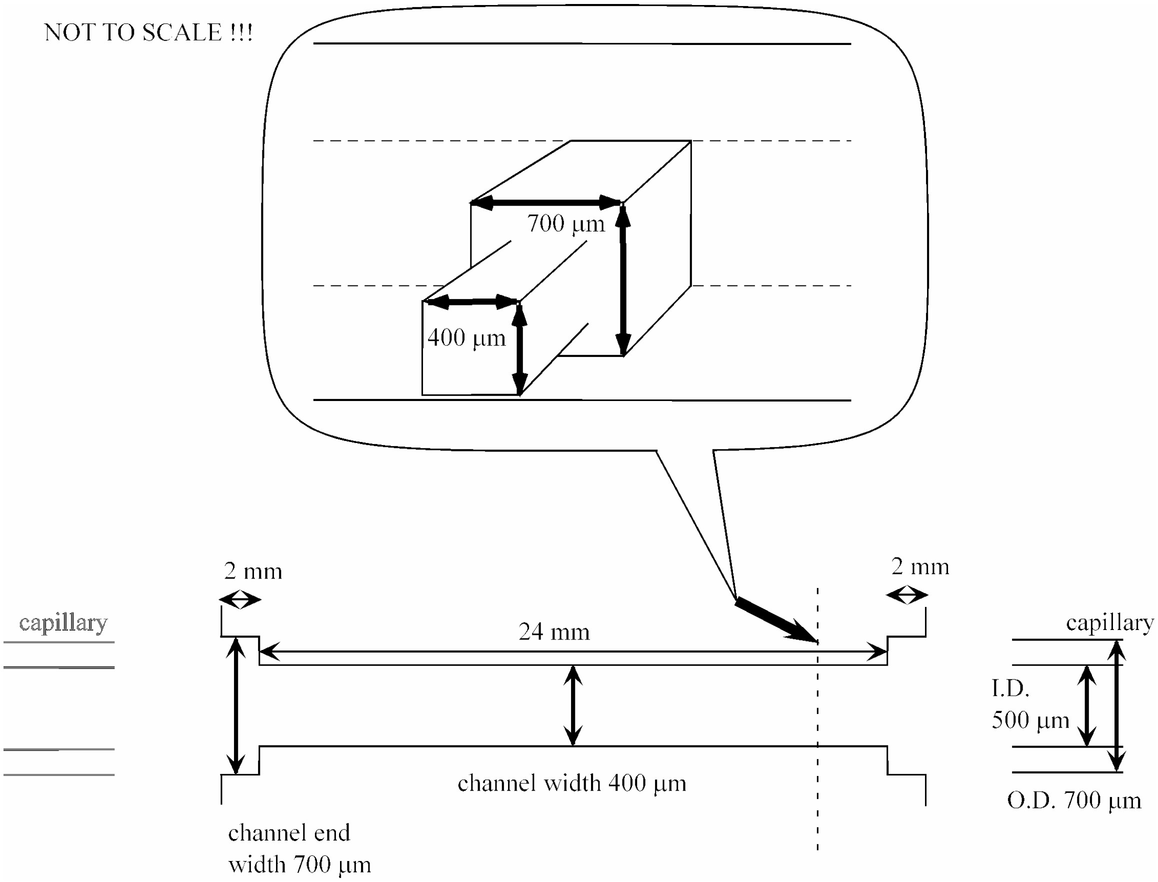
NOT TO SCALE !!!
700 µm
400 µm
2 mm
2 mm
capillary
24 mm
capillary
I.D.
500 µm
channel width 400 µm
O.D. 700 µm
channel end
width 700 µm

Figure 16 Schematic of the entrance and exit holes in the side-on connected channel for capillary connection inside the channel with reduced dead volume

4.3.3 Continuous flow system

Two flow systems relying on different pumping principles were developed for providing continuous flow inside the microchannels. The first system was pumped by a peristaltic pump and will be described as follows, whereas a later system was pumped by pressurized air and will be described afterwards.

A schematic of the general setup for peristaltic pump setup is shown in Figure 17. Biofilm source and nutrients were pumped continuously from a source bottle into the chip and then out into a waste bottle. Adsorption and growth studies in channels with flow provided by peristaltic pump were pumped by a Masterflex C/L peristaltic pump (Cole Palmer) using Tygon® tubes (inner diameter 0.020 inch, outer diameter 0.092 inch, Cole Palmer).

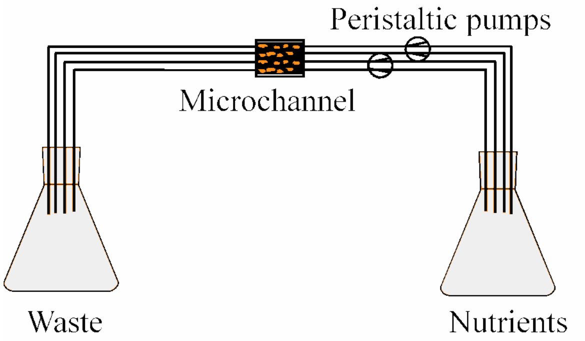

Figure 17 Schematic of the continuous flow-through setup containing the microchannel

Microbial samples were taken from a batch reactor, incubated with microbes from wastewater treatment plant activated sludge (provided by Ohgaki-Katayama-laboratory, Department of Urban Engineering, The University of Tokyo). For the top-on connected chips and the side-on connected I-channel, the microbe source was pumped into the parallel microchannels simultaneously and left standing overnight for initial attachment. Afterwards, the nutrient solution was pumped through the channels continuously to a waste bottle. For size comparison, the actual system with the side-on connected chip is shown in Figure 18.

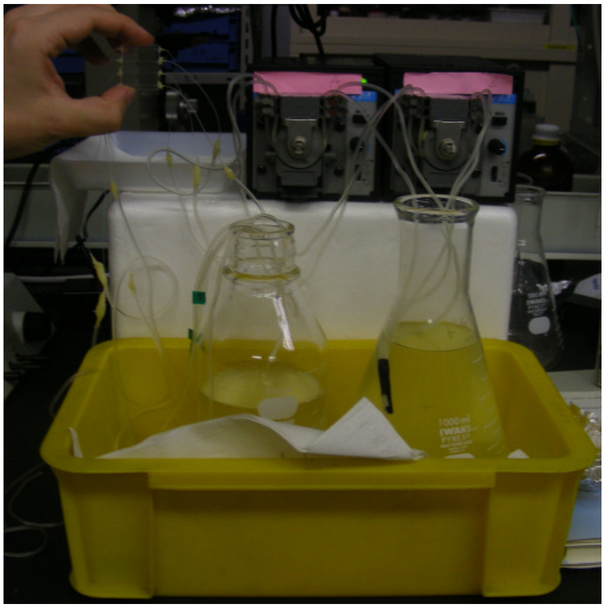

Figure 18 Flow-through system for continuous biofilm culture with the side-on connected channel: the nutrients are pumped from the flask on the left to the bottle on the right

During the experiments, the pulsation of the peristaltic pumped was observed in the microchannel, which might influence the growth of the biofilm. Also, the Tygon® tubes were prone to leakage and softening within the clamps of the pump and required repeated readjustment for providing a constant flow. Furthermore, increase of flow with the peristaltic pump in the microchannel was limited due to backpressure coming from the microchannel. An increase in flow rate for biofilm removal experiments is impossible with the peristaltic pump setup after some limit, as a further increase in pumping speed resulted only in a higher back pressure and a higher pulsating frequency at the pump, but the flow inside the chip was not increased.

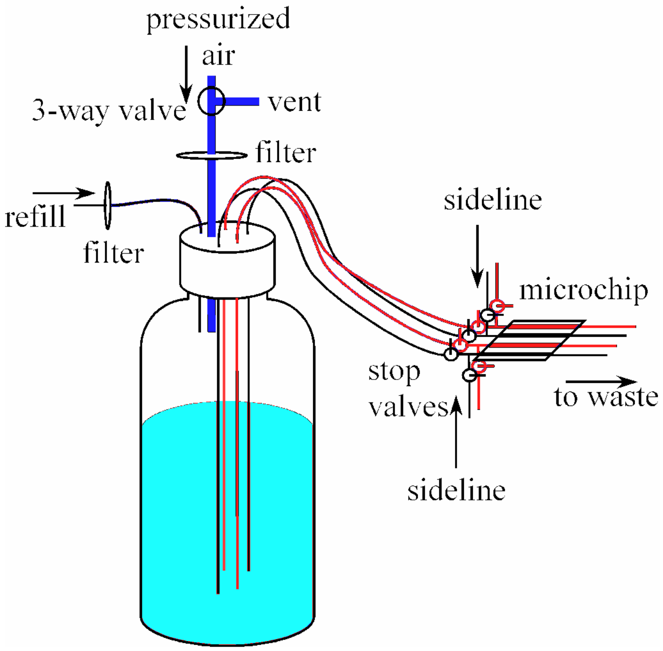

Figure 19 Schematic of the pressure-driven flow system; for detailed description see text

In order to overcome those problems and provide a constant, controlled flow in the microchannel, a pressure driven setup was conceived. The setup is illustrated in Figure 19. An autoclavable glass bottle is used as nutrient solution reservoir. The cap of the bottle was drilled to provide entrance and exit holes for several tubes, including one for gas supply, one for refill and four for liquid introduction into the microchannel. After fitting the tubes, the cap and tubes were sealed using acrylic resin (Araldite 2021). The tube for gas supply (Tygon®, inner diameter 1/8 inch, outer diameter ¼ inch, Saint-

Gobain Performance plastics) was fitted with a Millex GV 0.22-µm filter to avoid contamination. A silicon tube (inner diameter 5 mm, outer diameter 8 mm) was put on the other end of the filter and connected to a three-way-valve (polypropylene, inner diameter 5 mm, Bellewood). This valve was introduced in order to relieve pressure from the bottle if needed. After the valve, the gas supply was connected to a pressure calibrator PC34 (Nagano Keiki Co., Ltd.) with a Tygon® tube (inner diameter ¼ inch, outer diameter 5/16 inch, Saint-Gobain Performance plastics) and a 6x4 Polyurethane tube (TU0604, SMC).

For the refill tube and the tubes for liquid introduction to the microchannel, Tygon® tubes with an inner diameter of 1/32 inch and an outer diameter of 3/32 inch (Saint-Gobain Performance plastics) were applied. On the outside of the bottle, the refill tube was equipped with a DISMIC® 25 CS 0.20-µm cellulose acetate filter (Advantec) which was coupled to a Terfusion (テルフュージョン®) three-way R-type valve (Terumo). This in turn can be furthermore coupled to a 30-mL lock-type adapter syringe (テルモシリンジ®, Terumo) for refilling the bottle. The tubes for liquid introduction into the microchannel were glued to Teflon® capillaries (inner diameter 500 µm, outer diameter 700 µm) for connection to the channel system, which consisted of shut-off valves and a side stream for liquid introduction prior to the microchip. The channel system is shown in Figure 20.

Each capillary is introduced into a PEEK shut-off valve (P732, outer diameter 1/16 inch, thru-hole 0.020 inch, Upchurch Scientific, USA) with a PEEK tubing sleeve (1533, 0.75 mm, Upchurch Scientific, USA). The PEEK tubing sleeve is glued to the capillary with acrylic resin to avoid leakage and to keep the capillary fixed. The shut-off valve is installed to close the channel during refill, which is accompanied by a pressure increase in the system. This pressure increase would affect the microchannel otherwise. Also, the stop valve can be closed if liquid is pumped from the side stream, which is introduced into the main stream after the valve with a Tee (P727, 10-32 thread, thru-hole 0.020 inch, Upchurch Scientific, USA).

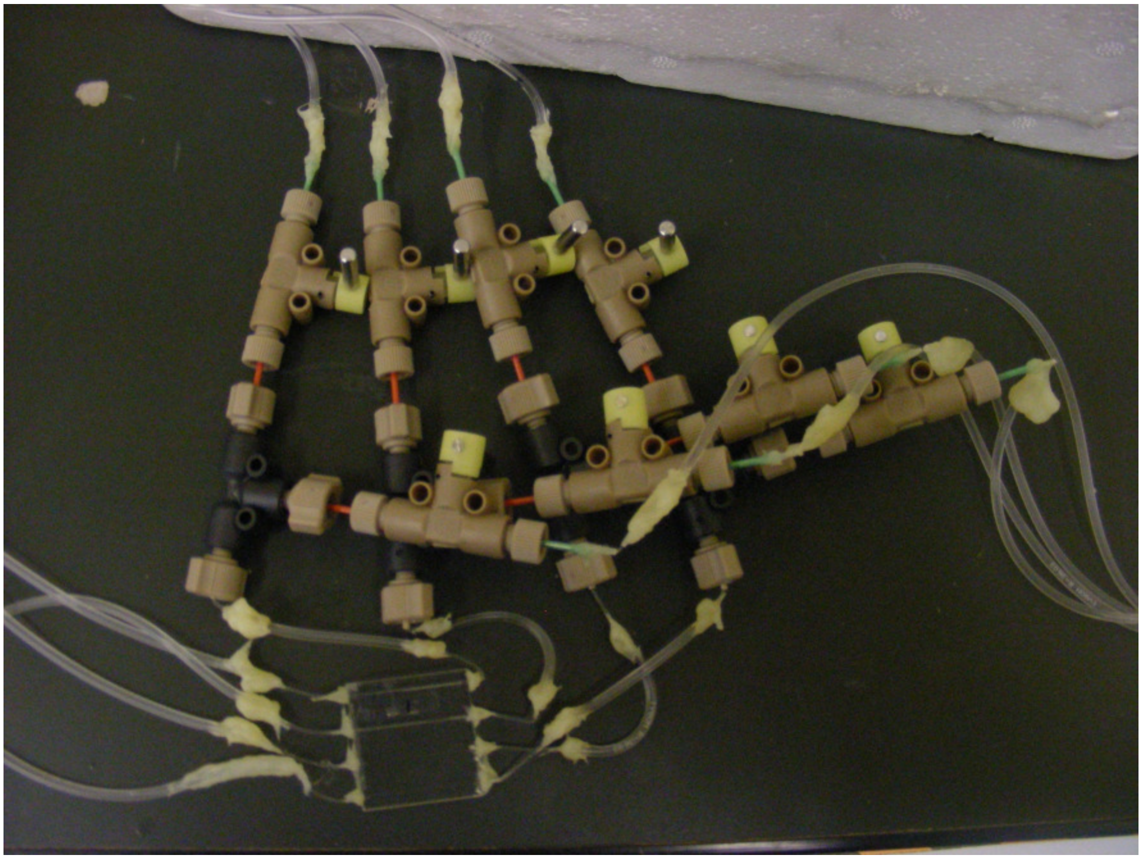

Figure 20 Channel system with stop valves and side channel before the microchannel; the main flow from the nutrient bottle is coming from the top and flowing to the exit on the left; side channels are refilled from the right

The connection between valve and tee is done with a PEEK tubing (1532, 0.50 mm, Upchurch Scientific, USA). The side stream is introduced into the tee the same way as the main stream, starting with a Tygon® tube, followed by the capillary inside the tubing sleeve, the shut-off valve and the 0.50 mm tubing. This way the side stream can be closed during the pressure-driven pumping in the main channel and opened for introducing reagents with the main stream closed. After the tee, the stream is introduced into the microchannel with a combination of Teflon® capillary, Tygon® tube and again Teflon® capillary to provide some space between the tee and the chip for easier observation on the microscope. Each connection between capillary and Tygon® tube as well as the connection to the chip is glued using acrylic resin. After the channels, a capillary and subsequently a Tygon® tube are glued to the system for removal of waste liquid from the channel to a waste bottle. The whole system is shown in Figure 21.

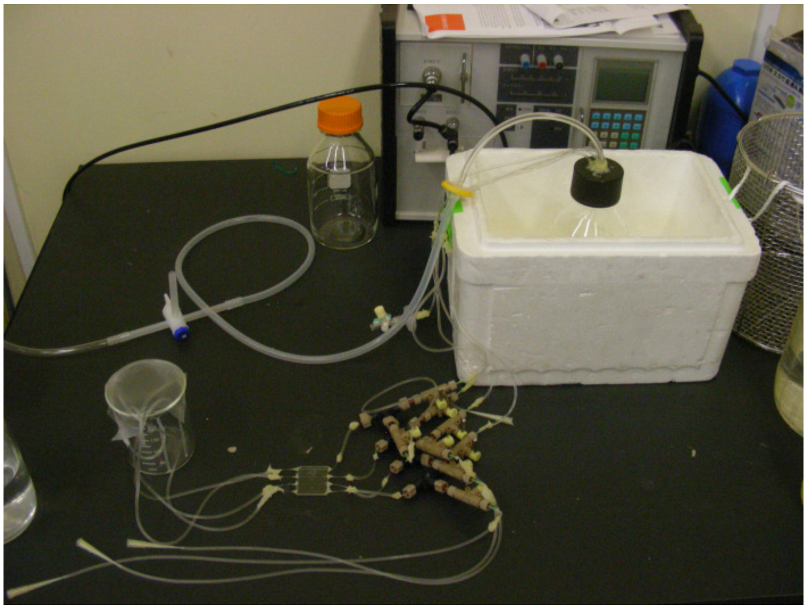

Figure 21 Photograph of the pressure-driven flow system; for detailed description see text

Prior to *Sphingomonas* biofilm experiments in the system, the glass bottle was autoclaved with a normal cap. As the acrylic resin was not resistant to autoclave procedures, the assembled flow system was cleaned in a clean bench. For this purpose, the whole system (excluding the tubes with filters) was flushed with 0.1 M NaOH. Also the inside of the cap was cleaned. After washing with autoclaved deionized water, the whole system was treated with 70 % ethanol and washed again with deionized water. The system was then left in the clean bench under UV illumination. System assembly as well as filling of the glass bottle with autoclaved nutrient solution was carried out in the clean bench after spraying the system parts with 70 % ethanol. Biofilm introduction also was carried out in the clean bench. To avoid contamination during transport of the system from the clean bench to the pressure controller that was positioned in the laboratory under non-sterile conditions, the tube ends were closed with stoppers. The stoppers were also left during operation on non-flowing lines and only removed after cleaning with 70 % ethanol for operation.

Flow rates inside each setup were measured prior to biofilm experiments for flow rate calibration using gravimetry. Deionized water was flown through the capillary and channels, respectively, at different flow speeds for the applied peristaltic pump and different pressures from the pressure controller. After exiting the setup, the water was collected in pre-weighed Eppendorf® caps for time intervals between thirty seconds and two minutes, depending on flow rate, and reweighed. Measurements were conducted in triplicate unless stated otherwise (see section 5.1). Gravimetric measurements were conducted with AB 265-S/Fact (Classic Plus) scales (Mettler Toledo).

Observation of biofilm adsorption and removal in the top-on connected channel, growth and removal in the side-on connected channel and adhesion and growth in the modified side-on connected channel were observed with an Olympus SZX12 zoom microscope equipped with a Sony 3CCD Exwave HAD CCD-camera powered by a Sony Model DXC-C33 power source. Videos of the channels were captured using the software ULead video studio 8SE (ULead Systems, Inc). A fluorescence microscope IX71 (Olympus) equipped with a mercury lamp, several optical filters and an Imaging Retiga Exi Camera (Imaging) was used for observation of stained adhered bacteria inside the channel. Biofilm in the S-type channel was observed with the fluorescence microscope in phase contrast mode and with TLM, as described in section 4.4.4.

4.3.4 Biofilm adsorption and growth studies

Biofilm experiments in the different setups were run for differing time periods and under different conditions, as given by the setup.

In the case of the top-on connected chip for adhesion studies, pumping was continued for 5 days at a flow speed of 0.1 m/s (shear stress at the channel wall, $\tau = 12.8$ N/m^2). The shear stress hereby is calculated according to equation 3-2.
In the top-on connected S-channel, biofilm was grown for 3 weeks at a flow velocity of 0.001 m/s.

In the side-on connected chip applied during growth studies on different surfaces, pumping was carried out for a period exceeding one month at a flow speed of 0.0013 m/s (shear stress at the wall, $\tau = \sim 0.015$ N/m^2).

In the pressure-driven setup, adhesion studies were carried out for 8 h at a pressure of 0.5 kPa (shear stress at the wall, τ = ~0.12 N/m^2). Only two channels were observed in the experiments due to a failed experiment in the remaining two channels. Growth studies of *Sphingomonas paucimobilis* were conducted for a period of 3 days at a pressure of 0.3 kPa (shear stress at the wall, τ = ~0.09 N/m^2). In the pressure-driven flow system, an initial increase in pressure up to 2.5 kPa was needed for a few channels to remove gas bubbles and fill the channel with liquid. However, gas bubbles only presented a minor problem and were not observed in all channels.

In the top-on connected channel and the pressure driven flow-system, adhesion and growth studies were conducted on the bare chip material. The surfaces of the four channels in the side-on connected chip were modified online, applying the peristaltic pump. A bare glass surface was prepared in one channel by firstly pumping 0.1 M sodium hydroxide solution for 20 minutes, and then deionized water for five minutes. The second surface was modified with MPC-copolymer (Poly[2-methacryloyloxyethyl phosphorylcholine(MPC)-co-methyl-carboxylic acid] (Mw= 100K, MPC: 90 mol%, methacrylic acid: 10%)) (provided by Ishihara-laboratory, Department of Material Engineering, The University of Tokyo) [216-218]. The channel was washed like the bare one, then washed with ethanol, filled with a five percent solution of APTS (3-aminopropyltriethoxysilane) in ethanol and left standing for two hours. After two further washing steps with ethanol and deionized water, a solution of 2.5% MPC-copolymer in 0.1M MOPS (3-Morpholinopropanesulfonic acid) buffer (pH 5.0) with 15 mM (1-[3[(dimethylamino)propyl]-3-ethylcarbodiimide) (EDC) hydrochloride for coupling was pumped in and left overnight. The treatment was completed with a final washing with deionized water. The third surface was modified with APTS according to the procedure for MPC polymer modification, which was terminated after the second washing with deionized water [219]. The fourth channel was washed with deionized water, washed with toluene, modified with ODS (octadecyltrichlorosilane) in toluene (1%) for 20 min, washed with toluene, washed with ethanol and finally washed with deionized water to produce a hydrophobic surface [74]. The chemical structures of the four modified surfaces are shown in Figure 22.

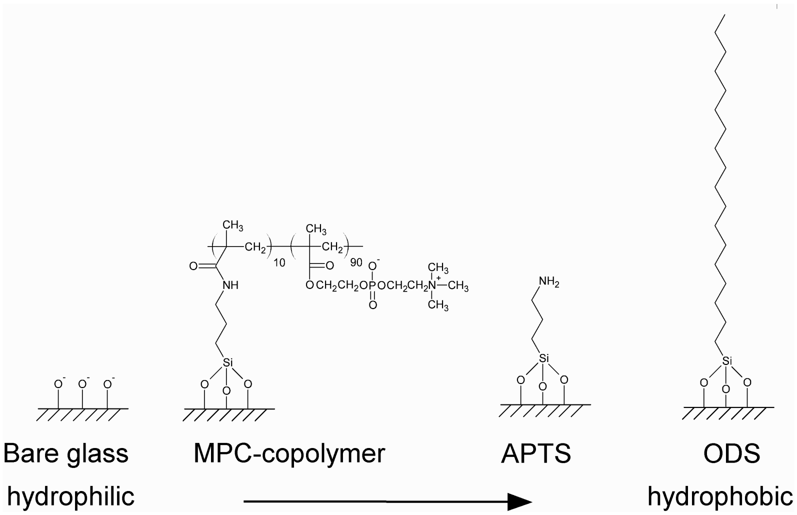

Figure 22 Surface composition of the four side-on connected microchannels after surface treatment with tendency in surface wettability written below

As a reference for contact angle measurements, glass slides were modified with the same chemicals and the same time intervals, without applying flow. Static contact angle measurements were conducted according to the sessile drop method with a Contact Angle Meter (DropMaster500, Kyowa Interface Science, Saitama, Japan) with automated picture acquisition and processing software (Famas, Kyowa Interface Science, Saitama, Japan). A drop of deionized water was put on each sample surface, and the static contact angle was measured at room temperature. Measurements were conducted in triplicate.

During the adhesion and growth experiments, the microchips were mounted on an inverted optical microscope for bright field observation and monitoring.

After the adsorption measurement in the top-on connected I-channel, biofilm was stained as described before. Staining was also conducted in the pressure-driven flow system after adhesion experiments of 8 h from the side channel with a peristaltic pump (Masterflex C/L) as described above. Bright-field and epifluorescence images were taken of the stained biofilm. A fluorescence microscope IX71 (Olympus) equipped with a mercury lamp, several optical filters and an Imaging Retiga Exi Camera (Imaging) was used for observation.

In the side-on connected chip, biofilm growth and removal were observed on the bottom of the channels with a microscope equipped with a CCD camera. Movies of each channel were recorded. The movies were cut into single non-overlapping pictures. Afterwards, the area surrounding the channel was cut from the pictures. The remaining pictures were then further reduced into equally big areas for each channel. Twenty pictures of each channel, excluding the entrance and exit areas near the capillaries, were further processed for statistical analysis using the software ImageJ. For this purpose, the images were converted to 8-bit format. Thresholding was applied to distinguish the bacterially overgrown surface from the channel. Manual thresholding was necessary for every observation day due to changing light conditions of the microscope, as it was used for other experiments in the laboratory. Surface coverage was determined as ratio of biofilm covered area to total area. Average values and standard deviations were calculated for each day and each channel.

4.3.5 Biofilm removal and microchip cleaning

In the top-on connected I-type channels, biofilm removal was first attempted applying a solution of hydrogen peroxide (1000 ppm), produced from deionized water and a 30% hydrogen peroxide solution (Wako, Japan). Subsequently, remaining biofilm was removed with a sodium hydroxide solution of pH ~ 12 which was produced by dissolving sodium hydroxide tablets (min 97%, Kanto Chemical Co., Inc., Japan) in deionized water. The removal chemicals were applied online by exchanging the tubes from the nutrient solution supply to the removal chemicals. During the exchange, a small air-bubble entered the system which did not affect the adhered biofilm.

In the side-on connected, surface modified I-type channels, removal was carried out using two pressure plugs. For this purpose, the channels were pumped with air overnight, and pumping with the nutrient solution was continued on the following day. This way, the newly pumped in nutrient solution applied a change in shear across the channel.

In the pressure driven flow-system, biofilm cleaning was attempted in various ways by pumping from the side line with a peristaltic pump (Masterflex C/L). One channel was pumped from the side line with hydrogen peroxide (1000 ppm) at pH 4.5 (addition of hydrochloric acid) and a flow rate of 0.002 m/s. The other channel was pumped with a solution of One Drop® (provided as gift at WaterMicro2008) with one drop inside 250 mL of water, which was older than 2 years though, at the same flow rate. After that, the channel was pumped with a solution of ~0.1 M NaOH in deionized water. As all methods proved to be unsuccessful, both channels were refilled with deionized water and left over the weekend. After the weekend, a large amount of biofilm was successfully removed with a combination of 1 M NaOH solution and air bubbles.

4.4 Adaptation of thermal lens microscopy for biofilm observation

A schematic of the basic thermal lens setup is shown in Figure 23.

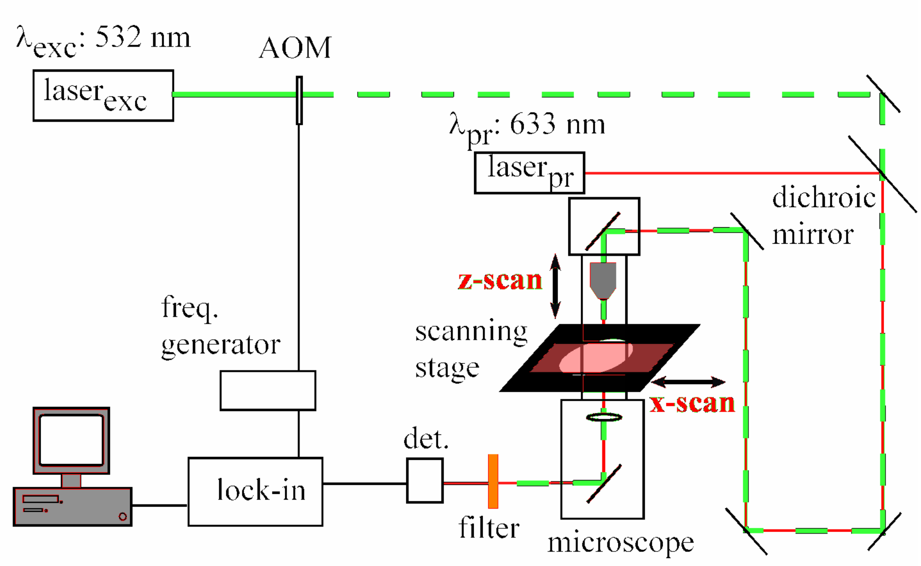

λ_{exc}: 532 nm
AOM
laser$_{exc}$
λ_{pr}: 633 nm
laser$_{pr}$
dichroic mirror
z-scan
freq. generator
scanning stage
x-scan
det.
lock-in
filter
microscope

Figure 23 Basic thermal lens microscope setup

All TLM measurements were carried out with a modulated, frequency-doubled Nd:YAG laser (Verdi TM, Coherent) at 532 nm as excitation source and a continuous He-Ne laser (Melles Griot) at 632.8 nm as probe beam. The excitation beam was modulated using an acousto-optic modulator (AOM, ISOMET Acousto-Optic Modulation Driver 232-A-1-70) triggered by a function generator (NF Wave Factory WF 1945 A 1) at a modulation frequency of 1003 Hz (rectangular pattern) unless stated otherwise. The beams were adjusted with beam expanders (Melles Griot 5x) for generation of parallel beam sources. They were coaxially aligned with a dichroic mirror and entered into a microscope (BX51, Olympus) by two prisms. For three-dimensional data acquisition, a manually controlled horizontal scanning stage controlled by a stage controller (Joystick, Sigma Koki) and the z-adjustment of the microscope were applied.

Adjustment of the beams for collinear alignment perpendicular was carried out in relation to the table at a fixed height and was found to be essential for three-dimensional observation. Alignment of the excitation beam was conducted first. For this purpose, the beam was centered into microscope optic field adjusting the prisms near the microscope. The perpendicular state of the beam was observed by observing the focus spots on the front and back of a glass objective slide, which was put on the stage, using *z*-scanning. After the alignment of the excitation beam, the probe beam was aligned collinear to the excitation beam with an optical mirror in the probe beam path and the dichroic mirror. The probe beam also was checked for perpendicularity. After alignment, the two beams were centered onto a further prism at the bottom of the microscope using an adjustable objective lens applied externally. The beams were led through two optical filters to filter the excitation beam and centered on a photodetector (EOT Silicon PIN detector ET-2030, Electro Optics).

After alignment, the probe beam focus point was adjusted for mode-mismatched TLM recording using a beam expander to lie below the focus of the excitation laser approximately one confocal length apart. Subsequently, a reference sample of either sunset yellow (10^{-4} M in deionized water) in a micrometer sized quartz cell or a thin sample of sputtered gold were put on the sample stage and the stage was moved in vertical direction until the excitation focus spot was in / on the sample. At this point, the modulated probe beam signal was detected with the photodetector and recorded with a multifunction digital lock-in amplifier (LI5640, NF Electronic Instruments). Maximum signal intensity was obtained by optimization of the foci difference of excitation and probe beam inside the sample using the beam expander in the probe beam path and by adjusting the detector position. All equipment is plugged to a low-noise power source to minimize influence of electrical noise on the thermal lens signal.

Thermal lens signal intensity and thermal lens signal phase were recorded simultaneously with home-built Labview software. TLM signal intensity is directly proportional to the absorption of the excitation laser, whereas TLM signal phase is related to the thermal characteristics of the sample material [193]. Data were stored for further evaluation.

4.4.1 Laser spot characterization

For imaging of samples with TLM, first the system has to be characterized. The results of this characterization are presented within this chapter, as they are essential for the further experiments.

As the thermal lens signal intensity is directly proportional to the applied excitation laser power, laser power measurements of the excitation laser were taken in the optical system prior to entering the microscope with different settings of the laser output. The relation of output setting and measured laser power is shown in Figure 24

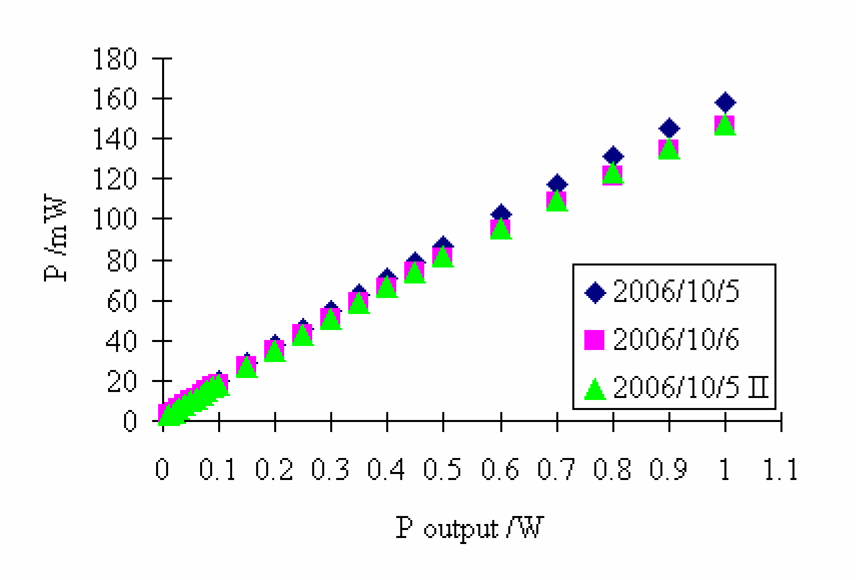

Figure 24 Laser power measurements of the excitation laser for different output settings before entering the microscope

Laser power was mostly linear over the observed power range and differences in recorded power were only observed for higher output settings. However, TLM measurements were conducted with output powers not exceeding 0.2 W output power. In this range, laser power was assumed constant and linear. Also, a significant power loss of the excitation laser was not observed in this range, as seen in repeated measurements on one day.

Next, the resolution of the instrument is of interest, which depends on the spot size of the excitation laser. The spot size is thereby determined by the diameter of the laser spot assuming circularity of the laser spot. While measuring the spot size, also the probe laser spot size was determined for comparison. For verification of the laser spot sizes of the excitation and probe laser at a given numeric aperture of the objective lens, laser power measurements through pinholes were conducted with a powermeter (Field mate, Coherent). Pinholes were produced by plasma-etching (Ulvac NE-500) on a sputtered chrome layer after patterning with electron beam lithography (ELONIX Electron Beam Lithography System ELS-7500M), with sizes from 0.6 to 10 µm on one glass slide. Pinhole sizes were verified using AFM (SPA-400, SII Nanotechnology Inc., Japan). A representative measurement of one pinhole is shown in Figure 25.

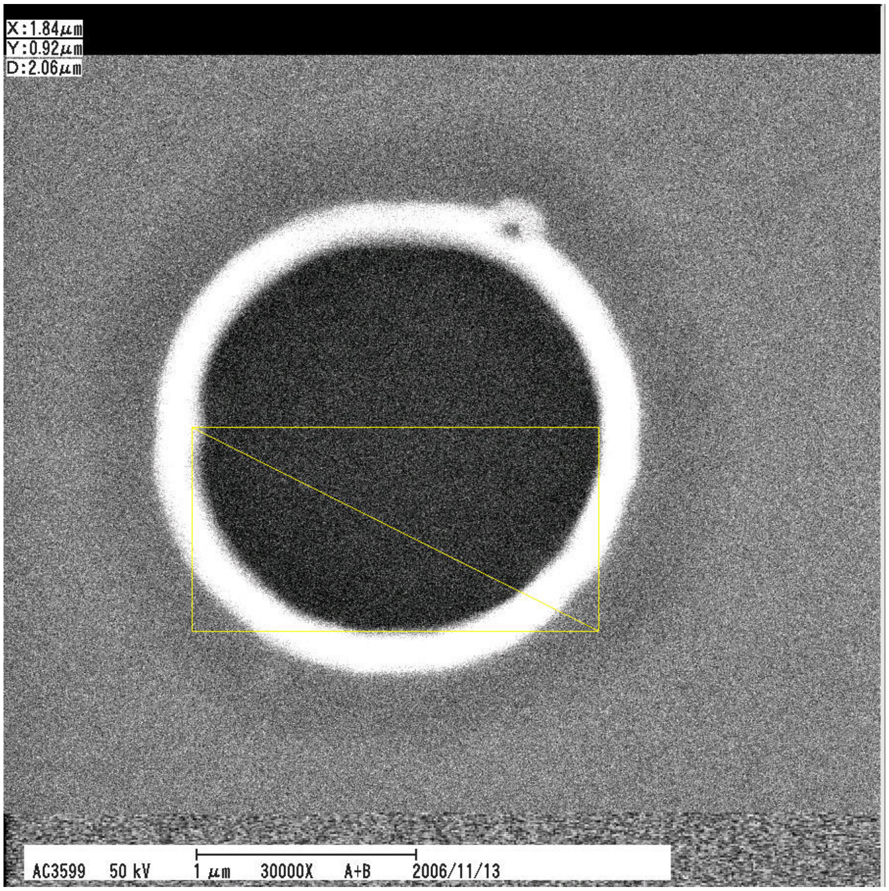

Figure 25 AFM image of a pinhole produced by plasma-etching onto a chromium sputtered glass-slide with a diameter of approximately 2 µm (scalebar at bottom 1 µm)

The pinhole slide was placed on the stage of the TLM instrument and each laser was measured separately. The measurement was conducted by maximizing the readout power on the powermeter using the scanning stage for optimization of the pinhole position. Measurements were conducted with an UPlanFLN 20x objective lens (Olympus) with a N.A. of 0.5. Measurements were conducted at varying output powers of the excitation laser and the set output power of the probe laser. The power readout of the measurement was transferred into spot diameters by the following formula:

$$\omega(z) = \sqrt{\frac{-2(d_{pin}/2)^2}{\ln(1-\frac{P_{pin}}{P_{w/o}})}} \qquad 4\text{-}1$$

In the equation, d_{pin} is the diameter of the pinhole as measured with AFM, P_{pin} the power measured through the pinhole and $P_{w/o}$ the power measured without pinhole. The theoretical spot size for the two lasers can be calculated using equation 3-14. For the excitation laser, a spot size of 1.298 µm is calculated, and the resulting size for the probe laser is 1.545 µm. The results for the laser spot measurements are shown in Figure 26.

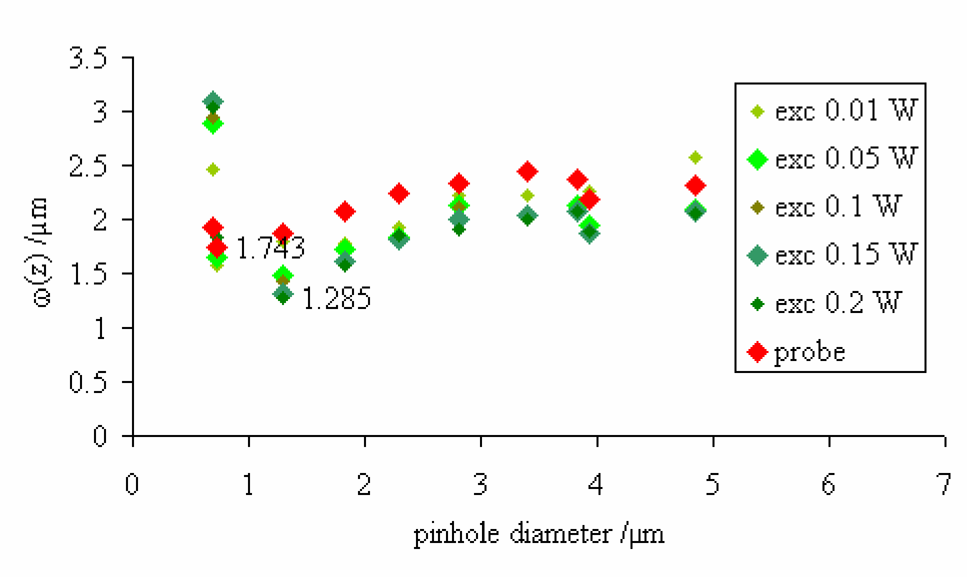

Figure 26 Calculated beam diameters ω(z) after measurement of laser power through a pinhole to determine spot sizes of a laser (for detailed description see text)

The spot sizes measured with the pinholes are in good agreement with the theoretical values. Deviations from the theoretical value can be explained by the uncertainty of pinhole diameter as measured with AFM, the non-circularity of the pinholes, and the non-circularity of the laser spots which were observed especially for the probe laser. Also the diameter size of pinholes was limited. For the excitation laser, which defines the resolution of the system, the results were in good agreement with theory.

4.4.2 Influence of instrumental parameters

In order to measure the influence of instrumental parameters, the detection system of the thermal lens setup was modified to reduce noise in the TLM signal. A preamplifier (5325 Isolation Amplifier, NF Electronic Instruments) and a frequency filter (3627 Dual Channel Programmable Filter, NF Electronic Instruments) were installed after the detector and prior to entering the signal into the lock-in amplifier.

With this setup, scanning of sputtered gold at different modulation frequencies was conducted to find an adequate modulation frequency with good signal to noise (S/N) ratio. Furthermore, scanning was conducted at different scanning speeds, which in return meant shorter time constants in the lock-in amplifier, to see the influence on S/N ratio. For the following experiments, the modulation frequency was set at 1003 Hz, unless noted otherwise. The slight offset from 1 kHz is added in each experiment to minimize the influence of electronic noise from the equipment on the thermal lens signal further.

For lateral resolution measurements, a gold stripe pattern was produced using photolithographic lift-off procedures. Photoresist was spin-coated onto a glass slide and developed under a UV-mask using UV-irradiation. Undeveloped photoresist was washed off, and gold was sputtered onto the surface. A lift-off of the remaining photoresist resulted in a pattern of a field with equidistant gold stripes (Figure 27). The resulting height of the gold stripes is about 100 nm, as confirmed with atomic force microscopy. The stripes act as a thin sample in regard to optical absorption and heat conduction. Fields with various widths of gold stripes, ranging from 20 to 100 µm, were produced for scanning experiments. The widths of the stripes were confirmed with optical microscopy (Nikon Eclipse TS100). Measurements were conducted on various sized stripes regarding scanning speed and repeatability. Following those measurements, edge resolution measurements were carried out on 40-µm-wide gold stripes. Scanning across three stripe patterns was conducted at different scanning speeds with different time constant and attenuation slope settings in the lock-in amplifier. The time constant thereby ranged from 1 to 300 ms and the scanning speeds ranged from 10 to 100 µm/s. The attenuation slopes of the lock-in amplifier were changed between 6, 12, 18 and 24 dB for each scanning speed and sampling time. Experiments were furthermore conducted at scanning speeds up to 1000 µm/s with time constants from 0.1 to 1 ms to confirm the trend observed during the previous measurements.

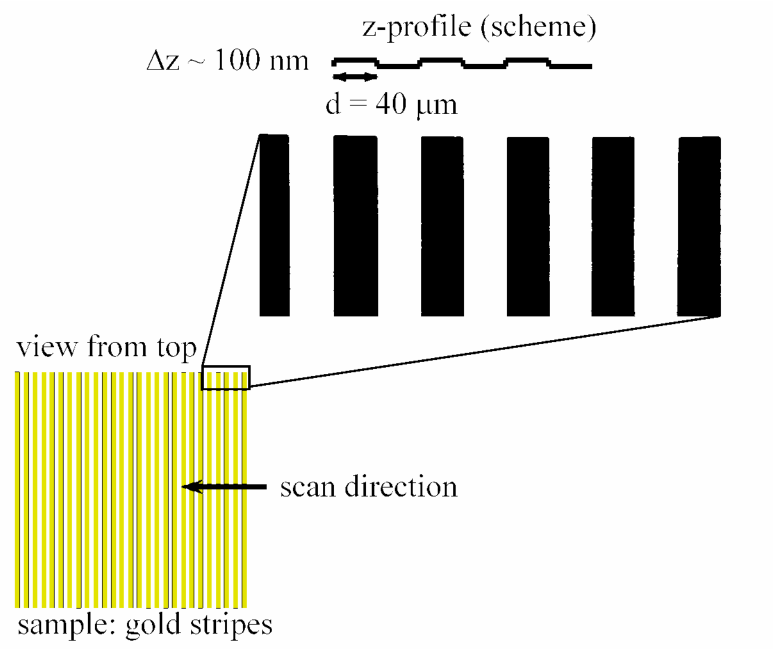

Figure 27 Schematic illustration and bright field microscopic image of gold stripe sample

A final change of the system was done after the two-dimensional scanning experiments and biofilm measurements in order to check for influence of a strongly scattering sample (e. g. biofilm) on the TLM signal. The measurements will be discussed here as they are in regard to instrumental setup. With the change in setup, the laser power of the excitation and probe beam, respectively, were monitored after exiting the sample to check for power losses during sample scanning. This way, a simple approximate measurement of the influence of scattering and out-of-focus absorption as well as absorption of the probe laser was attempted.

Additions to the setup were made as shown in Figure 28. In addition to the excitation laser (modulation frequency 1030 Hz), also the probe laser was modulated with an AOM (ISOMET Acousto-Optic Modulation Driver 232-A-1) triggered by a function generator (Tektronix AFG 3022 Dual Channel Arbitrary Function Generator) at a frequency of 1.0101 MHz (rectangular pattern). Both beams were applied to the sample as described above and left the microscope with a prism. After the prism, a dichroic mirror was installed to reflect the excitation laser to a photodetector (EOT Silicon PIN detector ET-2030, Electro Optics). In front of the photodetector, neutral density filters (10%, 30%, and 50%) and a bandpass filter (520 - 500nm) were installed to protect the detector from overload and to suppress scattered probe-light.

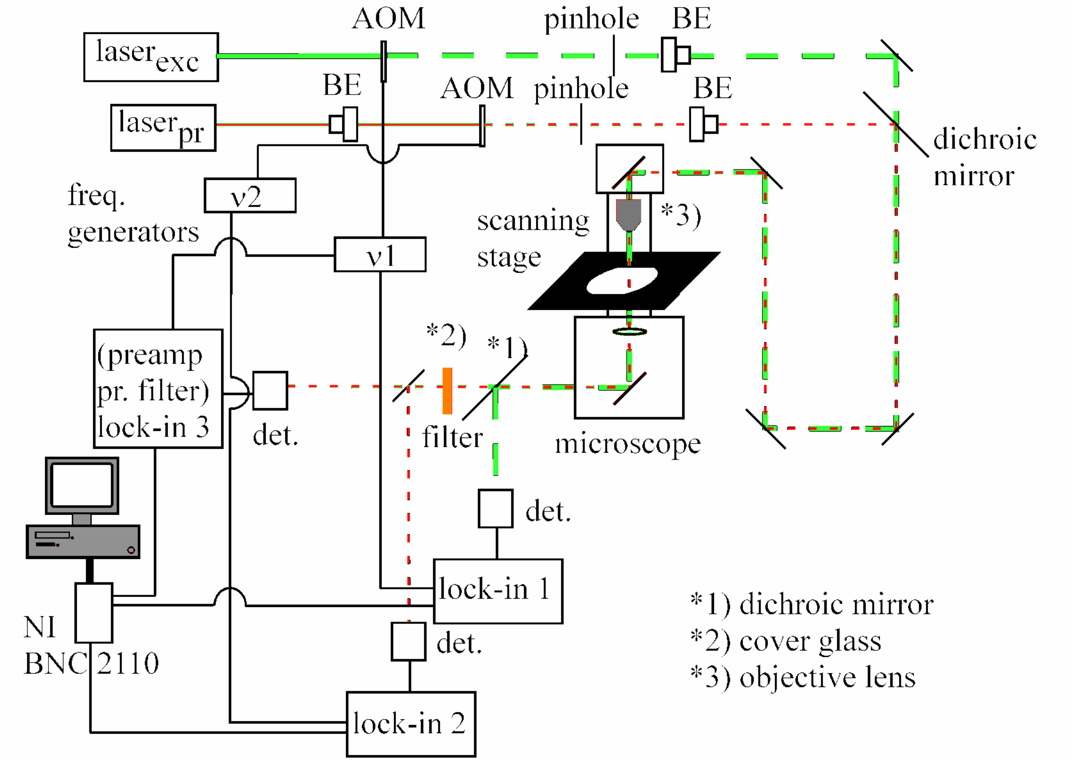
AOM
pinhole
BE
laser$_{exc}$
BE
AOM
pinhole
BE
laser$_{pr}$
dichroic
mirror
freq.
generators
ν2
scanning
stage
*3)
ν1
(preamp
pr. filter)
lock-in 3
det.
*2)
*1)
filter
microscope
det.
lock-in 1
NI
BNC 2110
det.
lock-in 2
*1) dichroic mirror
*2) cover glass
*3) objective lens

Figure 28 TLM setup for measurement of scattering samples

The photodetector signal was sampled with a lock-in amplifier (LI-575 Synchrotrack Lock-in Amplifier / Vector Voltage, NF Electronic Instruments). After the dichroic mirror, an orange filter was included to remove remaining excitation light. The probe light then was split by a cover glass slide. One beam was sent to a photodetector (EOT Silicon PIN detector ET 20-30, Traverse City, M1), and the probe laser power was sampled from this detector with a lock-in amplifier (Signal Recovery 7280 DSP). The other part of the probe beam was sampled for the TLM signal as described above. Thermal lens signal intensity and phase as well as the beam powers of excitation and probe beam were recorded simultaneously with the home-built Labview software and stored for further evaluation.

For the production of scattering samples, firstly 0.4 g agarose mixed with 2, 20 or 200 µL of bead solution was dissolved in 10 mL of deionized water by microwave heating (750 W, ~ 30 s). A glass slide was prepared as carrier for the samples by cleaning with deionized water and ethanol. On the two ends of the glass slides, glass slides were put as spacers. The hot sample solution was poured between the spacers and closed off with another glass slide that was put on top, this way producing scattering agarose gels of about 1 cm thickness. The samples were then left for drying to produce samples with thicknesses ranging from 25 to 35 µm, as confirmed by 3D-reflection microscopy (VK-9510 3D profile microscope, Keyence, Japan). Two sets of samples were prepared, one with black beads (Polybead® Polystyrene Black Died Microspheres, 1.00 µm: 2.5% aqueous suspension) as absorbing and scattering samples and one with white beads (Polystyrene solution, 2 wt % dispersion in H_2O, average diameter 1 µm, latex particles) as scattering samples. Scanning of the samples was conducted with a 20x lens (UPlan FL N, N.A. 0.50, Olympus) at a scan speed of 10 µm/s. Lines were scanned for distances around 150 µm, and parallel lines were scanned for a distance of 5 µm, 1 µm apart. Depth recordings were taken with Δz of 10 µm.

4.4.3 Three-dimensional scanning

Scanning experiments of biological samples were carried out before TLM in Kitamori-laboratory. However, scanning was conducted point-by-point, which makes measuring time for areas of 30 x 30 µm^2 with steps of 1 µm as long as 45 minutes with 3 second duration per measuring point [177]. For measuring biofilm in three dimensions, a minimal observation area of 100 x 100 µm^2 with a depth of 100 µm and step widths of at least 10 µm for thin biofilms is thought necessary. If this volume is measured step-by-step, the time needed for observation exceeds 83 hours. In order to enable a fast measurement of biofilm, continuous scanning of samples is needed. For this purpose, research on scanning characteristics and influence on the TLM signal was conducted. Scanning experiments were conducted at modulation frequencies at 1.003 kHz, as signal-to-noise ratio at this frequency was good for this frequency (see results).

For a first test of 2-dimensional scanning of a strongly scattering sample, a biofilm model sample of 1.5 % agar containing Fe_2O_3 particles (c = 9 mg/L) was prepared. The agarose and the iron(III)oxide were suspended in deionized water and heated in a microwave at 750 W until the agar dissolved (~ 30 seconds). The agar suspension was then poured onto a glass slide with further glass slides at each end of the slide as spacers. After filling the glass slide between the spacers, a final glass slide was placed on top of the spacers to produce an agar gel of homogeneous thickness of about 1 cm. After solidification of the gel, it was taken directly for TLM observation. The sample was scanned point by point with a 20 x objective lens (UPlan FL N, N.A. 0.50, Olympus). Triplicate measurements with a time constant of 300 ms of the lock-in amplifier at a laser output power of 0.1 W were conducted. Three lines with a length of 10 μm and data points 1 μm apart were recorded.

Stained polystyrene samples were prepared for determination of the depth-resolution of the system. Polystyrene was dissolved in solutions of toluene (100 mg/mL) stained with various amounts of the red dye Sudan IV. The stained samples were spincoated onto glass slides at 500 rpm for five seconds, a slope of 100 rpm/s for five seconds and at a constant rotation of 1000 rpm for 50 seconds. Depth resolution measurements were carried out in 10-fold repetition on 5 samples with dye concentrations of 1×10^{-5}, 2×10^{-5}, 1×10^{-4}, 2×10^{-4} and 1×10^{-3} mol/L. The thickness of the samples was determined to 4 μm with 3-D reflection microscopy. Depth scans of the samples with TLM were carried out at steps of 2 μm every second with a time constant of 100 ms, resulting in 10 data points per second.

A final reference sample was produced by patterning of stained SU-8. A suspension of 20 mL SU-8 2025 and 2 mg fluorescein in 15 mL ethanol was spincoated onto glass-slide (Visiol® Shin Etsu Chemical Co., Ltd., Japan) cleaned by acetone, ethanol, pressurized air and plasma cleaning (Ulvac NE-500). Spincoating was conducted 5 s at 500 rpm, followed by a ramp to 3000 rpm at 500 rpm/s, and a final 30 s at 3000 rpm with a IH-3605 spincoater (Mikasa Co., Ltd., Japan). The sample was softbaked at 65 °C for 3 minutes and 95 °C for 5 minutes. Afterwards, the sample was placed on a mask aligner (MA-10, Mikasa Co., Ltd., Japan) and irradiated through a photomask with UV light at 150 mW/s for 20 s. The photomask pattern was a 100 μm by 100 μm square. Following irradiation, the irradiated SU-8 was tempered 1 minute at 65 °C, 3 minutes at 95 °C, and developed for 4 minutes with SU-8 developer. Undeveloped SU-8 was washed off with acetone, and the slide was finally washed with ethanol and dried with pressurized air. The sample was scanned at a speed of 100 μm/s. Parallel lines, each 1 μm apart, were scanned for two-dimensional image generation. Reference pictures of the stained SU8 gel were obtained using a CLSM equipped with a Yokogawa spinning disc CSU21 scanner unit, which enables faster observation compared to point-scan or line-scan setups [220]. Fluorescence excitation was carried out with an Ar-laser at 488 nm with 10 mW power. Images were recorded with a Hamamatsu 1394 ORCA-ER digital camera.

4.4.4 Biofilm observation

Following the two-dimensional scanning experiments, three-dimensional scanning experiments were conducted on biofilm samples. Scanning of the biofilm samples was conducted manually. The three-dimensional scanning scheme is shown in Figure 29.

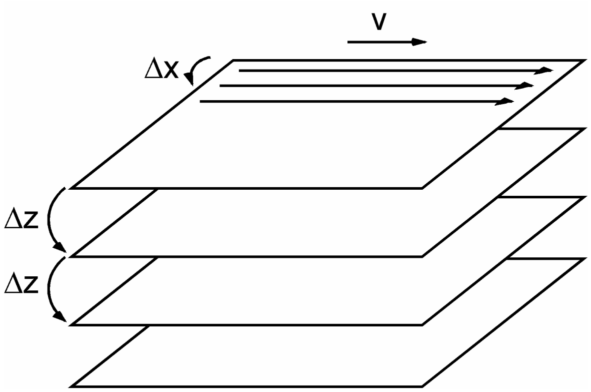

Figure 29 Scanning scheme for 3-dimensional biofilm observation, Δz = 10 μm, v = 100 μm, horizontal scanning lines are 1 μm apart

Scanning is conducted by scanning parallel lines in one sample layer that are a distance Δx apart. For three-dimensional scanning, parallel layers with a distance of Δz are scanned one after another by parallel line scans.

For the biofilm observation experiments, the beams were focused with an objective lens (UPlan FL N 20x, N.A. 0.50, Olympus) onto the sample. The excitation and probe beam laser focus spots were adjusted with beam expanders to be approximately one confocal distance (4.0 µm) apart vertically [187]. The modulation of the excitation beam was carried out with an AOM at a frequency of 1003 Hz.

In the first experiment, the sensitivity of TLM for biofilm observation was tested with a natural biofilm sample taken from a stone surface in a pond (Sanshiroike, Tokyo University). After sample-taking, the biofilm was taken directly to the laboratory and transferred to a special cuvette holder (height 40 µm) for observation. The sample was tested locally in a signal on-off experiment.

For testing the observation of adhered biofilm, the biofilm sample grown on a glass slide inside a flow channel was taken. A 100-µm square area within the unstained biofilm was observed with continuous scanning TLM with a scan speed of 10 µm/s and a time constant of 10 ms at an attenuation slope of 12 dB for line scans. Parallel lines 1 µm apart were scanned for two-dimensional image generation. For three-dimensional observation, a 10 µm wide strip of this square was monitored at depth intervals of 2 µm for a total distance of 10 µm.

For biofilm observation within a microchannel, biofilm grown in the S-type channel was placed with the holder onto the sample stage and continuously pumped with the nutrient solution. TLM observation was carried out by horizontal parallel line-scanning with lines 1 µm apart. Lines were scanned at a speed of 100 µm/s, with a time constant of the lock in amplifier of 1 ms. 1000 data points were recorded each second. The resulting layers of biofilm growth were recorded in different depths of the channel, 10 µm apart. A reference picture of the biofilm observed with TLM was recorded using a phase contrast microscope (IX71, Olympus) at 20x magnification.

Comparison experiments on resolution with two different objective lenses were conducted with a sample of biofilm grown in the-top-on connected I-channel growing on some dirt, probably a PEEK splinter. Two-dimensional scans of the sample were conducted by scanning parallel lines of 200 µm length at a scan speed of 100 µm/s and a time constant of the lock-in amplifier of 1 ms. Scans were conducted over a width of 100 and 70 µm, respectively, with lenses of numerical apertures of 0.5 (UPlan FL N 20x, Olympus) and 0.9 (LUMPlan FL 60x, Olympus). The excitation output powers were 0.05 and 0.1 W with sensitivities of the lock-in amplifier of 5 mV and 1 mV. As a reference, a transmission and fluorescence images were taken with the fluorescence microscope.

Data evaluation of biofilm signals was carried out with Matlab®. The two data sets representing thermal lens signal amplitude and signal phase were treated separately. The signal amplitude was taken as raw signal and plotted in false-color plot with color intensity normalized to amplitude value.

TLM signal phase images were generated by measuring the difference in phase value between adjacent points rather than absolute values. For this purpose, a Matlab® routine was developed that compared the phase values between points in one scan as well as between points in the parallel rows. This way, a new data set containing the phase differences as values was created. Only points with phase differences smaller than 18° in the two perpendicular directions (x/y, -x/-y, -x/y, x/-y) were considered for further evaluation. The values of the remaining phase differences were plotted on a black-white scale, with black areas presenting values of very small phase difference. This routine was continued over all scanned layers in the third dimension. A comparison between phase values in the z-direction was not done due to the distance between the layers.

5 Results and discussion

5.1 Biofilms in the microchannel

Before biofilm experiments could be conducted, channel flow had to be checked for linearity and the flow had to be calibrated.

For the flow channel, linearity is given over the whole range of the peristaltic pump, as shown in Figure 30. For this larger system, the coefficient of determination is near one.

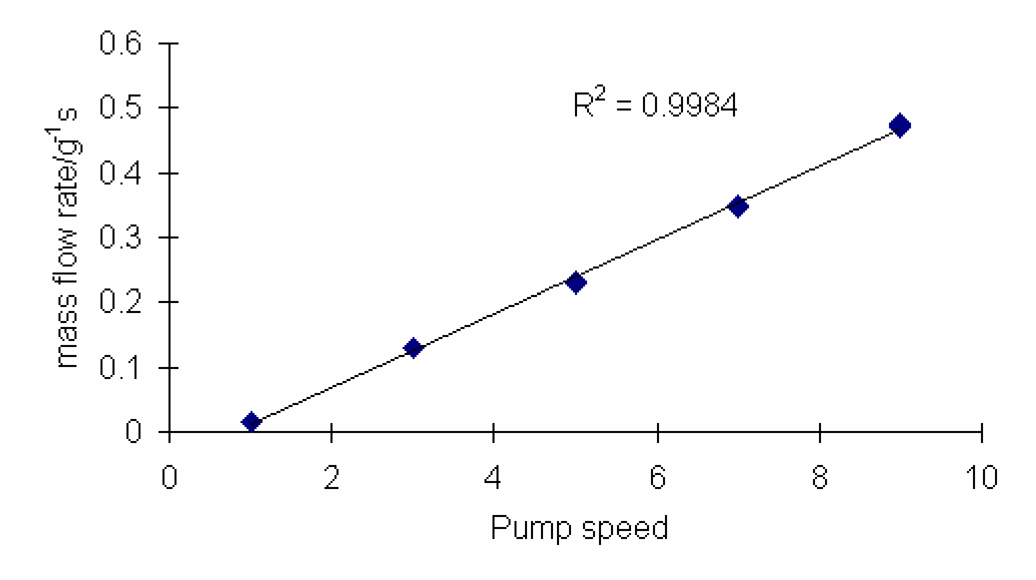

Figure 30 Calibration for flow rate inside the flow cell driven by peristaltic pump (n = 25, m = 5)

For the top-on connected microchannel system, the results for the flow calibration are shown in Figure 31. In the figure, the flow with one and two Tygon® tubes attached in the dual channel pump for two pumps of the same type is compared to the flow through tubes that are already glued to a PEEK capillary and a microchannel, respectively. With two tubes, double the amount of water is flown as with a single tube, and the attaching of a PEEK capillary has no significant influence on the flow rate. In contrast, the attaching to the top-on connected microchannel results in a decrease of flow rate within the system due to the back pressure coming from the chip.

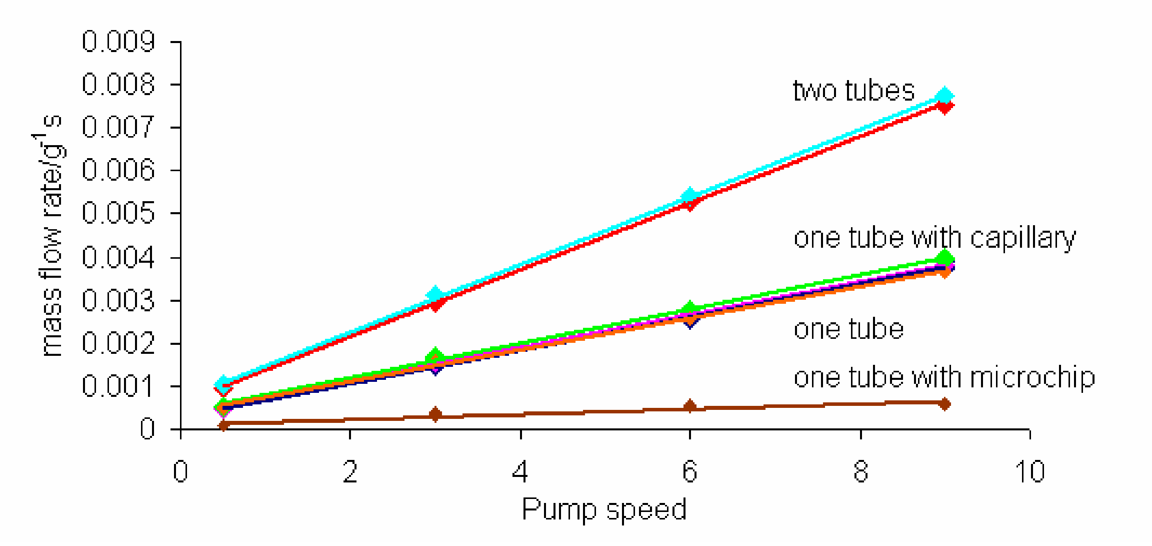

Figure 31 Flow calibration for the Masterflex pumps through Tygon® without and with attachment of a PEEK capillary and a top-on connected microchannel (n = 12, m = 3; except two tubes n = 4, m = 1)

However, all systems show a linear relation between arbitrary pump speed and flow rate over the pumping range of the peristaltic pump.

Following this calibration, the hydrodynamic conditions inside the microchannel have to be compared to existing biofilm growth systems for comparison. The hydrodynamic parameters of the top-on connected I-type channel system are summarized in Table 2. With the top-on connected chip setup, different hydrodynamic conditions having values comparable to literature can be realized [55, 112]. However, the values are slightly higher than in the other systems.

Table 2 Hydrodynamic data for the top-on microchannel system

flow [µL/s]	velocity [m/s]	Reynolds number	shear stress [N/m^2]
0.08	0.02	1.2	2.9
0.34	0.10	5.6	12.8
0.53	0.16	8.6	19.8
0.59	0.18	9.5	22.0

As the system with the top-on connected I-type channel ultimately failed due to clogging, the side-on connected I-type channel system was taken for experiments. The system showed linearity over the whole pump range as well (data not shown), and the hydrodynamic parameters are presented in Table 3 .

Table 3 Hydrodynamic data for the side-on microchannel system

flow [µL/s]	velocity [m/s]	Reynolds number	shear stress [N/m^2]
0.13	0.0005	0.26	0.006
0.32	0.0013	0.64	0.015
0.59	0.0023	1.17	0.028
0.92	0.0037	1.83	0.044
1.29	0.0052	2.58	0.062

Compared to other systems, the shear stress at the wall is slightly smaller. This, together with the fact that the peristaltic pumping is pulsating and prone to losses at the tube fixation, required the development of a new pumping system.

To minimize pressure loss within the system, capillaries were kept short and the major flow occurred in Tygon® tubes. This way the back pressure from the system was reduced and the pumping with a pressure calibrator at low pressure was possible, thus avoiding high pressure in the system and the need for special connections. The flow into the tubes was also easier with this setup. With smaller capillaries, it is especially difficult to remove gas bubbles inside the system. At this point, however, the resulting back pressure was too small, and pumping was already successful at 0.3 kPa, which is equal to three centimeters of water column. This causes flow differences inside the channels just by the relative position of the exit capillary. Therefore, the flow rate between channels deviated, as seen in Figure 32.

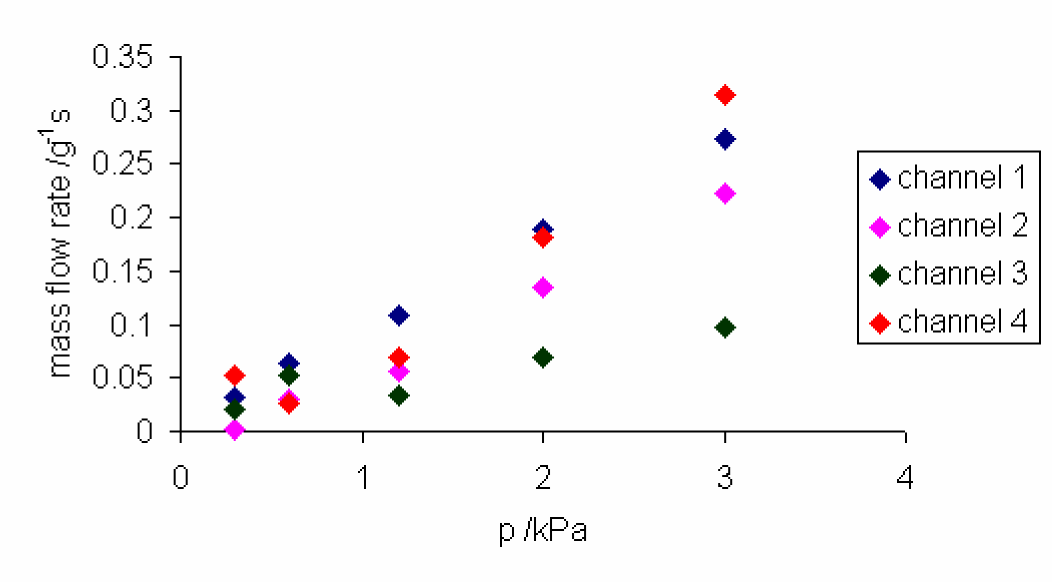

Figure 32 Flow rates for individual channels in the pressure-driven flow system

However, also measuring errors during gravimetric measurements cannot be neglected, especially at low flow rates. Another factor influencing the relative flow is the capillary length difference of capillaries connected to different channels. The pressure loss is highest in the system parts with low diameter, and apart from the channel the capillaries have the smallest diameters. Therefore they have a big influence on pressure loss inside channels, especially as they are longer than the channel itself.

Due to the differences in flow rates, only qualitative experiments were undertaken for growth of *Sphingomonas paucimobilis* biofilm. At the time of growth, the two channels chosen for growth experiments showed little difference in initial flow rate.

5.1.1 Biofilm adhesion in microchannels

In the top-on connected I-channels, some qualitative observations about biofilm growth were observed first in preliminary experiments. The results are presented in Figure 33 and Figure 34. Biofilms were growing strong in the channel flown at a higher flow rate of 0.1 m/s presented in Figure 33, and a dense mat of biofilm formed on the channel wall. In contrast, the biofilm colonies grown in the channel at a flow rate of 0.05 m/s (Figure 34) were growing less dense and patchy.

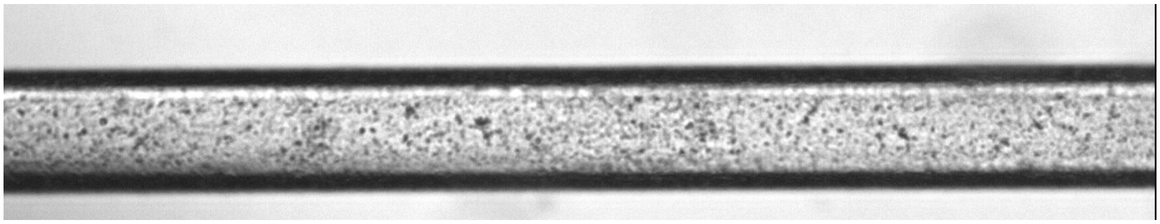

Figure 33 Biofilm growth in a top on connected channel at a flow rate of 0.1 m/s (Re = 18.5, $\tau \cong 12.8$ N/m^2)

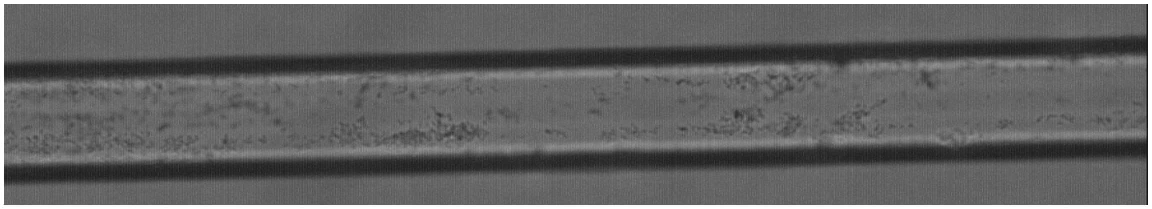

Figure 34 Biofilm growth in a top on connected channel at a flow rate of 0.05 m/s (Re = 9.2, $\tau \cong 6.4$ N/m2)

Further examination of the top-on connected channel revealed biofilm growth in the curves at the connection ports after more than one week. This growth resulted in clogging at those points (Figure 12). The clogging effect is most likely enhanced by the shallowness of the channel. The clogging of the curved path in microchannels with perpendicular connecting ports was also observed during growth of a *Staphylococcus epidermis* biofilm [70]. The clogging was observable in the channels as early as four days after inoculation. Disregarding the causes, prolonged biofilm growth in the top-on connected channel seems impossible, so a change to wider, side-on connected channels was taken. However, prior to this change, biofilm staining was attempted in order to prove the occurrence of biomaterial rather than dirt inside the channels.

5.1.2 Online biofilm staining in microchannels

In the shallow top-on connected microchannels, biofilm was attached and left in a high shear flow field for five days. Only a few biofilm colonies attached in the shallow channels, and growth was hardly observable. However, the biofilm stayed attached to the channel wall. In order to check for biofilm attachment, in contrast to attachment of other dirt particles, the channel was pumped with a staining solution containing DAPI and FITC-ConA. The resulting stained biofilm (Figure 35) shows that online staining was successfully carried out within twenty minutes of continued flow and a staining solution volume of 1 mL. Figure 35 presents one biofilm (left), where DNA stained with DAPI (middle) and stained α-mannosyl groups which are presumably a part of the EPS (right) are present. Therefore, the particles attached to the channel wall are likely biofilm.

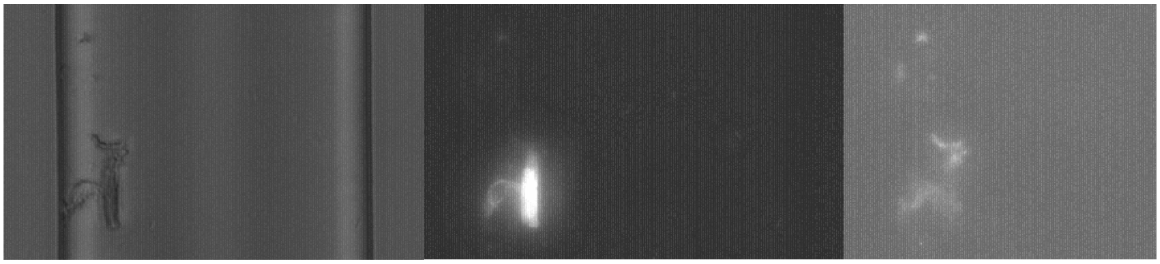

Figure 35 Bright-field image of biofilm in 100 µm wide microchannel after five days (left, scale bar 10 µm); fluorescent micrographs with DAPI and FITC-ConA staining as observed with DAPI-filter (middle) and FITC-filter (right)

The low amount of liquid needed for online staining is comparable to the volumes normally used for samples fixed on glass slides. As the staining can be carried out without disturbing the biofilm structure by opening the culture device, washing procedures or the staining procedure itself, online staining is preferable for observing biofilm structure. With the microchannel, this is possible with small amounts of reagents, thereby also limiting expenses and waste solution. Also, autoclaving procedures are simplified due to the minute amounts of reagents and small equipment applied. Utilizing parallel channels, many experiments can be carried out simultaneously using small reagent volumes. The advantage of microfluidic devices for fast online staining with a minimum consumption of reagents has already been reported in prior examinations [173].

Staining of biofilm was also undertaken in the pressure-driven flow system after 8 h flow in an adhesion experiment with *Sphingomonas paucimobilis* using DAPI. In this case, the successful adhesion of bacteria to wall was of interest prior to growth experiments. The results are shown in Figure 36

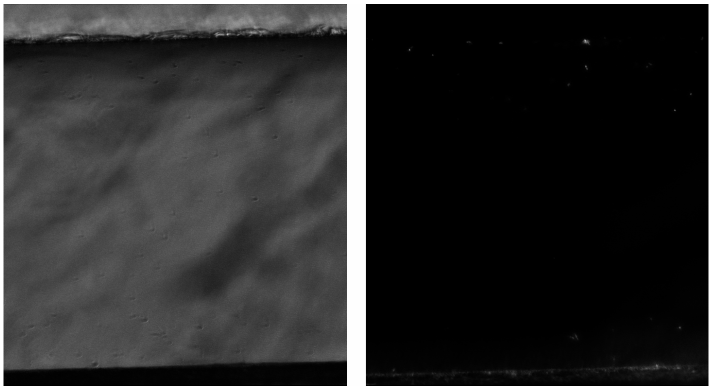

Figure 36 Transmission (left) and fluorescence image of *Sphingomonas paucimobilis* cells adhered to a microchannel in the pressure-driven flow setup after 8 h

Bacteria adhered mainly at the edges of the channel, where shear stress is reduced in comparison to the middle of the channel, as will be discussed below.

5.1.3 Biofilm growth in microchannel

The side-on connected microchannels showed reduced biofilm attachment in dead zones. No clogging of the channel was observed, a result similar to experiments of biofilm growth in monoliths with channels in the range of several hundred micrometers [94]. Dead zones were observed within a small distance of the capillary entrance, but not within the channel itself. The dead zones result from the insertion of the capillary in the bigger channel at the exit of each capillary. Biofilm growth in the dead zones surpassed biofilm growth in the rest of the channel initially, so the entrance of the channels was disregarded for further examinations. The effect of the dead zones on the rest of the channel was assumed to be minimal, which is supported by a triangular-looking shape of biofilm attachment and initial growth away from the capillary entrance within a few hundred micrometers (data not shown). However, extended growth in dead zones was limited with the side on connection, improving the system as compared to top-on connections where abundant biofilm growth, and possibly clogging, occurs. Furthermore, growth was observed predominantly at the bottom of the channels, which corresponds with former observations [70].

Growth of biofilm within one month was observed. Initial adhesion of biofilm was limited in the MPC polymer treated channel to mostly corner positions. In the glass microchannel, mostly round-shaped bacteria adhered initially, in contrast to mostly rod-shaped bacteria in the APTS and ODS channels, and also to a lesser extent in the MPC polymer channels. While the bare glass surface seemed to be not supportive to biofilm growth, biofilm growth was observed on most of the surface of the ATPS and ODS channels. In the ODS channel, thicker biofilm colonies formed, which appeared to have three-dimensional stalk-like structures. The stalks were mostly forming in the middle of the channel. Clogging of the channel, however, was not observed. Representative pictures of the biofilm growth in all four channels after one month are shown in Figure 37. After the growth phase, biofilm was flushed out of the channels with two pressure plugs, which will be discussed below.

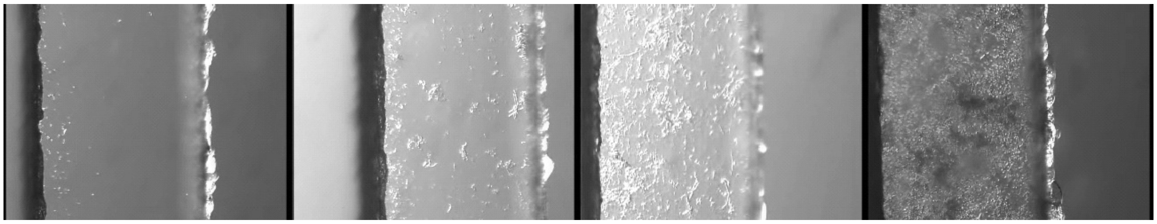

Figure 37 Growth of mixed population biofilm in microchannel with different surfaces (form left to right): glass, MPC-copolymer, APTS, ODS

Statistical analysis of biofilm growth in microchannels with different surfaces after one month showed surface-related coverage rates on the bottom plate of the channel, as can be seen in Figure 38.

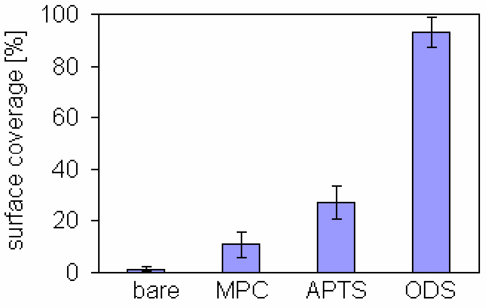

Figure 38 Statistical analysis (n = 20) of biofilm coverage of the side-on connected microchannels with differently modified surfaces after one month growth and the subsequent removal with two air plugs

On the hydrophilic glass walls, biofilm adhered only to a small extent, as already observed in the smaller microchannels. Also in other studies, borosilicate glass shows little amount of adhesion by homogenous biofilms, small amount of adhesion by mixed species biofilm [221]. Biofilm growth was hardly observed in the microchannel, which highlights the importance of initial bacterial/biofilm attachment for continued growth.
MPC polymer was applied successfully as surface modification method to prevent biofilm adhesion of pure culture biofilm from different bacteria on several surfaces, including intraocular lenses and dental material [71-73]. Also, MPC polymer was effective when applying low shear stress [72]. In this study, MPC polymer prevented adhesion and growth of a mixed species biofilm under low shear stress. However, an observed reduction of bacterial retention could not be confirmed, although the time frame of the study of Hirota and coworkers was significantly shorter [73]. Biofilm growth on MPC polymer surfaces occurred predominantly in the corners of the channel. This is in accordance with other microchannel experiments, where a field of lower shear stress was calculated for the corners and observed biofilm adhesion was enhanced [70].

On the other hand, ODS treated surfaces showed no reduced growth, as already observed by other researchers [74]. In the case of the ODS channel, biofilm growth extended in stalks to the upper wall of the channels, producing structures typical for biofilm grown under laminar flow conditions with an abundance of nutrients. The APTS channel showed results similar to the ODS channel, with bigger biofilm colonies and stalks developing, although the extent of biofilm growth was lesser.

Influence of surface properties on extensive biofilm growth contrasts prior results, where no influence of surface hydrophobicity on biofilm growth of E. coli was observed after 16 hours [106]. However, our experiments were carried out with a mixed species biofilm, and the primary adhering bacteria species could not be determined. However, during the adherence observation in the surface-modified microchannels, different kind of bacteria seemed to attach to different surfaces. Round type bacteria where mostly found on the hydrophilic surfaces, whereas rod-shaped bacteria attached predominantly to the hydrophobic surfaces. This indicates that the linking biofilm on different surfaces indeed could be varying. Therefore, biofilm formation could be started by only a small subgroup of bacteria, depending on surface properties. In order to prevent biofilm formation, it might therefore be possible to find effective means to only prevent a subgroup of bacteria from initial adhesion, or remove only this subgroup periodically. For example, biofilm morphology and growth behavior is influenced by surface characteristics, as was shown by the growth of *E. coli* K 12 biofilm on $–CH_3$ and $–NH_2$ modified surfaces [57]. Bacteria morphology is also influenced by the surface, as more round bacteria were observed on the methyl-like substrates, whereas the bacteria on the amino-modified surfaces were elongated. *Aquabacterium* commune, a member of various water distribution systems in Europe, was shown to preferably grow on medium density polyethylene in comparison to stainless steel [9].

However, although many papers about biofilm adherence on surfaces with different surface properties exist, a clear pattern for biofilm adherence, growth and removal is yet to be established [52]. Among the numerous influences, not only surface wettability, roughness, charge and other parameters are important, but also the bacteria itself as well as the nutrients provided are influencing bacterial adhesion and growth. Even bacteria with similar surface properties have been shown to have different adhesion behavior if they are recovered from different niches [53]. Our data with equal nutrient supply, big area to volume ratio and equal environmental conditions (shear stress, temperature) suggests a clear trend for biofilm from the same source adhering to surfaces with different wettability. Surface wettability therefore seems to have a direct effect on mixed species biofilm. The microchannel with its large surface-to-volume ratio might have influenced the results, as the surface availability for biofilm in the channel is high. Therefore, the available surface in relation to available volume might be of significance for bacterial attachment and biofilm formation studies, especially concerning bacteria growing in confined spaces and small tubes.

Biofilm growth in the pressure-driven flow system was only observed qualitatively in a first attempt to culture *Sphingomonas paucimobilis* inside a microchannel. Representative pictures are shown in Figure 39.

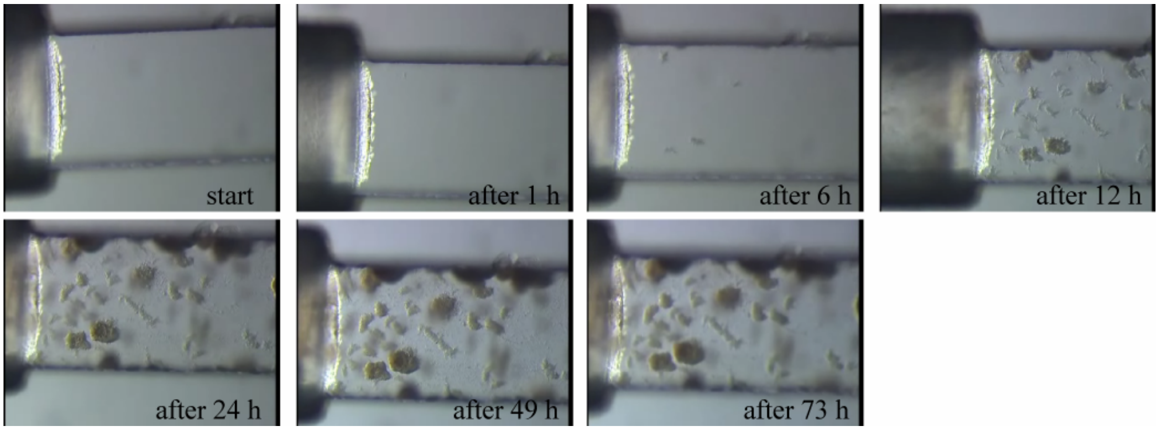

Figure 39 Growth of *Sphingomonas paucimobilis* biofilm in the pressure-driven flow system near the channel entrance

Biofilm development seems to be mostly finished within 24 h for this biofilm species, as no major change in colonies is observed afterwards. As noted, the pressure control in this system was not so good, though, so quantitative data were not obtained. As already seen with mixed biofilm before, the *Sphingomonas paucimobilis* biofilm did not clog the whole channel during growth, but left a wide area of the channel open for nutrient supply. Another observation is that dead zones near the capillary entrance were minimized with the new connection, and the flow in the whole channel seemed to be undisturbed by the new design.

5.1.4 Biofilm removal

Washout procedures in the top-on connected channels with hydrogen peroxide produced no significant effect in either channel (data not shown). However, as biofilm removal is essential for the reusability of the microchip, further chemical removal was undertaken. Attached biofilm was readily removed with sodium hydroxide solution. Differences in attachment strength of biofilm, resulting in different times of detachment, could be observed throughout the channel, as seen in Figure 40. Nevertheless, small particles which were most likely dirt from the capillary remained in the channel even after prolonged time.

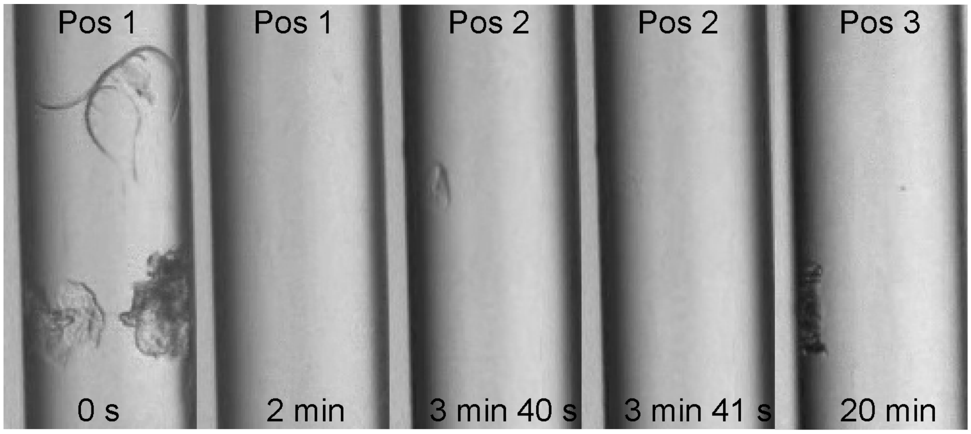

Figure 40 Removal of biofilm with sodium hydroxide solution (pH ~ 12) flown from top to bottom: While some parts of the biofilm in the microchannel are removed within 2 minutes, some colonies at different positions are only washed out after more than 3 minutes; after 20 minutes, further particles remain, in this case most likely splinters from the peak capillary (scale bar 20 µm)

In the attachment experiments in the small channels, attached biofilm is comparable to base biofilm. Comparable to other experiments, when applying hydrogen peroxide for removal this biofilm could not be removed [114]. As biofilm is expected to be removed in bigger aggregates and not disrupt, this suggest the strong bond between the biofilm materials. Also, the non-removal of base biofilm emphasizes the strong interaction of biofilm with the surface, which seems to be an important factor for this behavior.

The removal of biofilm with NaOH is in accordance with the results of Schmid et al. [116], but the prior flushing with hydrogen peroxide might have affected these results. Interestingly, biofilm was removed with NaOH as a whole, and the attached colony deformed, but did not break into pieces, as seen in Figure 41.

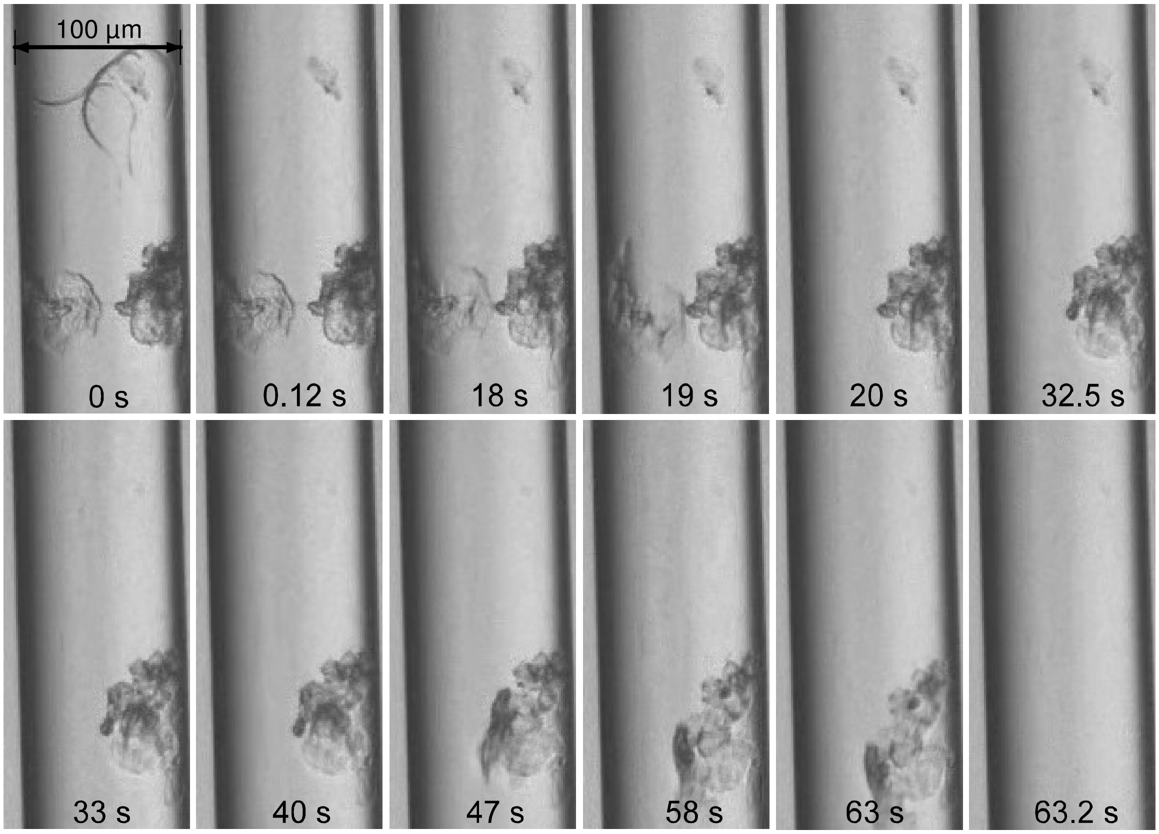

Figure 41Removal of attached biofilm colonies in a top-on connected microchannel (for detailed description see text)

This, together with the result from the hydrogen peroxide experiment, proves the importance of the linkage of biofilm with the surface, and a formerly proposed division into linking film and base biofilm seems justified [176]. The linking film is the bacterial layer in direct contact with the surface, and can therefore exhibit total different behavior than the base biofilm or the surface biofilm. On the other hand, our results also demonstrate that the forces holding a biofilm colony - formed prior to attachment - together are stronger than the interactions with the surface, at least for the glass surface of the microchannels.

In the side-on connected channels, biofilm was flushed out with two pressure plugs, as can be seen by representative pictures in the bottom of Figure 42. For comparison, the pictures with biofilm growth after one month are shown on the top.

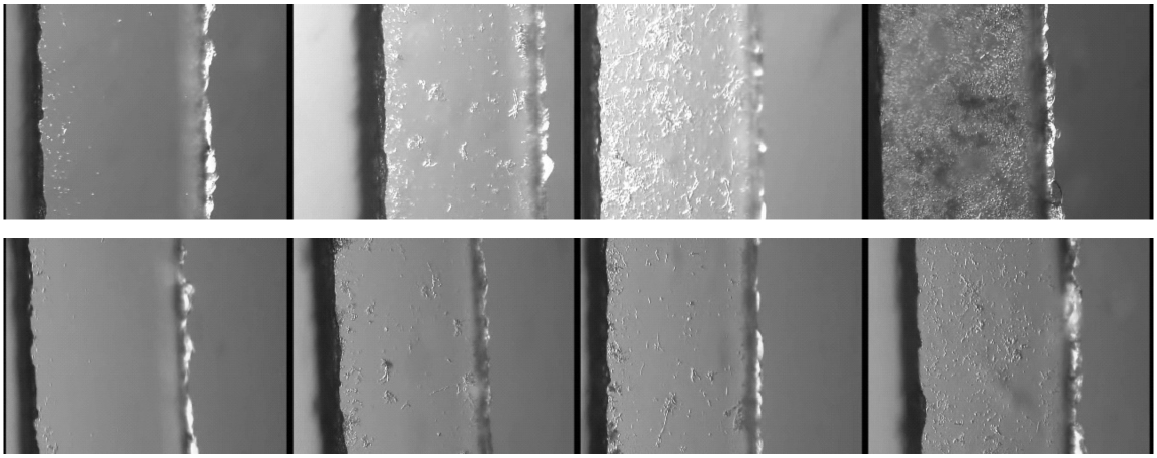

Figure 42 Biofilm growth in 500 µm wide surface-modified channels after one month (top row, scale bar 100 µm) and after two washout steps (bottom row); the pictures are representatives of the channels with (from left to right) bare glass surface, surface treated with MPC-copolymer, APTS and ODS

Conducting further analysis on biofilm coverage after the removal with two air plugs, and plotting the results for different surfaces against the contact angles obtained on modified glass surfaces, Figure 43 is obtained.

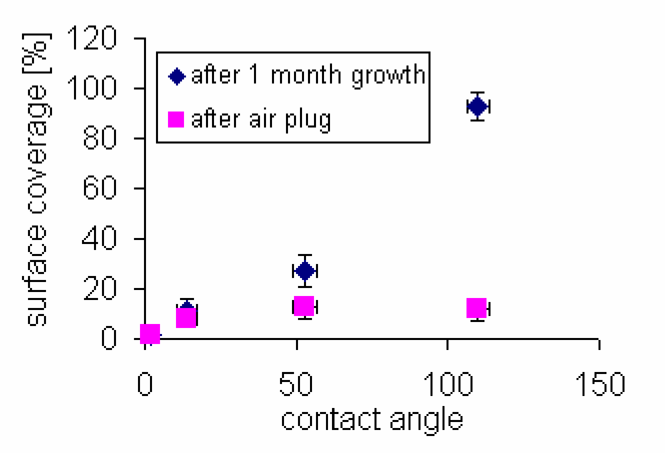

Figure 43 Effect of two air plugs on biofilm coverage: biofilm coverage (n = 20) in relation to contact angle (n = 3) before and after washout experiments with two air plugs after one month of biofilm growth

After the washout experiments, most of the biofilm remained on hydrophilic surfaces, whereas most of the biofilm was removed from the hydrophobic surfaces. This is in accordance with prior observations, where the interaction of the air plug with the hydrophobic surface was seen as major removal force [176]. Interestingly, about the same amount of biofilm remained attached to the different surfaces, independent of surface properties (with the exception of the glass surface, where biofilm occurrence was scarce). Shear stress on the biofilm structure during removal seemed to be the dominant factor for biofilm retention. Hydrophilic surfaces were not affected to a big extent by the introduced air, whereas biofilm on the more hydrophobic surfaces was strongly affected. The interaction of the hydrophobic surface with air is likely to be the major cause for the limited retention of biofilm on hydrophobic surfaces. The hydrophobicity of the material is the major cause for the removal event. This is similar to results where materials with higher hydrophobicity were less hampered by effects from surface roughness during biofilm removal [221]. The interaction of the lowermost biofilm layer with the surface seems to determine the removal efficiency. Therefore, a new model proposing consisting of three layers of biofilm, a linking film, the base biofilm and the surface biofilm, seems to be justified by these data [176].

Biofilm retention mainly occurred in the corners of the microchannel was observed. This behavior is similar to biofilm retention of *Staphylococcus epidermis* biofilm in a 100 μm wide and 100 μm deep microchannel [70]. In that case, flow modeling showed reduced shear in the corners to be the most likely reason for increased retention of biofilm in the corners. A similar result was also obtained during a cell adhesion assay with fibroblast cells [167].

After the removal experiments, washing of the big channels with NaOH successfully removed the remaining biofilm from the channels, enabling reuse of the system (data not shown).

In the growth and washout experiments, the microchannel proved to be a helpful tool for conducting multiple parallel experiments. With the recent development of combinatorial approaches in surface coating production [222], high-throughput, parallel systems for analyzing their efficiency in prevention of bacterial attachment and biofilm growth are needed. Also, as bacteria from different niches show different adhesion behavior, a small on-site multi-testing system seems to be favorable to extensive testing in the laboratory [53]. Apart from the possibility for multiplexing, microchannels have to offer also advantages for testing of new materials and material production methods, as they use limited amount of reagents and offer fast, cheap and reliable results. For example, surface patterning can be attempted in the microchannel which is already applied successfully in larger scale. For example, a patterned surface in a microchannel showed preferential retention of bacteria at the edges of hydrophilic surfaces [176]. And engineered surfaces were able to prevent biofilm adhesion and growth of *Staphylococcus aureus* to a big extent [48].

5.2 Thermal lens microscopy

5.2.1 Thermal lens scanning parameters

In thermal lens measurements, several settings of the instruments have to be taken in order to observe signals with a good S/N ratio. The first value to set is the modulation frequency of the AOM. In non-scanning cases, an optimum is found around 1 to 2 kHz. Also, during step-scan of gold stained cell surfaces, a frequency of 1.5 kHz was efficient [189]. For continuous scanning TLM, about the same frequency range seems to be good, as seen in Figure 44.

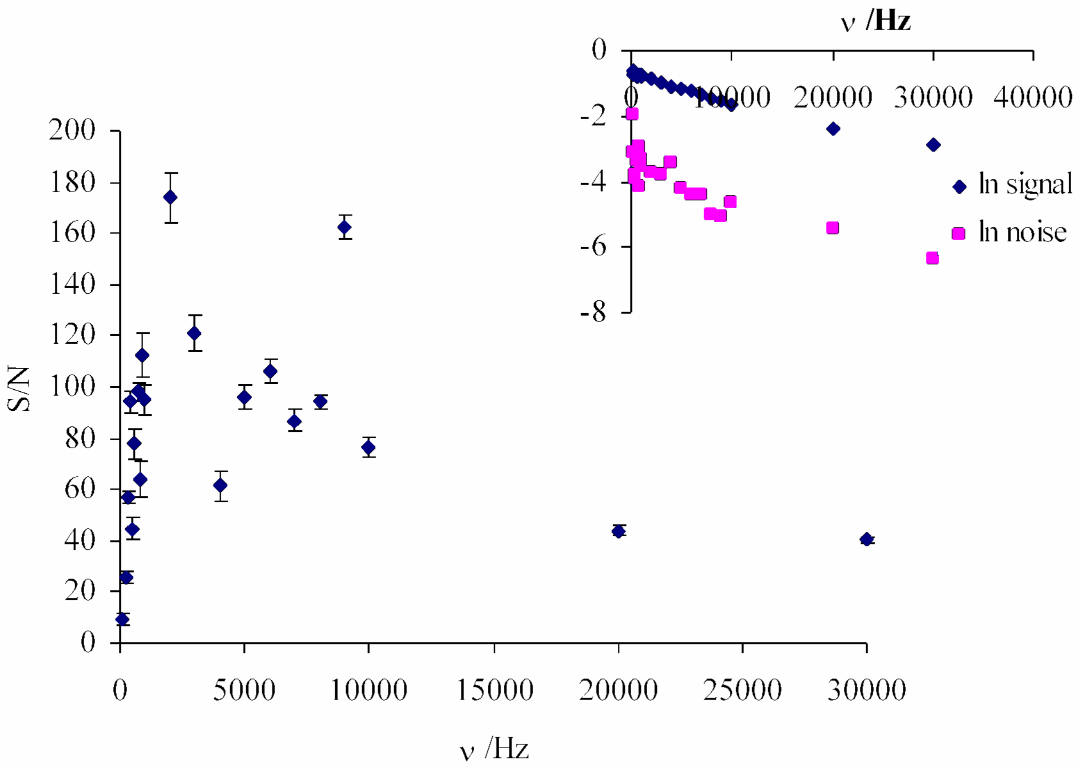

Figure 44 Signal-to-Noise ratio for scanning TLM at various AOM frequencies (scanning speed 10 µm/s)

The S/N ratio rises from 100 Hz until it reaches a maximum between 1 and 2 kHz and, neglecting an outlier at 9 kHz where the noise level was reduced, falls off again to higher frequencies.

The influence of the time constant of the lock-in amplifier influenced the signal, as shorter time constants and therefore shorter averaging time meant noisier signals. Over the whole scan speed range, the gold chip was measured with adequate S/N-ratio. However, the settings of the time constant in the lock-in amplifier became a more important factor regarding lateral resolution during continuous scanning, as will be discussed in the next section.

In order to see the influence of scan direction, a scan was taken across several stripes of the gold stripe sample, first in one direction and then after a brief stop back to the start. The result of this scan at an AOM frequency of 1503 Hz, and with a scanning speed of 10 µm/s, is shown in Figure 45.

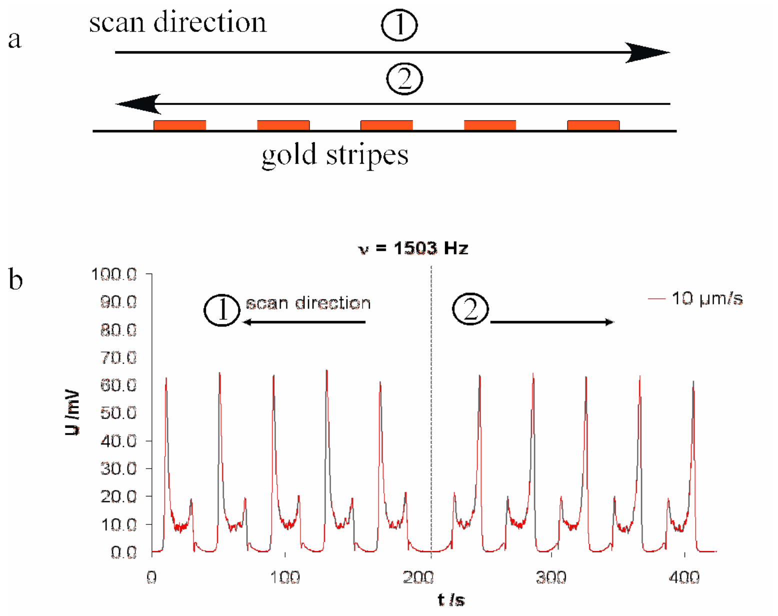

Figure 45 Influence of scan direction on TLM signal during continuous scanning over gold stripe sample: scanning scheme (a) and TLM signal (b)

The signal from the start to one point shortly after 200 s of scanning and back is virtually mirrored at a line which has been marked inside the figure by a dotted line. While the fact that the signal intensity is higher on one side of the gold stripes is higher than at the other makes this figure easier understandable and shows the results clearer, this is actually also a result taken with a wrong optical setup. The laser beams in this case were most likely not perpendicular to the sample surface in this case, as the signal intensifying at the edge normally should be symmetrical. This also shows one of the major problems of trying to quantify structures with TLM, as minor drifts in the optical pathway, for example caused by temperature effects on the setup from one day to the other, have strong influence on the thermal lens signal. With the present thermal lens setup, continued optimization has to be done frequently. In addition, interlaboratory research causes setup changes which then have to be readjusted, so quantification was not attempted. Rather, it was sought to determine the effect of sample properties on the thermal lens signal qualitatively.

5.2.2 Thermal lens resolution

Lateral resolution experiments

In order to determine the lateral resolution of the thermal lens microscope during continuous scanning, scanning experiments were carried out on the gold chip as an example of an object with restricted heat flow. Scanning across the gold stripe sample with 40 µm width resulted in peaks in the amplitude signal at the edge of the sample stripes (Figure 46). A similar observation was made with optical beam deflection spectroscopy by the group of Murphy [212]. Based on Murphy's model, the signal started rising from the noise level when the excitation beam spot started to overlap with the gold film, and fully overlapped at the peak of the signal. At the edge of the sample, heterogeneity of thermal conduction enhances the signal, and it relaxes in the central part of the gold film. The distance between the rising point and the peak was defined as lateral resolution here, which is expected to be the excitation beam spot size under an ideal condition.

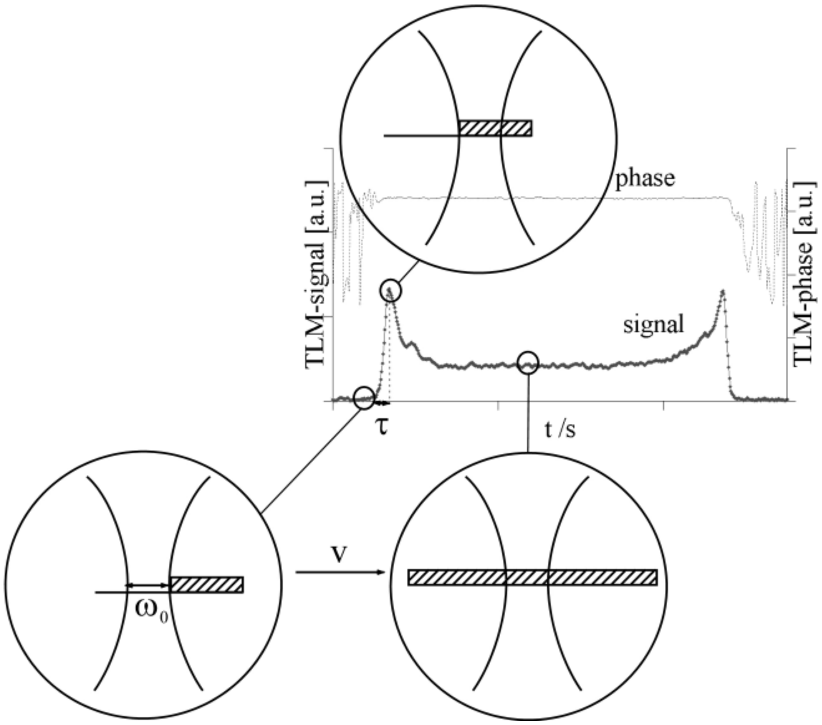

Figure 46 Thermal lens signal while scanning across a gold stripe: the thermal lens signal rises from noise level (beam with full width ω_0 outside the sample) in the response time τ to a maximum (beam just inside sample) and then falls to average signal amplitude (inside the stripe)

For clarification of the actual lateral resolution experimentally, the fraction of rise time τ from the noise level to the peak was discussed as functions of scanning velocity v and the electric system response, such as the time constant of the lock-in amplifier. The shape and position of the peaks, and therefore the rise time and resolution, was depending on the settings for scanning velocity v, time constant t_c and attenuation slope of the lock-in amplifier, as can be seen exemplary for different scan speeds and sampling times in Figures 47 and 48 (data for different attenuation slopes not shown). The time constants, t_c, were set as 10 ms and 30 ms, respectively.

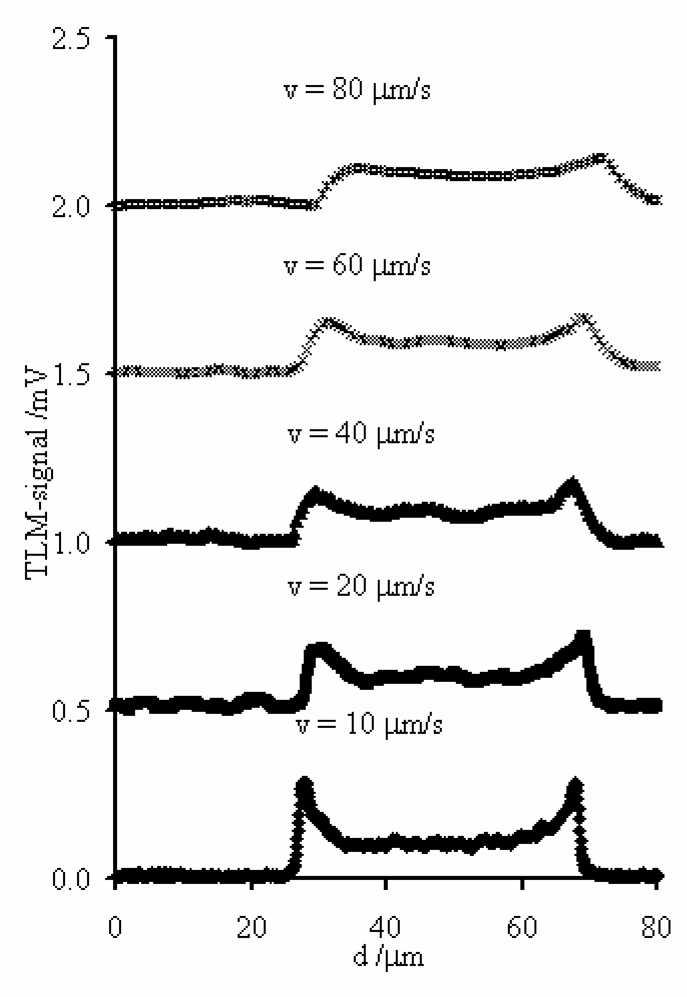

Figure 47 Signal of lateral scanning of one 40-µm wide gold stripe with different scanning velocities v at a lock-in attenuation slope of 12 dB and a time constant of 30 ms (signals shifted 0.5 mV): with rising scan velocity the edge peak disappears and the resolution at the edge becomes worse

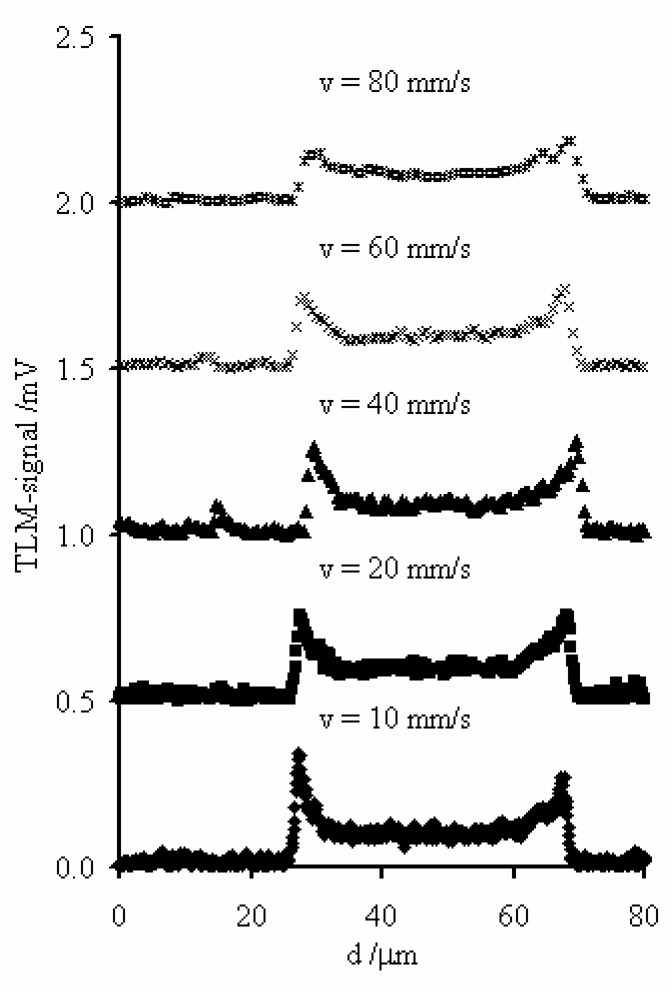

Figure 48 Signal of lateral scanning of gold stripe with different scanning velocities at a lock-in attenuation slope of 12 dB and a time constant of 10 ms (signals shifted 0.5 mV): in contrast to a time constant of 30 ms (Figure 4) the sample peaks are still established up to scanning speed of 40 µm/s

When the scanning speed was set higher, the signal became depressed and spread, the peak height became smaller and the rise time became longer.

In order to get actual spatial resolution, the rise time is multiplied by the scanning speed to obtain the signal rising distance, which corresponds to the lateral resolution. In Figure 49, the resolution (in units of beam diameters) is plotted against the scanning velocity at two time constants. For the current setup, two regimes can be distinguished. At scanning velocities between 10 and 40 µm/s of the time constant of 10 ms, the lateral resolution remains constant around twice the excitation waist diameter. In the responses at higher scanning velocities at 10 ms as well as those at a time constant of 30 ms in Figure 49, the resolution is getting worse with growing scanning velocities, where the response time remains constant.

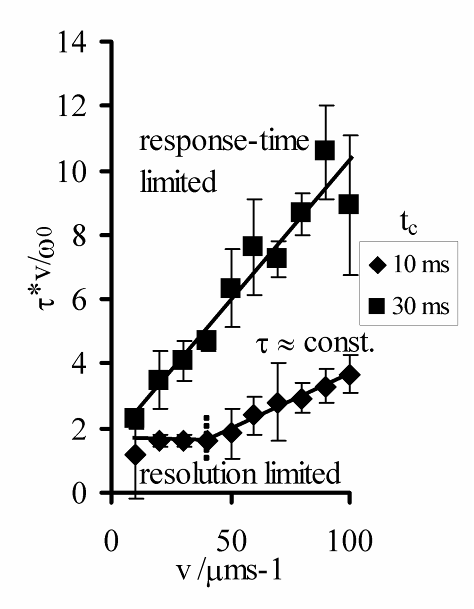

Figure 49 Lateral resolution (in units of beam width) in relation to lateral scanning velocity v at two different sampling times and an attenuation slope in the lock-in amplifier of 12 dB

The minimum resolution therefore depends on the time constant, scanning velocity and further instrumental parameters, and the following equation has to be matched for minimum resolution:

$$t_c < \frac{1}{A}\frac{d}{v} \qquad 5\text{-}1$$

A is the system factor concerning to the attenuation slope. With the applied lens with a focal spot size of 0.7 μm [eq. (1)], a resolution of about 1.4 μm is therefore possible, and the factor *A* in equation 5-1 can be calculated to 3.5, which means the time of 3.5 times more than t_c should be given for a single significant measurement. Although further investigation should be done, it is at least indicated that the continuous scanning with a speed of 40 μm/s is possible for TLM imaging, which requires only 22.5 s for 30-μm-square 2-D scan and is 100-times faster than conventional step-scan TLM. Subsequently, the relation was also confirmed for speeds up to 100 µm/s (data not shown).

Scanning experiments of the sample stripes with scanning velocities up to 1000 µm/s were also scanned successfully, but at this speed the time constant of the lock-in amplifier has to be set to 0.1 ms, which in return results in a higher noise level. At this scanning speed, biofilm measurement was therefore concluded to be difficult with the present setup, so biofilm scanning was conducted at speeds no higher at 100 µm/s.

Viewing from the opposite side of equation 5-1, a maximum scanning velocity can be calculated at a given time constant for minimum resolution at edges. In order to increase the scanning speed, the time constant should be shorter, but the time constant is restricted by the modulation frequency f, where the time constant should be larger than $1/f$. Therefore, when the modulation frequency is set higher, the scanning speed can be increased. However, the higher modulation frequency gives smaller thermal lens signal and reduces signal-to-noise ratio [178]. Furthermore, shorter time constant leads to a worse S/N ratio. In order to use high scanning speed with sufficient S/N ratio, we should investigate the optimum relationship, which may depend on absorbance, heterogeneity, refractive index, thermal conductivity and other factors.

Depth resolution experiments

Unlike in the cross-beam TLM setup, in a coaxial TLM setup the depth resolution is not limited by the irradiated spot, but also irradiation out of the focal plane results in the extension of generation of the concentration gradient above and below the sample. Those also affect the probe beam, resulting in a signal range during z-scanning wider than the sample depth [187].

The samples of stained polystyrene were scanned in z-direction with a step width of the stage of 2 µm. A signal was generated within 30 µm of depth, with linear signal response at different concentrations. The signal z-range with signals of half maximum intensity (FWHM) is taken as z-step width where signals of equal amplitude are still distinguishable. The widths of those measurements are given in Table 4.

Table 4 Signal depths for different stained polystyrene samples

Concentration (Sudan IV) [mol L^{-1}]	Signal Width (FWHM) [µm]
0.001	11.0 0 ± 2.6
0.0002	9.30 ± 2.6
0.0001	10.50 ± 3.3
0.00002	9.30 ± 3.3
0.00001	10.50 ± 4

The error of the measurement is predominantly given by the step width of the stage. With a sample thickness of 4 µm and a FWHM signal of about 14 µm, a z-step width of 10 µm for biofilm observation experiments can be assumed. As the biofilm structure reaches from about 10 µm to several 100 µm, this step width is sufficient for monitoring experiments. Nevertheless, further experiments have to be conducted to evaluate the influence of light scattering on the depth resolution in the future. A further improvement in step width can be achieved with cross-beam thermal lens experiments or a confocal TLM [191, 194, 223].

5.2.3 Two-dimensional scanning

In a first experiment for testing the ability of TLM to scan a biofilm model 2-dimensionally, a sample of agar and iron(III)oxide particles was observed. This was done point by point in distances of 1 µm. The resulting data is plotted in Figure 50.

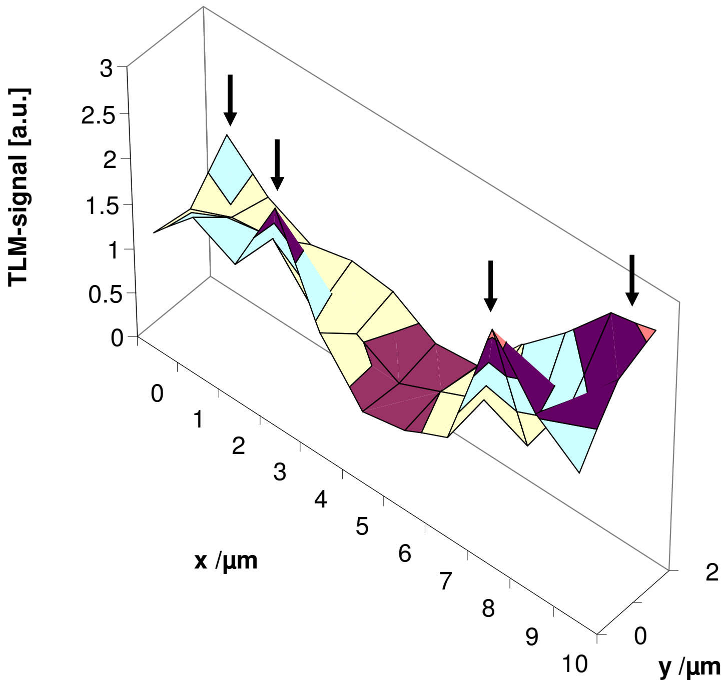

Figure 50 Two-dimensional scan of 1% agar containing Fe_2O_3 particles (c = 9 mg/L)

In the figure, differences in absorbance between sample points in neighboring lines are observed. Nevertheless, the differences are not too random, and even areas with roughly the same absorbance can be observed. Four peeks are also seen in the graph, two at the corners of the line with y = 2 µm and two at the side in the front line. These peaks could possibly be coming from iron oxide particles, as they are the strong absorbers inside the sample.

While this first measurement showed that two-dimensional spectra could be taken with the setup, a test was taken to check for stage alignment and movement. For this, two gold stripes on the gold chip were again scanned, this time in parallel rows with distances of 1 µm between each row. The results are shown in Figure 51.

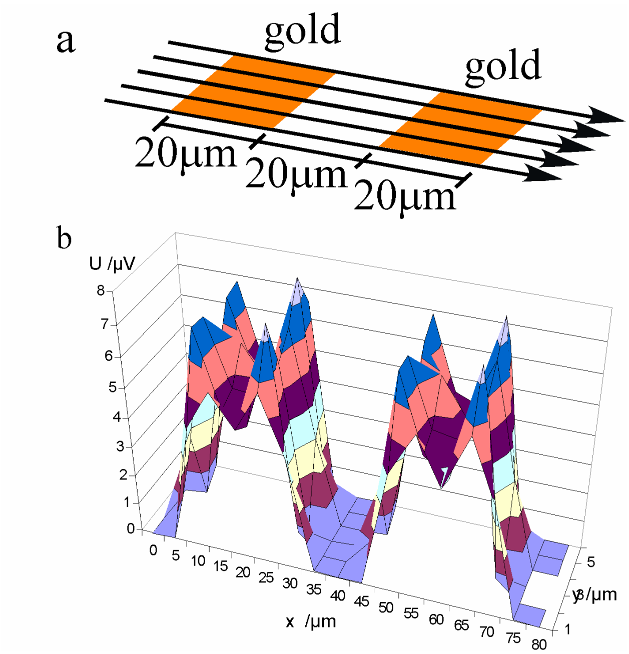

Figure 51 Two-dimensional line scan on the gold-chip: schematic (a) and TLM signal (b)

Although the signal in this experiment is not well resolved, as it was taken before the resolution optimization experiments, the graph shows that the stage is moving correctly and is well aligned.

In a next experiment, the obtained two-dimensional spectrum of a TLM measurement was compared to another imaging technique, in this case CLSM, to show the reliability of the obtained results. For this purpose, a square sample of fluorescein stained SU-8 was prepared. The obtained spectra for both CLSM and TLM are shown in Figure 52.

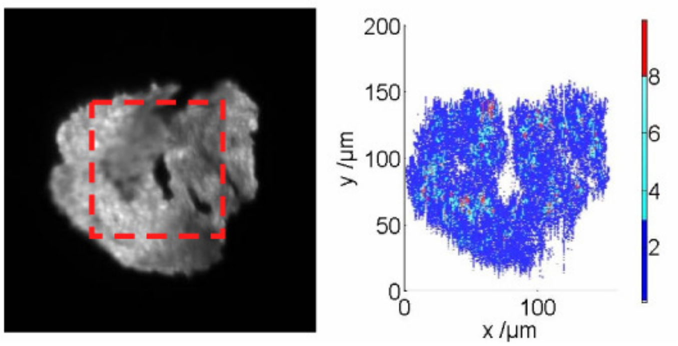

Figure 52 CLSM (left) and TLM (right) image of a SU-8 object stained with fluorescein; irradiated area (photo pattern) as red square in right image

While the pictures clearly indicate at first sight that the photopatterning of the SU-8 suspension was not totally successful, the shapes recorded by both methods look similar. The discrepancy from the square shape might arise from the suspension nature of the educt prior to photoactivation. The discrepancies in the two recorded images, seen in the bottom right corner, the middle and the small peninsula in the middle on the top can arise from images taken at different depths inside the sample. Another explanation also could be a limited sensitivity of the TLM or an overexposure with CLSM, as the missing parts in the TLM image are quite dark inside the CLSM image. Disregarding the cause, the sample was compared successfully with the two methods, and even finer structural details like the rift at right of the picture could be imaged.

A third sample for two-dimensional scanning were again scattering samples, although the purpose at this time was to find out about influences of scattering on the TLM signal. For this reason, three kinds of samples were made: samples with black particles inside (absorbing and scattering), samples with white particles inside (only scattering) and blank samples (reference). As the purpose was a little more complex, the applied samples were first characterized. For checking the difference in absorbance, TLM signal on-off experiments were conducted where the excitation beam is blocked during the off time. The results for the three sample types in this experiment are shown in Figure 53.

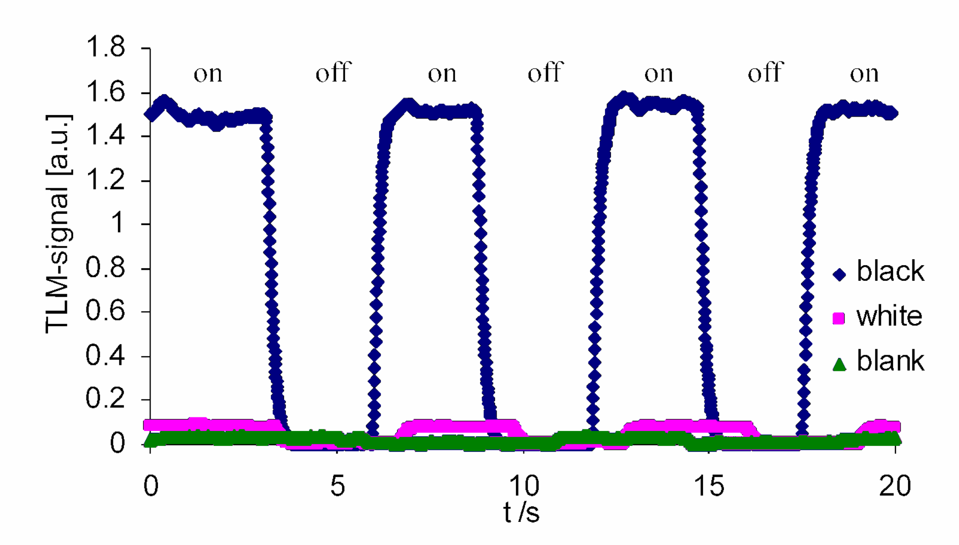

Figure 53 On-off-signal of black beads (200 µL), white beads (200 µL) and no beads in agarose gel

The black beads inside the agar gel absorb the excitation laser and therefore generate a strong TLM signal. The white beads, on the other hand, only have a very weak signal, which might arise from impurities or the agarose. Agarose itself gives of also a weak TLM signal, as was observed before and also by in earlier works [224].

The effect of different particle concentrations can be seen in Figure 54. The signal difference for black particles with 2 and 20 µL bead solution in 10 mL initial amounts can be seen in the different number of peaks. For 200 µL in 10 mL initial concentration, the peaks are not only more in number, they are also higher. This is most likely due to colocalization of particles.

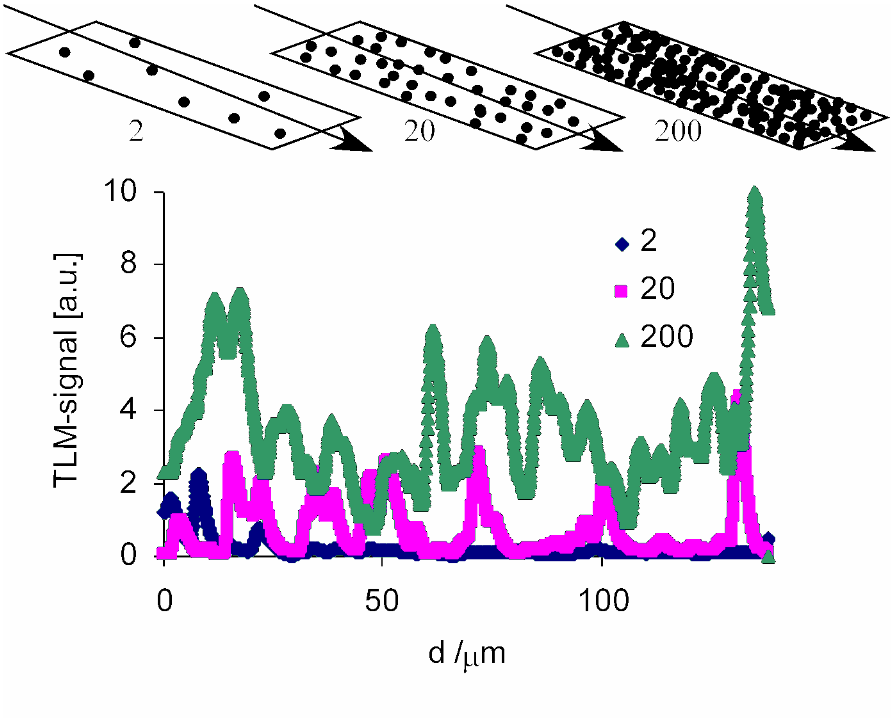

Figure 54 TLM signals of scattering black particles with different original concentrations

Signals were recorded over a range of 40 µm in depth, which is in good agreement with the results from 3D-reflection microscopy, where measured blank samples showed thicknesses between 25 and 35 µm (data not shown).

Information about thermal lens signal intensity and phase as well as the energy of the excitation and probe beam energy after passing through the sample were recorded simultaneously for the varying samples to check for correlation between the particles and scattering. A representative spectrum is shown in Figure 55.

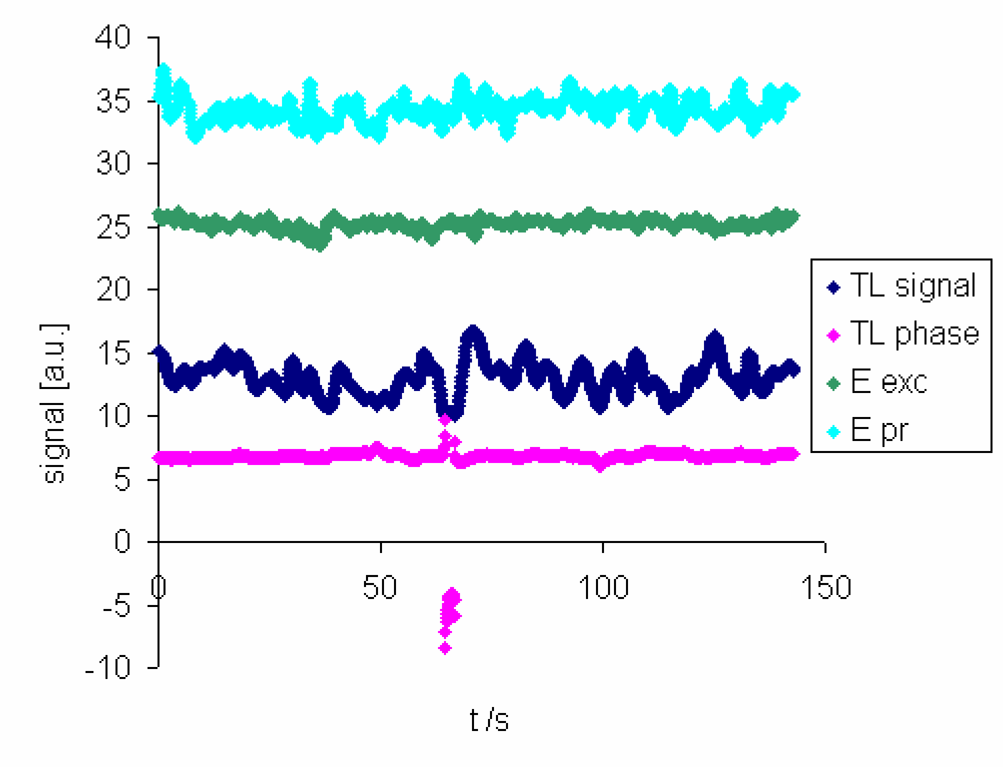

Figure 55 Thermal lens signal intensity and phase as well as energy of the excitation and probe laser after passing through the sample for one scan in the sample with 200 µL black bead solution in 10 mL water during gel preparation

For the samples, no correlation was found however between the thermal lens signal and either energy reading. This could be due to the fact that there are other factors influencing the energy readings. Most likely, however, the scattering is too complex to be found by line scans, and a more thorough three-dimensional modeling of the scattering inside the sample needs to be done to correlate measurements. As this is outside the scope of this thesis, however, further measurements for correlation were not continued. The samples, however, seem to be adequate for further experiments in this regard, as can be seen in the two-dimensional images of scanned planes inside the samples in Figures 56 to 58.

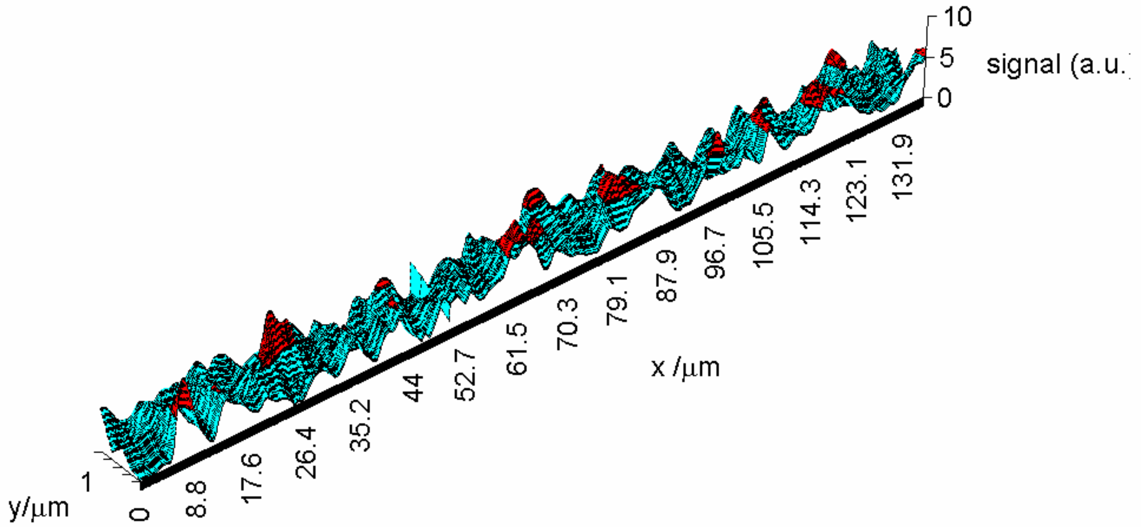

Figure 56 Two-dimensional image of TLM signal of black beads (200 µL bead solution in 10 mL water during gel preparation)

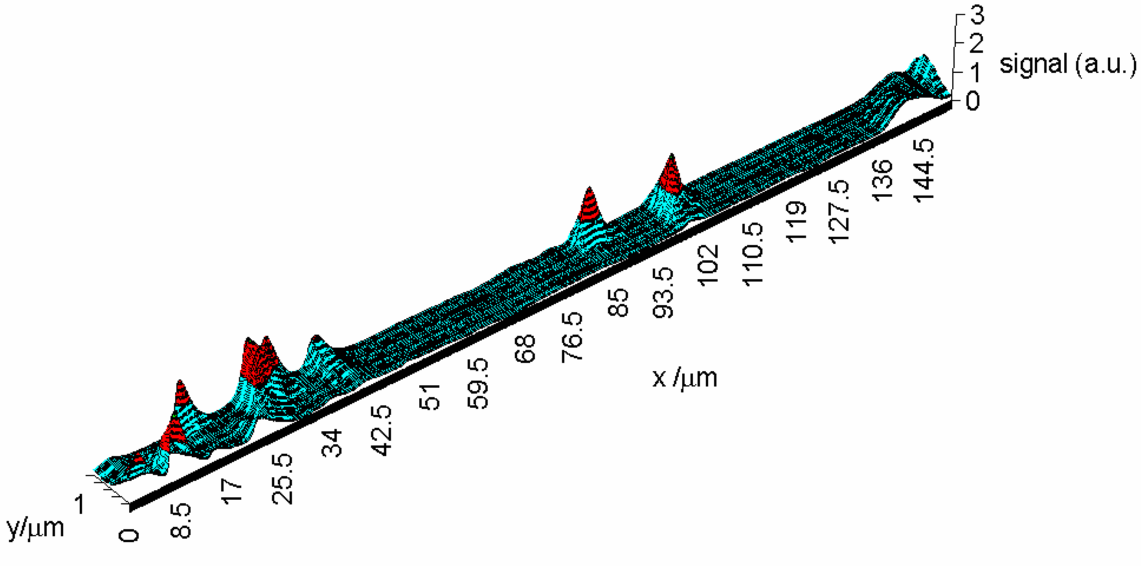

Figure 57 Two-dimensional image of TLM signal of black beads (2 µL bead solution in 10 mL water during gel preparation)

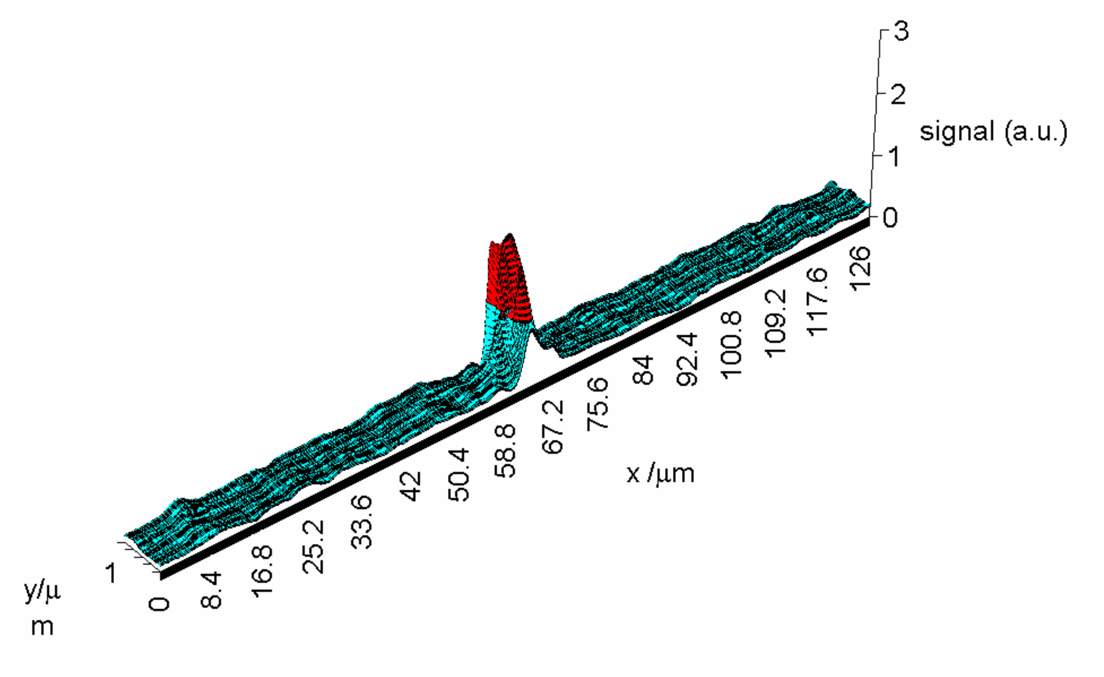

Figure 58 Two-dimensional image of TLM signal of white beads (200 µL bead solution in 10 mL water during gel preparation)

The sample with 200 µL black bead solution during gel preparation also looks 'overcrowded' in the two-dimensional view, and this concentration can be disregarded for future experiments. The sample with 2 µL black bead solution applied during gel preparation, on the other hand, shows well distinguishable peaks that are well resolved in either direction within 3 to 4 µm, which could also be confirmed with another data set. With the applied objective lens (N.A. 0.5), the minimum resolution during continuous scanning was expected to be above 2.5 µm. Only one big peak at 67 µm in *x* direction which could be attributed to contaminated dirt was seen in the sample with the white beads. The rest of this sample showed no significant TLM signal, as was expected.

5.3 Biofilm observation with TLM

In order to test the possibility of biofilm observation with TLM, a natural biofilm from a pond was tested without scanning for sensitivity during measurement. The recorded on-off signal is shown in Figure 59.

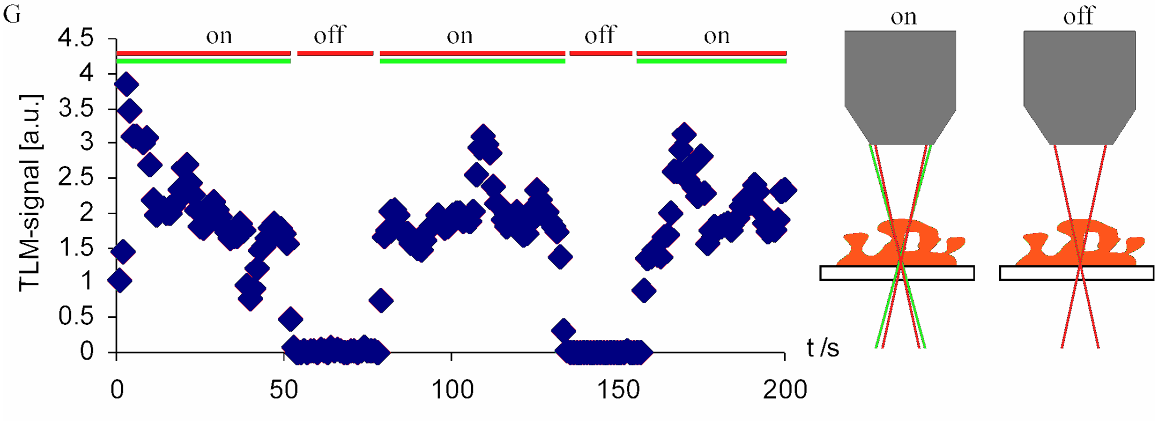

Figure 59 On-off signal of a natural pond biofilm in a glass cuvette

As can be seen, the biofilm gave a strong signal compared to the noise level. However, the signal did not remain constant over time. The reason for the change in signal amplitude is given by the fact that only planktonic biofilm was observed in this first experiment. Movement of the sample was likely to occur due to several reasons, be it the settling of the biofilm, the formation of a convective flow inside the cuvette due to the minute heating of the sample due to laser absorption or form diffusive flow. For the coming experiments, the need of attached biofilm for observation was therefore outlined. However, this first experiment showed that TLM is sensitive enough to observe biofilm samples. This result was expected, though, as TLM is a very sensitive measuring method with measurements at 10^{-4} cm^{-1} easily obtained, and biofilm absorption at about 1 cm^{-1} is quite strong for TLM application.

5.3.1 Biofilm grown on slides

Biofilm grown in flow cells grew into thick mushroom-like structures, which can be seen in picture of the unstained (left) and stained (right) biofilm in Figure 60.

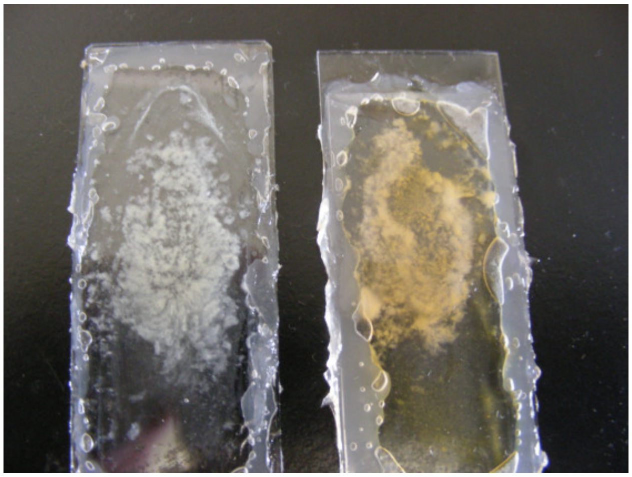

Figure 60 Pictures of unstained (left) and Acridine Orange stained (right) biofilm grown in flow cells

To gain a more detailed view of the structure of the biofilm, fluorescence pictures were taken of the stained biofilm. Representative pictures are show in Figure 61.

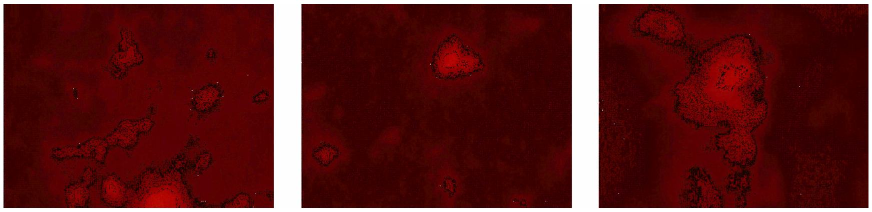

Figure 61 Detailed fluorescence images of the biofilm stained with Acridine Orange (c = 0.1 g/L)

The images show a biofilm with dense, but isolated colonies that are separated by areas free of biofilm coverage.

A detailed photograph of the biofilm grown in 9 days is seen in Figure 62(a). At the edges, the grease for sealing the biofilm in water is visible. The biofilm shows a mushroom-shaped structure as is usually seen under these growth conditions [4]. Inside the biofilm structure, a 100-μm square area observed with TLM was scanned continuously with the condition of equation 5-1 fulfilled. The result is shown in Figure 62(b). Strong absorption due to pigments within the biofilm matrix are distinguished from areas with no absorption, which is either due to no absorbing pigments or no biofilm growth in those areas. The objective lens with a numerical aperture of 0.7 allows for an edge resolution of less than 2 µm. With the scanning speed of 10 µm/s, image acquisition time for the square area is reduced to less than 20 minutes. This is a lot faster than TLM point-by-point scan, which would take some hours for the observed area. Compared to CLSM, the scanning speed is rather slow though. However, biofilm imaging of representative areas in one day is possible, even for statistical measurements. And higher scanning speeds with TLM up to 100 µm/s are possible with micrometer resolution, as described above. Therefore, the statistical measurement of biofilm growth at ten areas of 100 x 100 µm^2 within one day over a depth of several hundred micrometers with a step width of 10 µm, which is the limiting depth resolution, is possible. This is still slower than CLSM, which is the standard for biofilm *in situ* imaging with micrometer resolution. However, TLM is an observation method which can continuously monitor biofilm growth without the need for stains. Like PAS, continuous monitoring of natural biofilm is possible, but the resolution with TLM is superior.

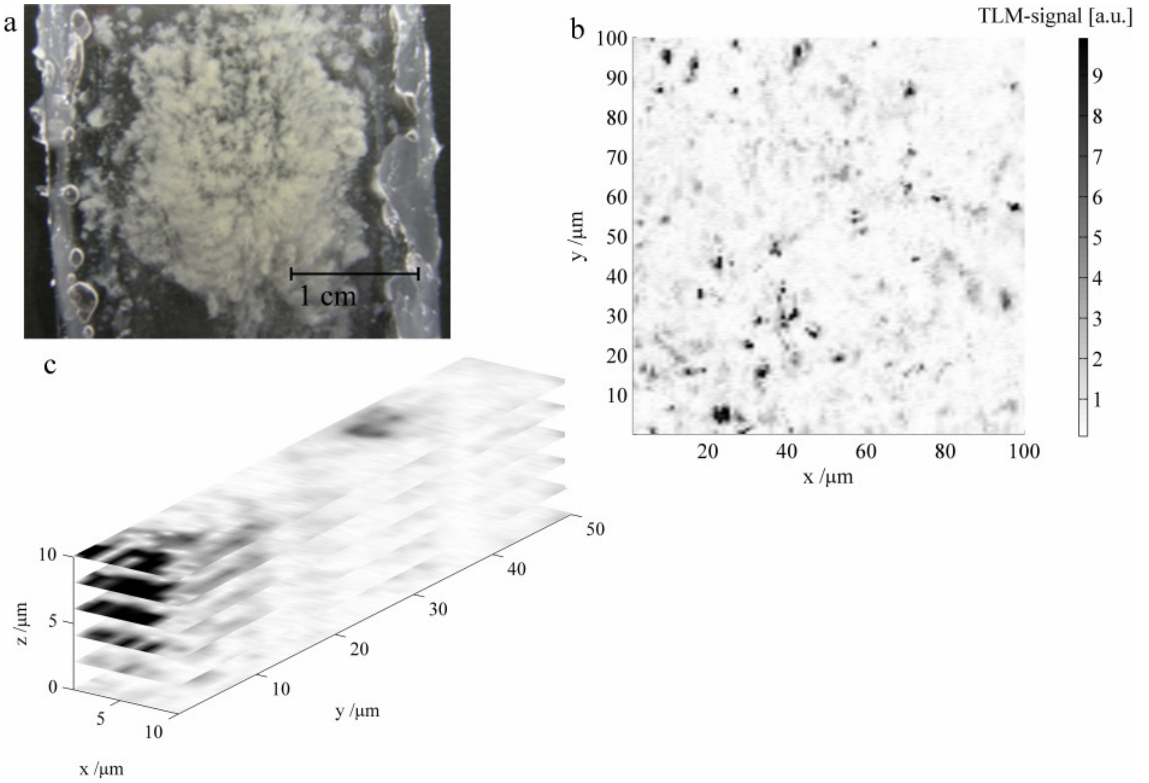

Figure 62 (a)Photograph of biofilm grown on a glass slide in a flow channel and sealed off with vacuum grease for TLM observation; (b) 2-dimensional and (c) 3-dimensional observation of unstained biofilm with TLM: stripe of (c) taken from the right hand bottom corner of (b)

For 3-dimensional visualization, a 10 µm wide and 50 µm long strip of the biofilm in the right hand lower corner of Figure 62(b) is shown in Figure 62(c). The biofilm structure at the bottom of the figure is clearly different from the structure 10 µm above at the top of the figure. A 10-µm z-step for biofilm observation is successfully applied. The results in Figure 62(c) even give a hint that depth resolution is actually better, as the biofilm structure gradually changes within the layers.

5.3.2 Biofilm grown in microchannel

For observation of biofilm inside a microchannel, the biofilm grown inside the top-on connected S-type channel was taken. Biofilm adhesion occurred throughout the S-channel. Little biofilm was observed, though, as biofilm does not adhere well to glass. A major colony formed throughout three weeks in the second curve of the channel away from the entrance (see Figure 63). Behind this colony, in flow direction, also smaller attachments were observed, which appeared probably due to seeding dispersal.

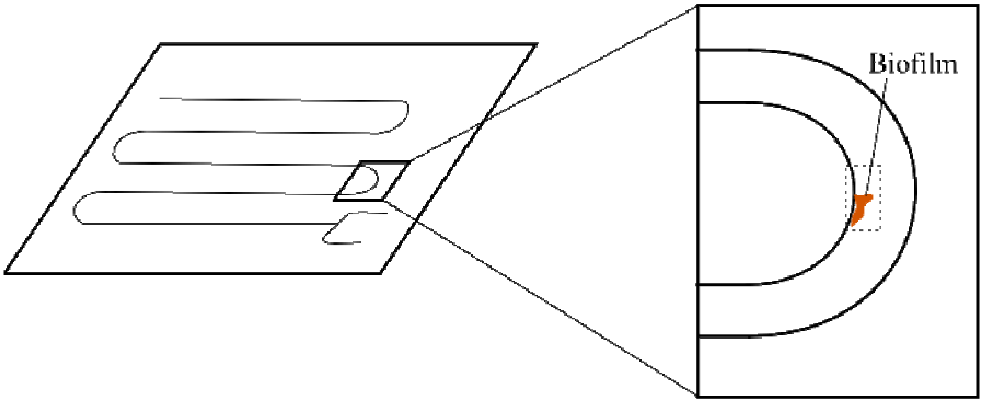

Figure 63 Schematic picture of the S-channel and the main biofilm occurrence in the second curve

The big colony in the second curve was taken for further examination with TLM. For comparison, a phase contrast image was recorded. It is shown in Figure 64 on the left. The biofilm formed in the inner side of the curve with a triangular shape, a shape that likely minimizes shear stress on the bacterial film. The biofilm formed a dense structure under the shear conditions present in the channel. The observation of one horizontal plane of the colony with TLM, shown in the middle of Figure 64, revealed that absorption of the excitation laser is not uniform within the biofilm. Localized centers of strong absorption exist, where pigments occur in higher concentration. This argues for localization of pigments in specific biofilm parts. Pigment formation by bacteria makes a colocalization of pigment absorption with bacterial cells likely. However, also a smaller background signal from the EPS might be present, as organic polymer molecules like agarose show a thermal lens signal [224].

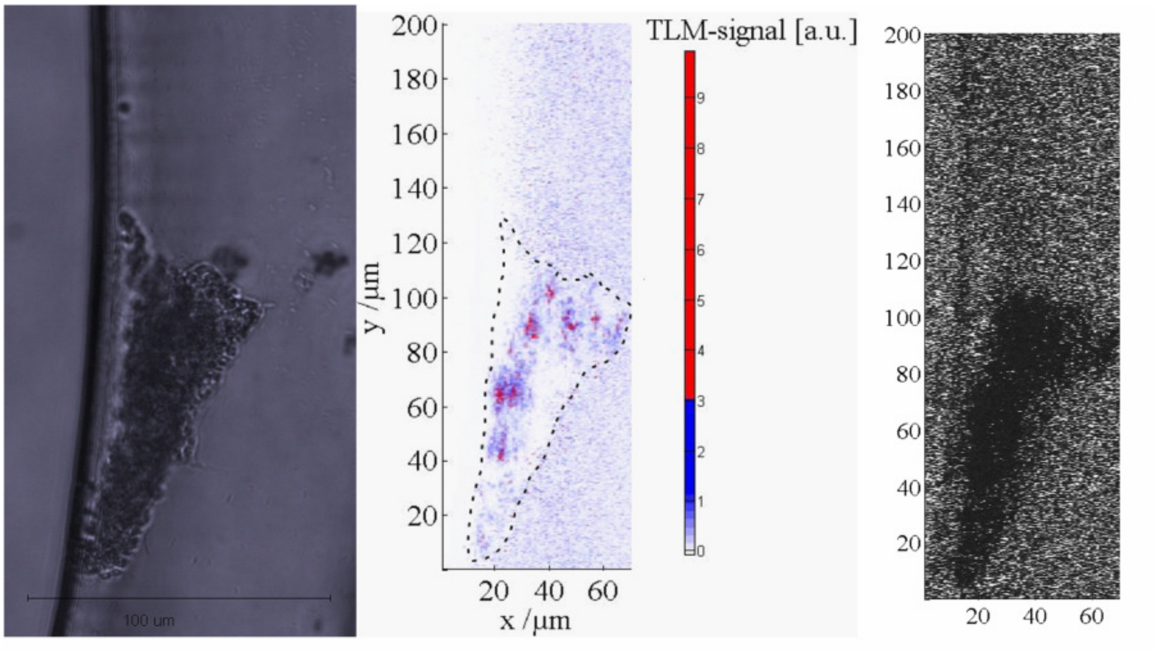

Figure 64 Phase contrast (left) and TLM image of one plane of the biofilm colony with an outline of the colony size in the TLM picture; TLM signal amplitude (middle) was not observed throughout the colony, showing that pigments are located in the biofilm at specific places; TLM signal phase (right) shows the whole biofilm structure

Figure 64 right shows the modified TLM phase image of the biofilm colony. As the phase is directly related to the thermal characteristics of the observed material, structures with similar characteristics are observed with a roughly equal TLM phase values. The biofilm, with its organic components in the bacteria and the EPS, exhibits more or less uniform thermal characteristics, as seen in contrast to the noise pattern observed in the surrounding, continuously flown water. A similar behavior was found when TLM signal phase was used to study yeast cell wall structure [193]. However, as noted at that time, a direct analysis of the TLM phase is difficult due to the manifold factors influencing the phase. In this thesis, the approach for image generation with the TLM phase is different, as the change of the TLM phase to adjacent points is compared. This way, regions that generate a similar TLM phase value are showing a strong signal. With this method, the biomaterial in the EPS contrasts the surrounding water. The thermal properties of proteins and polysaccharides, for example starch, are different from water, but approximate the value of water with rising water content [225, 226]. While this change in the thermal characteristics might not be a major influence while monitoring biofilm with PAS, the different thermal characteristics of the biofilm matrix compared to the surrounding water are evident. Even a weak absorption of the EPS components cannot be excluded, as agarose shows thermal lens signals when excited at a wavelength of 514 nm [224]. The water itself gives no homogeneous signal, as it is flown continuously. The flow affects the thermal conduction and therefore the TLM phase.

Another interesting feature of the TLM signal amplitude and phase pictures in Figure 64 is the microchannel wall. In the signal amplitude picture, the chip is seen as white surface, as the glass shows a very weak thermal lens signal, in contrast to the impure water (nutrients, biofilm parts, contaminations) in the channel. In the phase picture, the wall is seen as a dark line of similar thermal characteristics, which might be due to adsorbed proteins. Glass is not observed in the TLM signal amplitude and phase images. Similar results were observed also when imaging bacteria on a glass objective slide with a cross-beam TLM setup [191]. A higher thermal conduction at the glass wall leads to the generation of a thermal gradient upon absorption independent of the spatial distribution of the laser [178]. This might be the reason that the channel wall is clearly visible in the signal phase image of TLM.

During three-dimensional observation, the depth resolution with this coaxial TLM setup is limited to about 10 μm. Therefore, a step width of 10 μm was chosen for scanning of horizontal planes within the biofilm structure. A closer step width could be realized with a cross-beam TLM setup [191]. However, as the biofilm structure is normally in the range of a few tens of micrometers up to thicker structures of a millimeter, if not confined in microchannels, a step width of 10 μm is considered sufficient. The resulting pictures for TLM signal intensity and phase are shown in Figure 65. The biofilm colony shows a non-homogeneous growth at the channel wall. The tip of the biofilm structure (bottom in Figure 64 and right side in Figure 65) is located closer to the bottom of the microchannel, whereas the wider end of the biofilm (in flow direction) is located closer to the cover plate of the microchip.

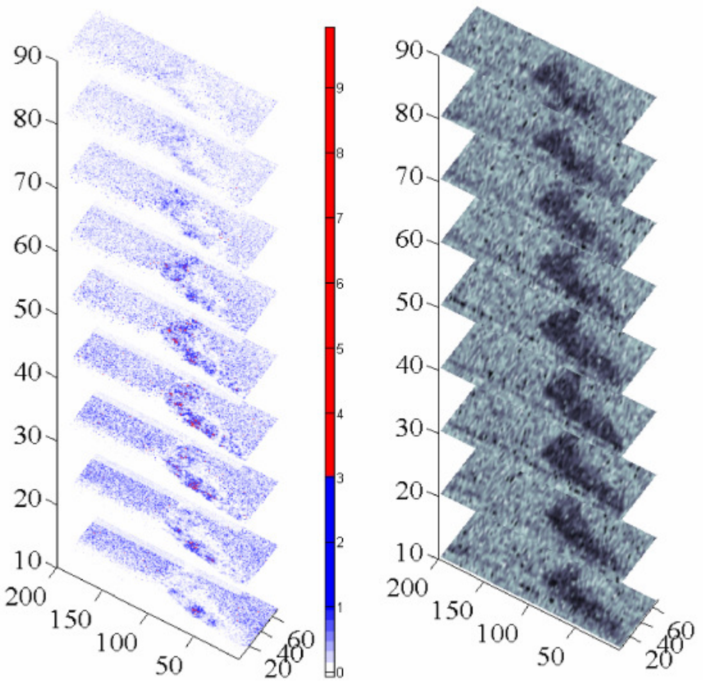

Figure 65 Three-dimensional plot of TLM signal intensity (left) and signal phase (right) of biofilm colony in the microchannel

With TLM, for the first time the pigment structure in a biofilm can be observed with micrometer resolution. The common method for measuring pigment levels in biofilm is still the application of a spectrophotometer [5, 227-229]. Using this method, pigments cannot be located in the biofilm matrix, though. Other methods for pigment observation in biofilm exist, but focus on chemical elements for observation. For example, the manganese oxidation state can be monitored by STXM in combination with NEXAFS [132] Zinc sorption measurements were taken with X-ray absorption fine structure spectroscopy, but no 3-D structure was obtained [151]. Pigments observed with the TLM measurements show absorption at 532 nm. Examples of pigments absorbing radiation at this wavelength are derivates of cytochrome c’, which have been purified from several bacteria [230-232].

Many other pigments like carotenoids, riboflavin and chlorophyll can be found [229, 233, 234]. The separation of pigments from biofilm is tedious, and the pigments are not easy to identify [233, 235]. TLM should be able to image those pigments and can elucidate the function of those pigments in biofilms by varying the excitation laser wavelength. In addition, the localization of colloids inside biofilms, their removal and their chemical disposal might be elucidated using TLM. Pollutants bound to colloids and their influence on biofilms are of interest, as well as the effect of colloids on biofilm stability (for example in WWTP) [124]. With TLM, the influence of pigments and particles on biofilm structure should be determined in upcoming experiments. In addition, further roles of pigments in biofilms might be elucidated. By localizing pigments, also useful information about their need and their functions might be gained. Interestingly, slightly more pigmented bacteria were found in biofilm than in bulk bacteria in a drinking water distribution system [14]. The amount of pigmented bacteria could not be related to water quality parameters, though. Understanding the functions of pigments, this could help determining biofilm occurrences in water systems.

In the future, it should furthermore be possible to image other components of the biofilm matrix with TLM, as absorption spectra of biofilm could be generated with PAS [142]. UV lasers as well as white light sources could function as light sources in this case, which recently were reported as excitation sources in thermal lens measurements [193, 236]. With TLM, information about biofilm structure can be obtained staining-free in flow systems. This way, a nondestructive observation of biofilm in its natural state without a possible interference of stains is possible. As no stains are needed, TLM can also be applied for continuous online, *in situ* monitoring of biofilm with micrometer-resolution, even in thicker biofilms. In addition, the influence of particles or pigments on biofilm stability and their role in biofilm formation, growth and maturation can be studied using TLM.

A further biofilm monitoring experiment was conducted to elucidate the improvements resulting from an increase in numerical aperture of the objective lens. The biofilm grew on a splinter inside an I-type top-on connected channel. The images of the splinter with the biofilm are presented in Figure 66.

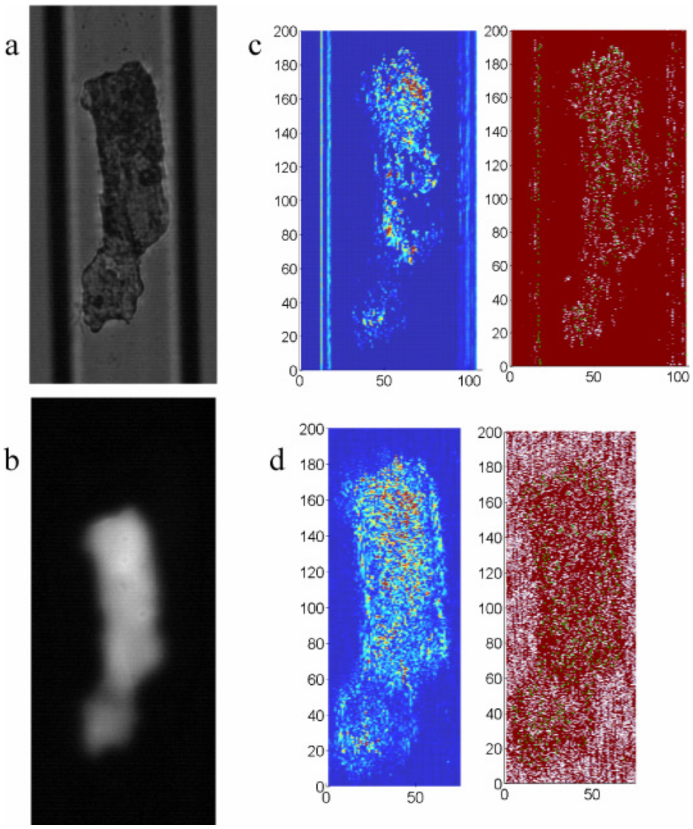

Figure 66 Bright field (a), fluorescence (b), and thermal lens images (c, d) of biofilm grown on a PEEK splinter inside a microchannel; thermal lens signal and phase were recorded with an objective lens with a numerical aperture of 0.5 (c) and 0.9) (d)

The fluorescence in image Figure 66 (b) results most likely from background fluorescence from either biofilm or, more likely, the PEEK splinter. The comparison of TLM observation with objective lenses with different numerical apertures in Figure 66 (c) and (d) revealed that the higher numerical aperture resulted in images with a better resolution. This was accompanied by a need for higher excitation beam intensity and a simultaneous loss in sensitivity. The theoretical resolution for continuous scanning TLM with an objective lens with a numerical aperture of 0.9 is about 1.4 µm.

In the image with the higher numerical aperture (Figure 66 (d)), more detail of the sample is gained. This is most likely due to the smaller excitation beam spot size, as the TLM signal is a result of averaging over the beam spot. On the other hand, the sensitivity with the lower numerical aperture of 0.5 within the observation spot during observation might not be high enough to image the complete biofilm, as can be seen in Figure 66 (b). As a result, not the whole sample is imaged. The question of the origin of the TLM signal remains for this sample, though, as also the PEEK splinter can be considered as a source for a TLM signal. However, the application of the higher numerical aperture is justified, as more detail of the sample is gained.

6 Summary and outlook

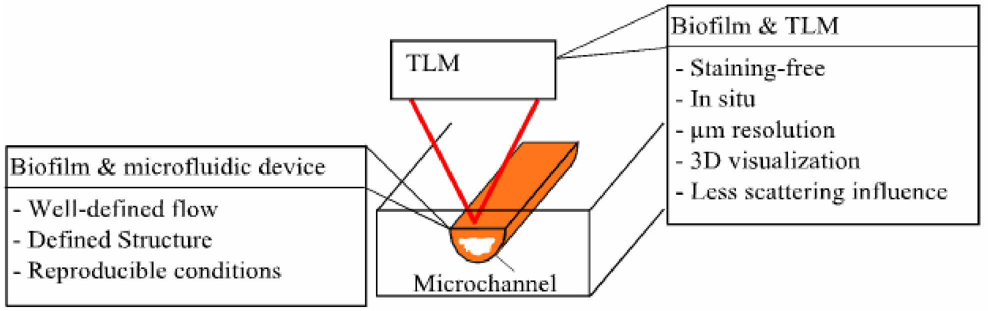
TLM
Biofilm & TLM
- Staining-free
- In situ
- µm resolution
- 3D visualization
- Less scattering influence
Biofilm & microfluidic device
- Well-defined flow
- Defined Structure
- Reproducible conditions
Microchannel

Figure 67 Advantages of microfluidics and TLM for biofilm research

In this thesis, the applicability and possible benefits of microchannels and thermal lens microscopy for biofilm research were presented. The main advantages of each application are summarized in Figure 67. Microfluidic devices are applied as flow channels with well-defined flow that can easily be produced and modified and grow biofilm under reproducible conditions. They are easy to handle and easy to observe. Further advantages include the small amounts of reagents needed and waste produced as well as the possibility for multiplex parallel experiments in limited space. TLM is a microscopic technique that allows staining-free, *in situ*, online observation of biofilm structures with micrometer resolution. Three-dimensional images can be taken. Whereas other non-staining observation techniques have problems with *in situ* observation of biofilms due to the strongly light-scattering biofilm matrix, TLM is hardly influenced by it. A detailed description regarding the aims and scope of this thesis follows.

Microchannel as pipe model for biofilm growth

The microchannel was adapted to biofilm research due to a number of setup changes, mostly in regard to capillary connection to the channel. While prior systems led to clogging inside the microchannel, a side-on connection proved to be useful. Also, it seemed necessary for biofilm growth observation to have channels with a minimum width and height, which was chosen at 400 µm and proved useful for the experiments. By further optimization of the connection port, dead zones near the capillary entrance and exit were reduced in biofilm growth experiments. Another setup change was made from a pump-driven flow system to a pressure-driven flow system. Both systems can be applied to continuous biofilm growth experiments. The pressure-driven flow system seemed favorable in the end as no pressure pulses occur. Also, the system can be easier upgraded to a multiplexing system, as parallel flow experiments are not limited by the availability of pump ports. In fact, a system with 12 lines is currently being tested for further research and showed a good pumping performance. Depending on the application, a system with pulsed flow or with continuous flow might be favorable though.

Bacterial growth could be observed with both systems, and both systems could be cleaned afterwards, so recycling of the equipment is possible. This is especially important for the microchannel, which is the most expensive part of the setup. However, with other production methods or mass production, the costs for the microchannel can also be cut. In the course of the thesis, however, the production of other channels using soft lithography failed.

The experiments conducted in the channel showed biofilm behavior that is similar to macroscale experiments. During application of surface modification procedures in parallel microchannels hydrophilic surfaces limited the amount of biofilm growth, whereas hydrophobic surfaces limited biofilm retention during the application of an air plug. Both surfaces therefore had pronounced effects on the biofilm during the one month experiment. A clear judgment for either approach cannot be made, though, as both methods showed about the same amount of biofilm remaining. As recently surface modification methods for implants, intraocular lenses or medical devices are increasing in number and usage, surface modification chemicals become cheaper. Therefore, it seems reasonable to consider surface modification methods for water conducting systems, water storage systems and wastewater treatment systems in the future. This has to be done with consideration to applied cleaning procedures and removal chemicals, where even synergetic effects might arise. Also, the bacterial composition at the start influences biofilm growth, which makes a multi-experiment approach reasonable. For this purpose a fast, easily observable and well defined multi-test system is needed. A non-flow, screening device for biofilm removal and disinfection strategies has been introduced before [120]. However, biofilm grown under dynamic conditions differ from those grown under static conditions. The microchannel can be applied in future as a pipe-like, high throughput testing device for flow systems, where parallelization and easy online observation is possible. Tests on surface modification chemicals and removal strategies can then be carried out in combination with combinatorial approaches for surface modification procedures, enabling manifold new suggestions for future water system engineering [222].

An interesting observation was made during biofilm removal experiments. An adhered biofilm removed from the surface as a whole rather than breaking into pieces upon application of sodium hydroxide solution. The same observation was made with biofilms grown in the pressure-driven flow system, although the actual removal conditions in the channel remain unclear at this point. However, the results hint on the importance of the linking film, the biofilm part that connects the surface and the biofilm. Future removal could eventually concentrate on breaking the linking film rather than try to break up whole biofilm.

In summary, the microchannel has met the requirements for application as a model for biofilm growth in pipe-like structures:

1. Shear stress in the existing systems was comparable to conditions found in literature, showing the applicability of microchannels to biofilm research.
2. Biofilm adhesion and growth were observed online and staining-free in various microchannel systems.
3. Dead zones in the microchannel system and problems with the connection between channel and capillary were recognized. Clogging occurred in the top-on connected channels. Optimization of the setup then focused on avoiding those problems, and new systems were devised.
4. Clogging in the microchannel was avoided by using microchannel systems with side-on connection. Through enlarging of the entrance and exit holes for the capillary, the dead zones inside the microchannel were minimized.
5. Biofilm grown in the various setups could be removed by chemical or physical means or a combination thereof, making the channels available for reuse.

6. Parallel experiments in the channel were conducted with varying surface conditions, showing the versatility of the setup. All other parameters influencing biofilm growth could be kept constant in the setup.
7. The hydrodynamic conditions can be varied in a broad range and enable detailed research of biofilm behavior under varying shear conditions. The application of the shear range is limited with the present method to laminar flow conditions, but microchannel research under turbulent conditions was carried out before. With the pressure-driven setup, parallelization of experiments in high numbers is possible, as a system with twelve parallel channels was tested successfully for parallel flow. Future experiments in this system and bigger systems should enable multiple parallel biofilm experiments with systematically varied conditions.

For the future, the following statements can be made for the application of microchannels to biofilm research:

I. The microchannel as a model for a water-bearing pipe is an efficient tool for observation of biofilm attachment, and biofilm growth under defined flow conditions and shear conditions comparable to real pipes for a period extending one month is feasible.
II. The microchannel offers the possibility for online, *in situ* observation of biofilm development without sample removing and of the influence of change of experimental parameters on biofilm structure.
III. Parallelization of experiments in microchannel enables the research of multiple experimental parameters (surface condition, flow, removal agent …) at the same time, making it a possible device for combinatorial approaches to biofilm research.
IV. With the microchannel, screening of biofilm growth under various conditions can be carried out. As the microchannel setup is small, even screening for biofilm growth at sampling sites with microchannels modified to simulate the existing site situation should be possible.
V. As the microchannel shape can easily be modified, biofilm growth in different setups (curves, branches, etc) can be compared.

TLM for online observation of biofilm

TLM experiments were carried out to characterize the system and show its applicability to biofilm experiments. In the course of experiments, factors that limit the image quality, resolution and quantification were determined and tried to resolve.

With TLM, like with PAS, staining-free online observation of biofilm is achieved. In contrast to PAS, a lateral resolution comparable to bacteria size is possible while depth resolution in TLM is comparable to PAS. With a higher numerical aperture, a z-resolution in the micrometer range should be possible. Unlike CLSM, micrometer resolution is possible without staining, and, therefore, the biofilm structure can be monitored for a long time without fluorescent staining or addition of hybridized bacteria. TLM can be applied as a long time online monitoring device for biofilm growth and removal, without influences from staining procedures. After a research regarding scattering irradiation losses within the biofilm matrix, also a direct quantification of the biofilm structure should be possible.

With the thermal lens microscope, the online observation of biofilm parts which are not observable even with staining, e. g. pigments, is possible. The pigment structure of a biofilm was observed online with micrometer resolution for the first time using TLM. But the observation is not limited to pigments, but any other molecule class in the biofilm absorbing radiation can be observed with the proper excitation laser. With PAS, another photothermal method, biofilm spectra also were recorded for carbohydrates in biofilm [142]. However, lateral averaging is done for spectra, whereas TLM enables a lateral resolution in the micrometer range. In yeast cells, proteins were recorded successfully with TLM [193]. Unlike fluorescent methods like CLSM, TLM measurements are not limited by effects like photobleaching, and sensitivity of measurement is very high [190]. As TLM can observe other biofilm components than CLSM, it can also be applied for comparative studies. A recent study reported on the combination of TLM and CLSM observation method in one setup [199].

With the continuous-scanning TLM setup, sample areas of 100 x 100 x 100 µm, with a z-step width of 10 µm, can be scanned within a little more than 15 minutes, which is comparably fast to spot-by-spot scanning [177]. This way, several sample areas for statistical analysis can be recorded in one day, making online monitoring of biofilm growth possible. In the future, we plan on monitoring of biofilm growth in the microchannel with the present TLM setup, and compare the results of the TLM observations with CLSM measurements.

TLM was successfully applied in observation of online, *in situ* biofilm 3-D pigment structure. The biofilm was grown in a microchannel, and formed a structure which minimizes shear force on the colony, in the inner wall of a curve. Pigments were not spread homogeneously throughout the film, but were localized. The lateral resolution of the continuous scanning TLM of about 2.6 μm enables the observation of structures which are about the size of bacterial cells. Combining TLM with microchannel, the system will be a powerful tool for biofilm online structure monitoring under varying conditions in parallel.

The following statements can be regarding the aims of this thesis for the online observation of biofilm with TLM:

1. A continuous scanning system for TLM measurements was devised and characterized regarding instrumental parameters.
2. Signal output was optimized for instrumental settings.
3. Heterogeneous systems were measured with the TLM, and the measurements showed the applicability of TLM for micrometer-resolved experiments in those systems.
4. Biofilm structure was observed with the TLM system for various biofilms.
5. A three-dimensional online observation of TLM structure grown inside a microchannel was successfully conducted.
6. The TLM measurements were compared to various observation methods, including CLSM measurements with a reference sample and bright field and fluorescence measurements for biofilm samples.
7. The TLM system with its excitation laser of 532 nm was applied successfully to probe absorbance inside a biofilm sample. This way, the pigment structure inside biofilms, which is not easily observable with other methods, can be observed with micrometer resolution.

To summarize the findings made during the characterization and application of TLM for biofilm observation, the system is compared to the other systems in Table 1.

TLM, like all microscopic methods, is able to perform online, *in situ* measurements on biofilm. It is non-invasive and, in contrast to CLSM and other fluorescent methods, does not require staining, enabling the observation of the 'raw' biofilm structure. Structural observation can be made with resolution of a few micrometers in both directions, which is sufficient for biofilm imaging. Quantization of the structure is of now not possible, but semi-quantitative results are recorded as the TLM signal is proportional to the absorbance inside the sample. The depth penetration of the system remains unclear at the moment, as no biofilm with a thickness higher than 100 μm was observed. As TLM is comparable in signal generation to PAS, depth penetration should be possible for thicker biofilms. The sensitivity of TLM to biofilm methods was not researched in this thesis. However, TLM is a very sensitive method for measurement of trace amounts of samples in liquids [183]. TLM records sample absorbance inside the biofilm, and therefore information about the chemical composition can be gained. Also, whole biofilm can be recorded, especially if it is localized inside a microchannel. Otherwise, TLM at the present stage should be able to perform statistical measurements on bigger biofilms with numerous repetitions, comparable to CLSM. The scanning speed with TLM remains slower compared to CLSM at this moment, though. Biological information cannot be recorded with TLM, but could be possible in future applications using immunogold-staining, which has already been applied to other biological samples [188-190]. Information about the bacterial environment can be recorded with the TLM system. With the present setup, pigments inside the biofilm were measured. Pigments can also be applied externally, e.g. iron oxide particles, and the interception of those particles has already been monitored with PAS [124].

In conclusion, TLM should be capable of measuring the whole biofilm with micrometer resolution and give insight into its structure and its constituents. Further experiments are needed, though, for signal quantification, and at this point scattering theory should be included. Also, further improvements can be made to the system, one being the combination with CLSM for simultaneous recording of multiple parameters inside a biofilm. TLM is not a system that should replace CLSM, but it seems an appropriate method that can easily complement it.

7 Appendix

7.1 Abbreviations

AHL	acylated homoserine lactone
AOM	acousto-optic modulator
APTS	3-aminopropyltriethoxysilane
CAM	contact angle measurement
CLEM	correlative light electron microscopy
CLSM	confocal laser-scan microscopy
CTC	cyanoditoryl tetrazolium chloride
DIC	differential interference contrast
EDC	1-[3[(dimethylamino)propyl]-3-ethylcarbodiimide
DAPI	4',6-diamidino-2-phenylindole
EB	electron beam
EPS	extracellular polymeric substances
FCS	fluorescence correlation spectroscopy
FISH	fluorescence *in situ* hybridization
FLIM	fluorescence lifetime imaging microscopy
FRAP	fluorescent recovery after photo-bleaching
FRET	Foerster resonance energy transfer
FITC-ConA	Concanavalin A tagged with fluorescein isothiocyanate
FTIR-ATR	Fourier-transform infrared attenuated total internal reflection
HDPE	high-density polyethylene
HPC	heterotrophic plate count
IR	infrared
LISNA	light induced scattering around a nano-absorber
MAR	microautoradiography
MATH	microbial adhesion to hydrocarbons
MOPS	3-Morpholinopropanesulfonic acid
MPC	2-methacryloyloxyethyl phosphorylcholine

MUO	micro unit operation
OCT	optical coherence tomography
ODS	octadecyltrichlorosilane
MRD	modified Robbins device
MUO	micro-unit operation
NEXAFS	near-edge X-ray absorption fine structure spectroscopy
P. aeruginosa	*Pseudomonas aeruginosa*
PAS	photoacoustic spectroscopy
PBS	phosphate buffered saline
PDMS	poly(dimethylsiloxane)
PIC	photothermal interference contrast
PQS	*Pseudomonas* quinolone signal
PTFE	polytetrafluorethylene
PVC	polyvinylchloride
QS	quorum sensing
SEM	scanning electron microscopy
S/N	signal-to-noise
SPR	surface plasmon resonance
STED	stimulated emission depletion
STXM	scanning transmission X-ray microscopy
TEM	transmission electron microscopy
TLM	thermal lens microscopy
TLS	thermal lens spectroscopy
TOC	total organic carbon
WWTP	wastewater treatment plant
XPS	X-ray photoelectron spectroscopy
µTAS	micro total analysis system

7.2 Letters and symbols

a	depth of the microchannel
b	width of the microchannel
C_p	specific heat capacity
d_{pin}	diameter of pinholes used for laser spot measurements
k	thermal conductivity
D	equivalent diameter
F	friction factor
$I(r)$	intensity of the excitation beam
L	path length
n	refractive index
$N.A.$	numerical aperture of objective lens
P_e	power of excitation laser beam
P_{pin}	laser power measured through a pinhole
$P_{w/o}$	laser power measured without pinhole
$Q(r)$	heat generated after absorbance
r	radius
Re	Reynolds number
T	temperature
t_c	thermal time constant
$\overline{u}$	average velocity
z_c	confocal distance
α	thermal diffusity
Δp	pressure drop
ΔT	temperature change
ε	absorption coefficient
λ	wave length
λ_{pr}	wave length of probe beam
ν	frequency
Φ	phase shift

ρ	density
τ	rise time of TLM signal from noise level to maximum
τ_w	wall shear stress
ω_0	laser spot size at beam waist
ω_e	beam radius of excitation beam
ω_{pr}	beam radius of probe beam

7.3 Japanese pipe materials

Japanese pipe materials were briefly tested for their surface characteristics for reference measurements to compare them to the applied surface modification methods inside the microchannels. As they are not connected to the biofilm research part except for the reference to contact angles, the procedures and results regarding those pipe materials will be introduced here. Pipe materials for which experiments were conducted were made of high-density polyethylene (HDPE), polyvinylchloride (PVC), coated steel and concrete, which are shown in Figure 68. They were provided by Dr. D. Simazaki, Japanese Institute of Public Health.

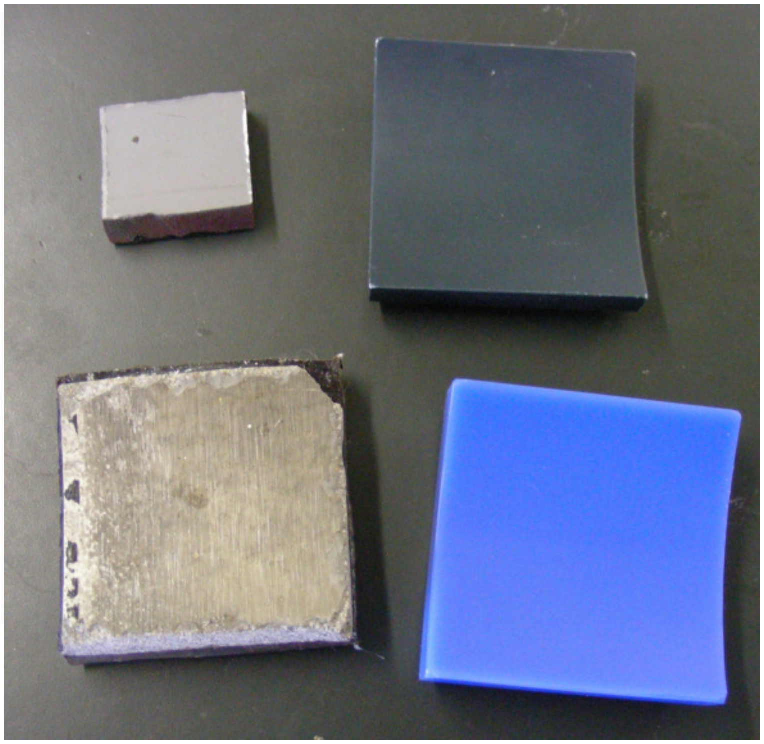

Figure 68 Pipe materials in Japan: coated steel (top left), PVC (top right), coated concrete (bottom left) and HDPE (bottom right)

For surface characterization, CAM, AFM measurements and coating experiments (with a TOC measurement for combined liquids) were conducted.

Contact angle measurements were conducted as described above directly on the samples. To check on the influence of water contaminants on the surface properties, further contact angle measurements were conducted after one and 24 hours while dipping the materials in tap water. Contact angle measurements were conducted in triplicate. The results of the contact angle measurements are shown in Figure 69 to Figure 71.

The contact angle of all materials was between 70 and 85 degrees and didn't change significantly by dipping the materials in tap water. The pipe materials therefore all are hydrophobic and most similar to surfaces modified with APTS.

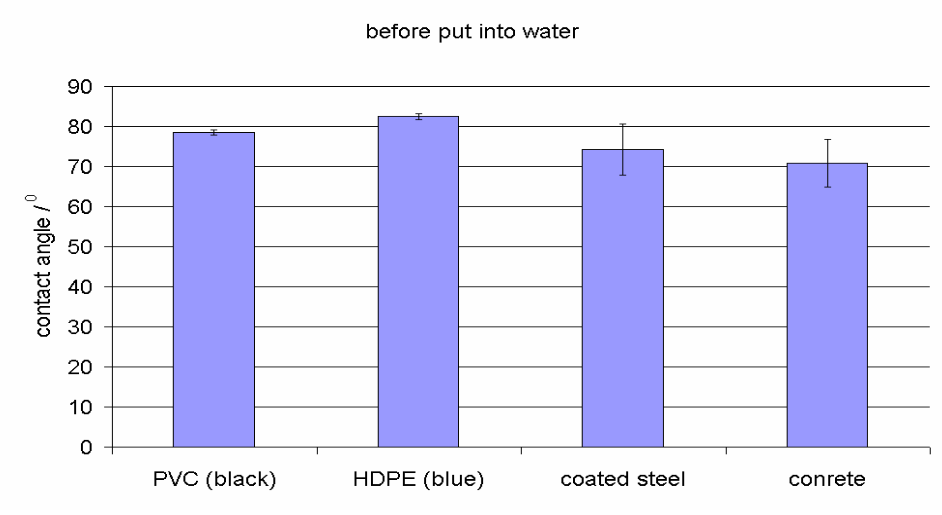

Figure 69 Contact angles of Japanese pipe materials

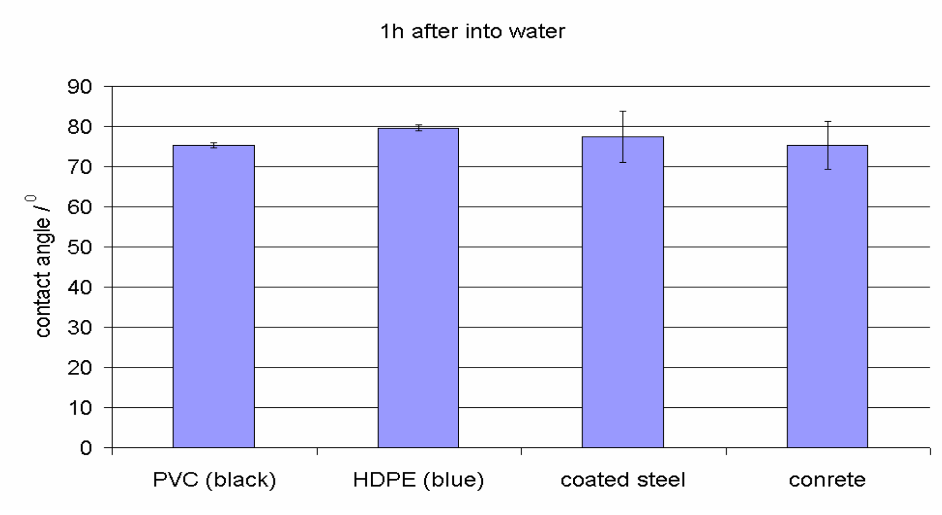

Figure 70 Contact angles of Japanese pipe materials after remaining 1 h in tap water

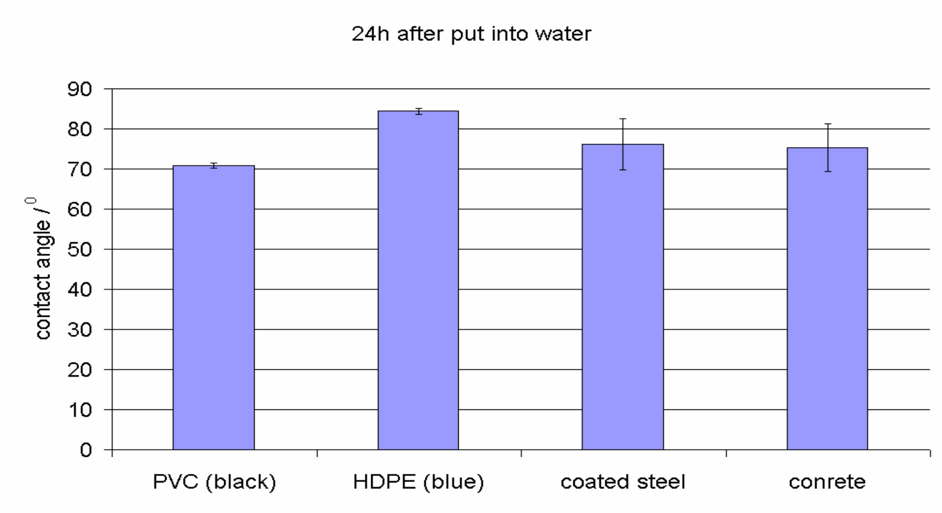

Figure 71 Contact angles of Japanese pipe materials after remaining 24 h in tap water

AFM measurements showed a roughness of about 100 nm for PVC, HDPE and coated steel and 500 nm for coated concrete. Therefore, concrete was the only material with a micro-roughness that is maybe relevant to initial adhesion. For the other materials, attachment experiments on glass, and therefore inside a microchannel, seem to be sufficient for modeling.

Coating experiments were conducted with tap water, where sufficient amounts of proteins, lipids, etc. should be contained. After 24h of dip-coating the samples in water, they are stained with a solution of Biotin-FITC in PBS buffer (1mg/mL) for 60 minutes, washed with PBS buffer and examined for epifluorescence with a FITC filter. All samples showed localized fluorescence, with slightly less fluorescence observed on the HDPE sample. For biofilms grown in systems with those materials, the occurrence of a conditioning film prior to biofilm attachment is therefore likely. However, the results of this preliminary testing are insufficient for actual knowledge about occurrence of a conditioning film. TOC measurements showed a decline from 2.13 to 2.02 ppm within one hour for the combined liquid of the samples, which was followed by a rise to 2.95 ppm after 24 h. This rise was accompanied by rusting of the coated steel sample at the cutting edges, which is the likely cause for this increase. For more exact determination of surface states of pipe materials, a more thorough testing is necessary. However, the preliminary results about pipe materials show the possibility to test materials and model them by other surface coatings inside model systems.

7.4 Design drawings

Bottom of flow chamber, as designed by S. Wiesemann, Institute of Hydrochemistry, Technical University Munich.

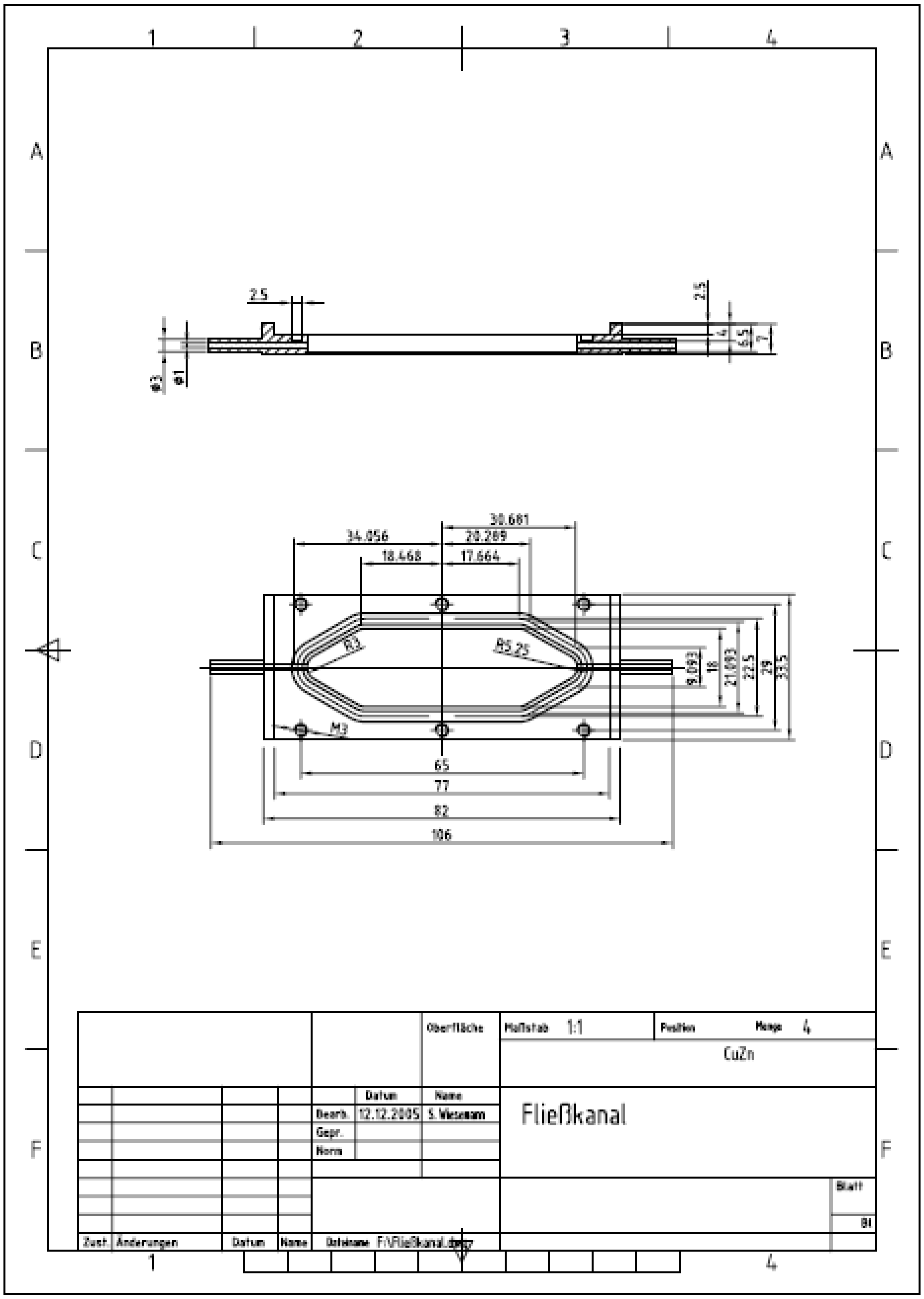
1
2
3
4
A
B
C
D
E
F
2.5
2.5
ϕ3
ϕ1
4
6.5
7
34.056
18.468
30.681
20.289
17.664
R3
R5.25
M3
9.093
18
21.093
22.5
29
33.5
65
77
82
106
Oberfläche
Maßstab 1:1
Position
Menge 4
CuZn
Datum
Name
Bearb. 12.12.2005 S. Wiesemam
Gepr.
Norm
Fließkanal
Blatt
Bl
Zust.
Änderungen
Datum
Name
Dateiname F:\Fließkanal.dwg

Side-on connected I-type channel, as designed by K. Uchiyama, IMT Corporation (in Japanese).

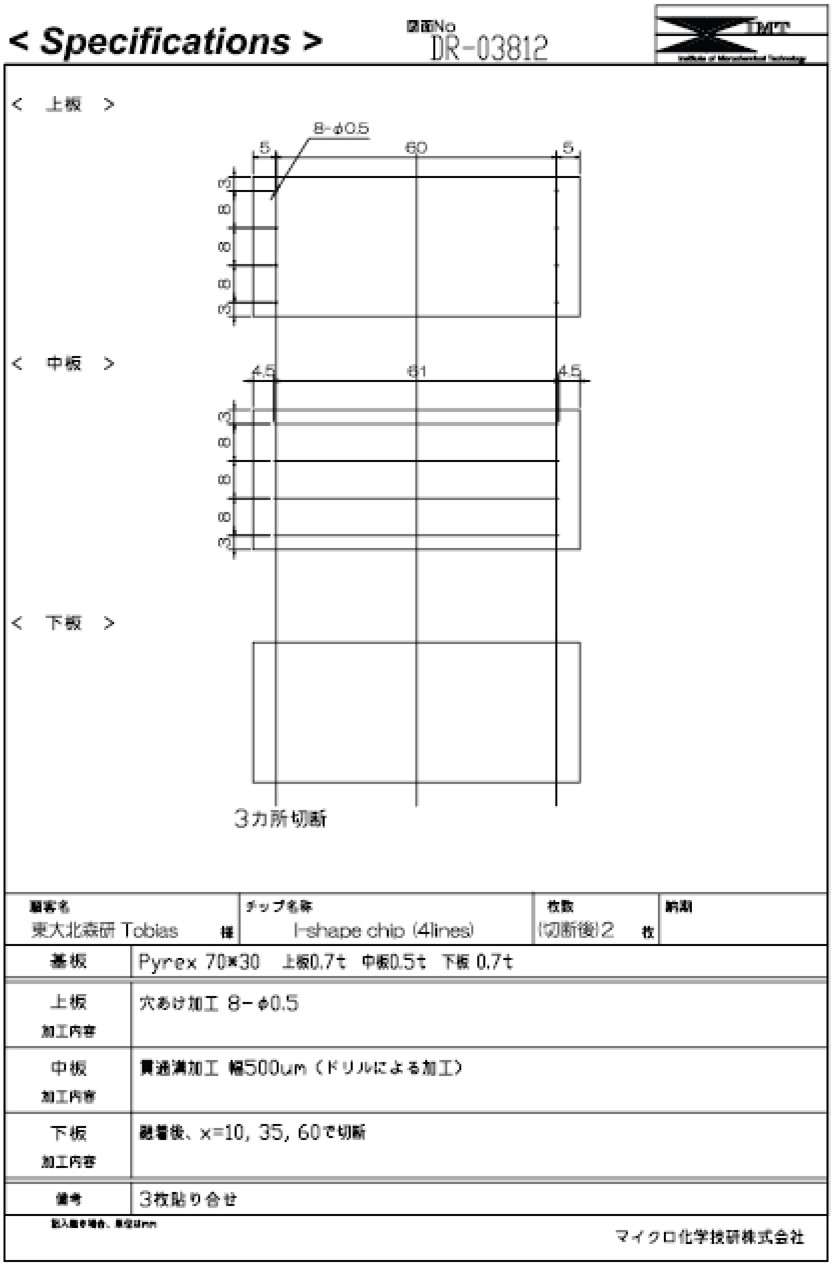

< Specifications >

図面No DR-03812

IMT

< 上板 >
8-φ0.5
5
60
5
3
8
8
8
3
< 中板 >
4.5
61
4.5
3
8
8
8
3
< 下板 >
3カ所切断

顧客名 東大北森研 Tobias 様	チップ名称 I-shape chip (4lines)	枚数 (切断後)2 枚	納期

基板	Pyrex 70×30　上板0.7t　中板0.5t　下板 0.7t
上板 加工内容	穴あけ加工 8−φ0.5
中板 加工内容	貫通溝加工 幅500um（ドリルによる加工）
下板 加工内容	融着後、x=10, 35, 60で切断
備考	3枚貼り合せ

記入無き場合、単位はmm

マイクロ化学技研株式会社

Side-on connected I-type channel with special entrance and exit holes, as designed by Y. Kikutani, IMT Corporation (in Japanese).

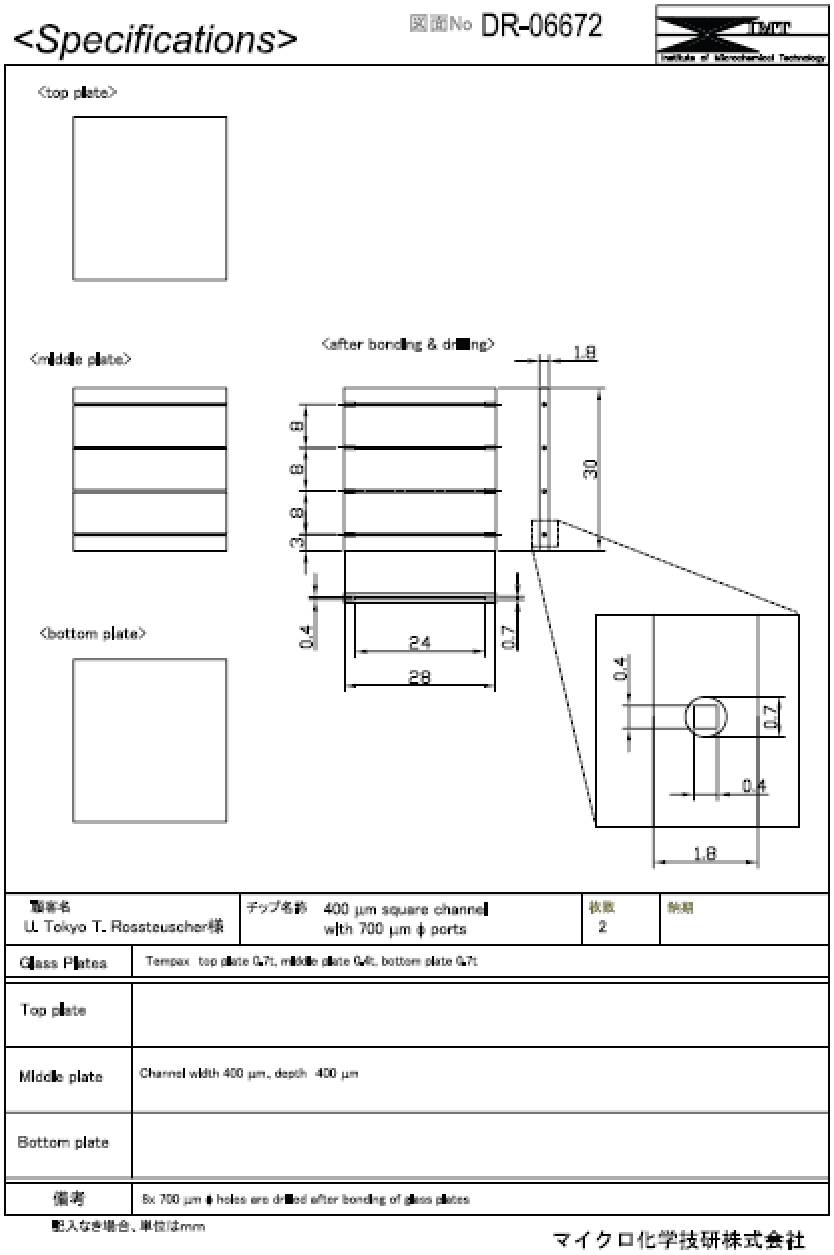
IMT
Institute of Microchemical Technology
<top plate>
<middle plate>
<after bonding & drilling>
<bottom plate>
1.8
8
8
8
3
30
0.4
24
28
0.7
0.4
0.7
0.4
1.8

<Specifications>

図面No DR-06672

顧客名 U. Tokyo T. Rossteuscher様	チップ名称 400 µm square channel with 700 µm ϕ ports	枚数 2	納期
Glass Plates	Tempax top plate 0.7t, middle plate 0.4t, bottom plate 0.7t		
Top plate			
Middle plate	Channel width 400 µm, depth 400 µm		
Bottom plate			
備考	8x 700 µm ϕ holes are drilled after bonding of glass plates		

記入なき場合、単位はmm

マイクロ化学技研株式会社

8 References

1. Wacey, D., et al., *The ~3.4 billion-year-old Strelley Pool sandstone: a new window into early life on earth.* International Journal of Astrobiology, 2006. **5**(4): p. 333-42.

2. Wilderer, P.A., et al., *Modern scientific methods and their potential in wastewater science and technology.* Water Research, 2002. **36**(2): p. 370-393.

3. Murakawa, T., *Slime production by Pseudomonas aeruginosa. IV. Chemical analysis of two varieties of slime produced by Pseudomonas aeruginosa.* Japanese Journal of Microbiology, 1973. **17**(6): p. 513-20.

4. Branda, S.S., et al., *Biofilms: the matrix revisited.* Trends in Microbiology, 2005. **13**(1): p. 20-26.

5. Sheng, G.P., H.Q. Yu, and Z. Yu, *Extraction of extracellular polymeric substances from the photosynthetic bacterium Rhodopseudomonas acidophila.* Applied Microbiology and Biotechnology, 2005. **67**(1): p. 125-130.

6. Allesen-Holm, M., et al., *A characterization of DNA release in Pseudomonas aeruginosa cultures and biofilms.* Molecular Microbiology, 2006. **59**(4): p. 1114-1128.

7. Danese, P.N., L.A. Pratt, and R. Kolter, *Exopolysaccharide production is required for development of Escherichia coli K-12 biofilm architecture.* Journal of Bacteriology, 2000. **182**(12): p. 3593-3596.

8. Tomlinson, S., et al. *Surface hydrophobicity of particles and bacteria in Melbourne's water storage system. 1st Australian Young Water Professionals Conference*. 2006. UNSW Sydney: International Water Association (Australia).

9. Bachmann, R.T. and R.G.J. Edyvean, *AFM study of the colonisation of stainless steel by Aquabacterium commune.* International Biodeterioration & Biodegradation, 2006. **58**(3-4): p. 112-118.

10. Christensen, B.E., *The Role of Extracellular polysaccharides in biofilms.* Journal of Biotechnology, 1989. **10**(3-4): p. 181-201.

11. Schmitt, J. and H.C. Flemming, *Water binding in biofilms.* Water Science and Technology, 1999. **39**(7): p. 77-82.

12. Lawrence, J.R., et al., *Optical Sectioning of Microbial Biofilms.* Journal of Bacteriology, 1991. **173**(20): p. 6558-6567.

13. Barberousse, H., et al., *Capsular polysaccharides secreted by building facade colonisers: characterisation and adsorption to surfaces.* Biofouling, 2006. **22**(6): p. 361-370.

14. Carter, J.T., et al., *Relationships between levels of heterotrophic bacteria and water quality parameters in a drinking water distribution system.* Water Research, 2000. **34**(5): p. 1495-1502.

15. Turetgen, I., *Comparison of the efficacy of free residual chlorine and monochloramine against biofilms in model and full scale cooling towers.* Biofouling, 2004. **20**(2): p. 81-85.

16. Kjellerup, B.V., et al., *Evaluation of analytical methods for determining the distribution of biofilm and active bacteria in a commercial heating system.* Biofouling, 2006. **22**(3): p. 145-151.

17. Brown, D.A., et al., *Evaluation of microscopic techniques to observe iron precipitation in a natural microbial biofilm.* Fems Microbiology Ecology, 1998. **26**(4): p. 297-310.

18. Danhorn, T. and C. Fuqua, *Biofilm formation by plant-associated bacteria.* Annual Review of Microbiology, 2007. **61**: p. 401-422.

19. McNab, R. and H.F. Jenkinson, *Altered adherence properties of a Streptococcus gordonii hppA (oligopeptide permease) mutant result from transcriptional effects on cshA adhesin gene expression.* Microbiology-UK, 1998. **144**: p. 127-136.

20. Sliepen, I., et al., *Aggregatibacter actinomycetemcomitans adhesion inhibited in a flow cell.* Oral Microbiology and Immunology, 2008. **23**(6): p. 520-524.

21. Reith, F., et al., *Biomineralization of gold: Biofilms on bacterioform gold.* Science, 2006. **313**(5784): p. 233-236.

22. Stoodley, P., et al., *Biofilms as complex differentiated communities.* Annual Review of Microbiology, 2002. **56**: p. 187-209.

23. Whiteley, M., et al., *Gene expression in Pseudomonas aeruginosa biofilms.* Nature, 2001. **413**(6858): p. 860-864.

24. Bassler, B.L., E.P. Greenberg, and A.M. Stevens, *Cross-species induction of luminescence in the Quorum-sensing bacterium Vibrio harveyi.* Journal of Bacteriology, 1997. **179**(12): p. 4043-4045.

25. Manefield, M. and L. Turner Sarah, *Quorum sensing in context: out of molecular biology and into microbial ecology.* Microbiology, 2002. **148**(12): p. 3762-4.

26. McLean, R.J.C., et al., *Evidence of autoinducer activity in naturally occurring biofilms.* FEMS Microbiology Letters, 1997. **154**(2): p. 259-263.

27. Eberhard, A., et al., *Structural identification of autoinducer of Photobacterium fischeri luciferase.* Biochemistry, 1981. **20**(9): p. 2444-9.

28. Spoering, A.L. and M.S. Gilmore, *Quorum sensing and DNA release in bacterial biofilms.* Current Opinion in Microbiology, 2006. **9**(2): p. 133-137.

29. McKnight, S.L., B.H. Iglewski, and E.C. Pesci, *The Pseudomonas quinolone signal regulates rhl quorum sensing in Pseudomonas aeruginosa.* Journal of Bacteriology, 2000. **182**(10): p. 2702-2708.

30. Pesci, E.C., et al., *Quinolone signaling in the cell-to-cell communication system of Pseudomonas aeruginosa.* Proceedings of the National Academy of Sciences of the United States of America, 1999. **96**(20): p. 11229-11234.

31. Schauder, S., et al., *The LuxS family of bacterial autoinducers: biosynthesis of a novel quorum-sensing signal molecule.* Molecular Microbiology, 2001. **41**(2): p. 463-476.

32. McNab, R., et al., *LuxS-based signaling in Streptococcus gordonii: autoinducer 2 controls carbohydrate metabolism and biofilm formation with Porphyromonas gingivalis.* Journal of Bacteriology, 2003. **185**(1): p. 274-284.

33. Chen, X., et al., *Structural identification of a bacterial quorum-sensing signal containing boron.* Nature, 2002. **415**(6871): p. 545-549.

34. Xavier, K.B. and B.L. Bassler, *LuxS quorum sensing: More than just a numbers game.* Current Opinion in Microbiology, 2003. **6**(2): p. 191-197.

35. Waters, C.M. and B.L. Bassler, *Quorum sensing: Cell-to-cell communication in bacteria.* Annual Review of Cell and Developmental Biology, 2005. **21**: p. 319-346.

36. O'Toole, G.A., *To build a biofilm.* Journal of Bacteriology, 2003. **185**(9): p. 2687-2689.

37. Medina, G., K. Juarez, and G. Soberon-Chavez, *The Pseudomonas aeruginosa rhlAB operon is not expressed during the logarithmic phase of growth even in the presence of its activator RhlR and the autoinducer N-butyryl-homoserine lactone.* Journal of Bacteriology, 2003. **185**(1): p. 377-380.

38. Davey, M.E., N.C. Caiazza, and G.A. O'Toole, *Rhamnolipid surfactant production affects biofilm architecture in Pseudomonas aeruginosa PAO1.* Journal of Bacteriology, 2003. **185**(3): p. 1027-1036.

39. Mashburn, L.M. and M. Whiteley, *Membrane vesicles traffic signals and facilitate group activities in a prokaryote.* Nature, 2005. **437**(7057): p. 422-425.

40. Davies, D.G., et al., *The involvement of cell-to-cell signals in the development of a bacterial biofilm.* Science, 1998. **280**(5361): p. 295-298.

41. Moller, S., et al., *In situ gene expression in mixed-culture biofilms: evidence of metabolic interactions between community members.* Applied and Environmental Microbiology, 1998. **64**(2): p. 721-732.

42. Gantner, S., et al., *In situ quantitation of the spatial scale of calling distances and population density-independent N-acylhomoserine lactone-mediated communication by rhizobacteria colonized on plant roots.* Fems Microbiology Ecology, 2006. **56**(2): p. 188-194.

43. Frymier, P.D., et al., *Three-dimensional tracking of motile bacteria near a solid planar surface.* Proceedings of the National Academy of Sciences of the United States of America, 1995. **92**(13): p. 6195-9.

44. Vigeant, M.A.S. and R.M. Ford, *Interactions between motile Escherichia coli and glass in media with various ionic strengths, as observed with a three-dimensional-tracking microscope.* Applied and Environmental Microbiology, 1997. **63**(9): p. 3474-3479.

45. Van Loosdrecht, M.C.M., et al., *Bacterial adhesion - a physicochemical approach.* Microbial Ecology, 1989. **17**(1): p. 1-15.

46. Zobell, C.E., *The effect of solid surfaces upon bacterial activity.* Journal of Bacteriology, 1943. **46**(1): p. 39-56.

47. Vigeant, M.A.S., et al., *Reversible and irreversible adhesion of motile Escherichia coli cells analyzed by total internal reflection aqueous fluorescence microscopy.* Applied and Environmental Microbiology, 2002. **68**(6): p. 2794-2801.

48. Chung, K.K., et al., *Impact of engineered surface microtopography on biofilm formation of Staphylococcus aureus.* Biointerphases, 2007. **2**(2): p. 89-94.

49. Carman, M.L., et al., *Engineered antifouling microtopographies - correlating wettability with cell attachment.* Biofouling, 2006. **22**(1): p. 11-21.

50. Van der Mei, H.C., M.M. Cowan, and H.J. Busscher, *Physicochemical and structural studies on Acinetobacter-calcoaceticus Rag-1 and Mr-481 - 2 standard strains in hydrophobicity tests.* Current Microbiology, 1991. **23**(6): p. 337-341.

51. Kjelleberg, S. and M. Hermansson, *Starvation-induced effects on bacterial surface characteristics.* Applied and Environmental Microbiology, 1984. **48**(3): p. 497-503.

52. Van der Mei, H.C., R. Bos, and H.J. Busscher, *A reference guide to microbial cell surface hydrophobicity based on contact angles.* Colloids and Surfaces B-Biointerfaces, 1998. **11**(4): p. 213-221.

53. Bakker, D.P., et al., *Bacterial strains isolated from different niches can exhibit different patterns of adhesion to substrata.* Applied and Environmental Microbiology, 2004. **70**(6): p. 3758-3760.

54. Park, S., et al., *Motion to form a quorum.* Science, 2003. **301**(5630): p. 188-188.

55. Horn, H., H. Reiff, and E. Morgenroth, *Simulation of growth and detachment in biofilm systems under defined hydrodynamic conditions.* Biotechnology and Bioengineering, 2003. **81**(5): p. 607-617.

56. De Saravia, S.G.G. and M.F.L. De Mele, *Non-invasive methods for monitoring biofilm growth in industrial water systems.* Latin American Applied Research, 2003. **33**(3): p. 353-359.

57. Ploux, L., et al., *Quantitative and morphological analysis of biofilm formation on self-assembled monolayers.* Colloids and Surfaces B-Biointerfaces, 2007. **57**(2): p. 174-181.

58. Purevdorj-Gage, B., W.J. Costerton, and P. Stoodley, *Phenotypic differentiation and seeding dispersal in non-mucoid and mucoid Pseudomonas aeruginosa biofilms.* Microbiology-UK, 2005. **151**(5): p. 1569-1576.

59. Kugaprasatham, S., H. Nagaoka, and S. Ohgaki, *Effect of turbulence on nitrifying biofilms at non-limiting substrate conditions.* Water Research, 1992. **26**(12): p. 1629-38.

60. Eisenmann, H., et al., *Interception of small particles by flocculent structures, sessile ciliates, and the basic layer of a wastewater biofilm.* Applied and Environmental Microbiology, 2001. **67**(9): p. 4286-4292.

61. Klausen, M., et al., *Involvement of bacterial migration in the development of complex multicellular structures in Pseudomonas aeruginosa biofilms.* Molecular Microbiology, 2003. **50**(1): p. 61-68.

62. Blehert, D.S., et al., *Autoinducer 2 production by Streptococcus gordonii DL1 and the biofilm phenotype of a luxS mutant are influenced by nutritional conditions.* Journal of Bacteriology, 2003. **185**(16): p. 4851-4860.

63. Webb, J.S., et al., *Cell death in Pseudomonas aeruginosa biofilm development.* Journal of Bacteriology, 2003. **185**(15): p. 4585-4592.

64. You, L., et al., *Programmed population control by cell-cell communication and regulated killing.* Nature, 2004. **428**(6985): p. 868-871.

65. Balagadde, F.K., et al., *Long-term monitoring of bacteria undergoing programmed population control in a microchemostat.* Science, 2005. **309**(5731): p. 137-140.

66. Padden, A.N., et al., *Clostridium used in mediaeval dyeing.* Nature, 1998. **396**(6708): p. 225.

67. Balaban, N., et al., *Prevention of staphylococcal biofilm-associated infections by the quorum sensing inhibitor RIP.* Clinical Orthopaedics and Related Research, 2005(437): p. 48-54.

68. Bjarnsholt, T., et al., *Garlic blocks quorum sensing and promotes rapid clearing of pulmonary Pseudomonas aeruginosa infections.* Microbiology-UK, 2005. **151**(12): p. 3873-3880.

69. Orgaz, B., R.J. Neufeld, and C. SanJose, *Single-step biofilm removal with delayed release encapsulated Pronase mixed with soluble enzymes.* Enzyme and Microbial Technology, 2007. **40**(5): p. 1045-1051.

70. Lee, J.H., J.B. Kaplan, and W.Y. Lee, *Microfluidic devices for studying growth and detachment of Staphylococcus epidermidis biofilms.* Biomedical Microdevices, 2008. **10**(4): p. 489-498.

71. Huang, X.D., et al., *Surface modification of silicone intraocular lens by 2-methacryloyloxyethyl phosphoryl-choline binding to reduce Staphylococcus epidermidis adherence.* Clinical and Experimental Ophthalmology, 2007. **35**(5): p. 462-467.

72. Patel, J.D., et al., *Phospholipid polymer surfaces reduce bacteria and leukocyte adhesion under dynamic flow conditions.* Journal of Biomedical Materials Research Part A, 2005. **73A**(3): p. 359-366.

73. Hirota, K., et al., *Coating of a surface with 2-methacryloyloxyethyl phosphorylcholine (MPC) co-polymer significantly reduces retention of human pathogenic microorganisms.* Fems Microbiology Letters, 2005. **248**(1): p. 37-45.

74. Nikawa, H., et al., *Immobilization of octadecyl ammonium chloride on the surface of titanium and its effect on microbial colonization in vitro.* Dental Materials Journal, 2005. **24**(4): p. 570-582.

75. Carlen, A., et al., *Surface characteristics and in vitro biofilm formation on glass ionomer and composite resin.* Biomaterials, 2001. **22**(5): p. 481-487.

76. Lin, Y.-H., et al., *Acyl-homoserine lactone acylase from Ralstonia strain XJ12B represents a novel and potent class of quorum-quenching enzymes.* Molecular Microbiology, 2003. **47**(3): p. 849-860.

77. De Nys, R., et al., *New halogenated furanones from the marine alga Delisea pulchra (cf. fimbriata).* Tetrahedron, 1993. **49**(48): p. 11213-20.

78. Manefield, M., et al., *Halogenated furanones inhibit quorum sensing through accelerated LuxR turnover.* Microbiology-UK, 2002. **148**(4): p. 1119-1127.

79. Givskov, M., et al., *Eukaryotic interference with homoserine lactone-mediated prokaryotic signaling.* Journal of Bacteriology, 1996. **178**(22): p. 6618-6622.

80. Bramucci, M. and V. Nagarajan, *Bacterial communities in industrial wastewater bioreactors.* Current Opinion in Microbiology, 2006. **9**(3): p. 275-278.

81. Ekman, M., B. Bjoerlenius, and M. Andersson, *Control of the aeration volume in an activated sludge process using supervisory control strategies.* Water Research, 2006. **40**(8): p. 1668-1676.

82. Lopez, C., M.N. Pons, and E. Morgenroth, *Endogenous processes during long-term starvation in activated sludge performing enhanced biological phosphorus removal.* Water Research, 2006. **40**(8): p. 1519-1530.

83. Liao, B.Q., et al., *Effect of solids retention time on structure and characteristics of sludge flocs in sequencing batch reactors.* Water Research, 2006. **40**(13): p. 2583-2591.

84. Ichihashi, O., H. Satoh, and T. Mino, *Effect of soluble microbial products on microbial metabolisms related to nutrient removal.* Water Research, 2006. **40**(8): p. 1627-1633.

85. Arnz, P., et al., *Simultaneous loading and draining as a means to enhance efficacy of sequencing biofilm batch reactors.* Water Research, 2000. **34**(5): p. 1763-1766.

86. Barnard, J.L. and M.T. Steichen, *Where is biological nutrient removal going now?* Water Science and Technology, 2006. **53**(3): p. 155-164.

87. Chung, J., R. Nerenberg, and B.E. Rittmann, *Bio-reduction of soluble chromate using a hydrogen-based membrane biofilm reactor.* Water Research, 2006. **40**(8): p. 1634-1642.

88. Minamiyama, M., S. Ochi, and Y. Suzuki, *Fate of nonylphenol polyethoxylates and nonylphenoxy acetic acids in an anaerobic digestion process for sewage sludge treatment.* Water Science and Technology, 2006. **53**(11): p. 221-226.

89. Buitron, G., K.M. Martinez, and A. Vargas, *Degradation of acid orange 7 by a controlled anaerobic-aerobic sequencing batch reactor.* Water Science and Technology, 2006. **54**(2): p. 187-92.

90. Frijters, C.T.M.J., et al., *Decolorizing and detoxifying textile wastewater, containing both soluble and insoluble dyes, in a full scale combined anaerobic/aerobic system.* Water Research, 2006. **40**(6): p. 1249-1257.

91. Li, J. and P.L. Bishop, *Adsorption and biodegradation of azo dye in biofilm processes.* Water Science and Technology, 2004. **49**(11-12): p. 237-245.

92. Ichihashi, O., H. Satoh, and T. Mino, *Sludge-sludge interaction in the enhanced biological phosphorus removal process.* Water Science and Technology, 2006. **53**(6): p. 1-6.

93. Zhang, B., et al., *Floc size distribution and bacterial activities in membrane separation activated sludge processes for small-scale wastewater treatment/reclamation.* Water Science and Technology, 1997. **35**(6): p. 37-44.

94. Kreutzer, M.T., et al., *Monoliths as Biocatalytic Reactors: Smart Gas-Liquid Contacting for Process Intensification.* Industrial & Engineering Chemistry Research, 2005. **44**(25): p. 9646-9652.

95. Dos Santos, A.B., F.J. Cervantes, and J.B. van Lier, *Potentials of high-temperature anaerobic treatment and redox mediators for the reductive decolorization of azo dyes from textile wastewaters.* Water Science and Technology, 2006. **54**(2): p. 151-6.

96. O'Flaherty, V., G. Collins, and T. Mahony, *The microbiology and biochemistry of anaerobic bioreactors with relevance to domestic sewage treatment.* Reviews in Environmental Science and Bio/Technology, 2006. **5**(1): p. 39-55.

97. Ahn, Y.T., et al., *Modeling of extracellular polymeric substances and soluble microbial products production in a submerged membrane bioreactor at various SRTs.* Water Science and Technology, 2006. **53**(7): p. 209-216.

98. Manser, R., W. Gujer, and H. Siegrist, *Decay processes of nitrifying bacteria in biological wastewater treatment systems.* Water Research, 2006. **40**(12): p. 2416-2426.

99. Whittington-Jones, K.J., J.B. Molwantwa, and P.D. Rose, *Enhanced hydrolysis of carbohydrates in primary sludge under biosulfidogenic conditions.* Water Research, 2006. **40**(8): p. 1577-1582.

100. Meyer, B., *Approaches to prevention, removal and killing of biofilms.* International Biodeterioration & Biodegradation, 2003. **51**(4): p. 249-253.

101. Williams, M.M., J.W.S. Domingo, and M.C. Meckes, *Population diversity in model potable water biofilms receiving chlorine or chloramine residual.* Biofouling, 2005. **21**(5-6): p. 279-288.

102. Fracchia, L., et al., *Site-related airborne biological hazard and seasonal variations in two wastewater treatment plants.* Water Research, 2006. **40**(10): p. 1985-1994.

103. Masago, Y., et al., *Assessment of risk of infection due to Cryptosporidium parvum in drinking water.* Water Science and Technology, 2002. **46**(11-12): p. 319-24.

104. Otaki, M., et al., *Inactivation differences of microorganisms by low pressure UV and pulsed xenon lamps.* Water Science and Technology, 2003. **47**(3): p. 185-90.

105. Hwang, M.G., H. Katayama, and S. Ohgaki, *Accumulation of copper and silver onto cell body and its effect on the inactivation of Pseudomonas aeruginosa.* Water Science and Technology, 2006. **54**(3): p. 29-34.

106. Davidson, C.A.B. and C.R. Lowe, *Optimisation of polymeric surface pre-treatment to prevent bacterial biofilm formation for use in microfluidics.* Journal of Molecular Recognition, 2004. **17**(3): p. 180-185.

107. Keskinen, H., et al., *Titania and titania-silver nanoparticle deposits made by Liquid Flame Spray and their functionality as photocatalyst for organic- and biofilm removal.* Catalysis Letters, 2006. **111**(3-4): p. 127-132.

108. Pasmore, M., et al., *Effect of polymer surface properties on the reversibility of attachment of Pseudomonas aeruginosa in the early stages of biofilm development.* Biofouling, 2002. **18**(1): p. 65-71.

109. Jullien, C., et al., *Physico-chemical and hygienic property modifications of stainless steel surfaces induced by conditioning with food and detergent.* Biofouling, 2008. **24**(3): p. 163-172.

110. Sathasivan, A., et al., *Role of inorganic phosphorus in controlling regrowth in water distribution system.* Water Science and Technology, 1997. **35**(8): p. 37-44.

111. Czechowski, F. and T. Marcinkowski, *Sewage sludge stabilization with calcium hydroxide: Effect on physicochemical properties and molecular composition.* Water Research, 2006. **40**(9): p. 1895-1905.

112. Lehtola, M.J., et al., *The effects of changing water flow velocity on the formation of biofilms and water quality in pilot distribution system consisting of copper or polyethylene pipes.* Water Research, 2006. **40**(11): p. 2151-2160.

113. Florjanic, M. and J. Kristl, *Microbiological quality assurance of purified water by ozonization of storage and distribution system.* Drug Development and Industrial Pharmacy, 2006. **32**(10): p. 1113-1121.

114. Schmid, T., et al., *Investigation of biocide efficacy by photoacoustic biofilm monitoring.* Water Research, 2004. **38**(5): p. 1189-1196.

115. Haisch, C. and R. Niessner, *Visualisation of transient processes in biofilms by optical coherence tomography.* Water Research, 2007. **41**(11): p. 2467-2472.

116. Schmid, T., et al., *A photoacoustic technique for depth-resolved in situ monitoring of biofilms.* Environmental Science & Technology, 2002. **36**(19): p. 4135-4141.

117. Nandakumar, K., et al., *In vitro laser ablation of natural marine biofilms.* Applied and Environmental Microbiology, 2004. **70**(11): p. 6905-6908.

118. Nandakumar, K., et al., *Recolonization of laser-ablated bacterial biofilm.* Biotechnology and Bioengineering, 2004. **85**(2): p. 185-189.

119. Hu, J.Y., et al., *Investigation into biofilms in a local drinking water distribution system.* Biofilms, 2005. **2**: p. 19-25.

120. Pitts, B., et al., *A microtiter-plate screening method for biofilm disinfection and removal.* Journal of Microbiological Methods, 2003. **54**(2): p. 269-276.

121. Goeres, D.M., et al., *Statistical assessment of a laboratory method for growing biofilms.* Microbiology-Sgm, 2005. **151**: p. 757-762.

122. Flemming, H.-C., U. Szewzyk, and T. Griebe, *Biofilms investigative methods & applications*. 2000, Lancaster, PA, USA: Technomic Publishing Company, Inc.

123. An, Y.H.H., et al., *An open channel flow chamber for characterizing biofilm formation on biomaterial surfaces.* Microbial Growth in Biofilms, Pt B, 2001. **337**: p. 79-88.

124. Schmid, T., et al., *Process analysis of biofilms by photoacoustic spectroscopy.* Analytical and Bioanalytical Chemistry, 2003. **375**(8): p. 1124-1129.

125. Abdi-Ali, A., M. Mohammadi-Mehr, and Y. Agha Alaei, *Bactericidal activity of various antibiotics against biofilm-producing Pseudomonas aeruginosa.* International Journal of Antimicrobial Agents, 2006. **27**(3): p. 196-200.

126. Aoi, Y., *In situ identification of microorganisms in biofilm communities.* Journal of Bioscience and Bioengineering, 2002. **94**(6): p. 552-556.

127. Costerton, J.W., et al., *Biofilms, the customized microniche.* Journal of Bacteriology, 1994. **176**(8): p. 2137-2142.

128. Kuhl, M., L.F. Rickelt, and R. Thar, *Combined imaging of bacteria and oxygen in biofilms.* Applied and Environmental Microbiology, 2007. **73**(19): p. 6289-6295.

129. Surman, S.B., et al., *Comparison of microscope techniques for the examination of biofilms.* Journal of Microbiological Methods, 1996. **25**(1): p. 57-70.

130. Minsky, M., *Memoir on Inventing the Confocal Scanning Microscope.* Scanning, 1988. **10**(4): p. 128-138.

131. Semwogerere, D. and E.R. Weeks, *Confocal microscopy*, *Encyclopedia of Biomaterials and Biomedical Engineering*, G.L. Bowlin and G. Wnek, Editors. 2005, Taylor & Francis.

132. Lawrence, J.R., et al., *Scanning transmission X-ray, laser scanning, and transmission electron microscopy mapping of the exopolymeric matrix of microbial biofilms.* Applied and Environmental Microbiology, 2003. **69**(9): p. 5543-5554.

133. Giepmans, B.N.G., et al., *Review - The fluorescent toolbox for assessing protein location and function.* Science, 2006. **312**(5771): p. 217-224.

134. Frischknecht, F., O. Renaud, and S.L. Shorte, *Imaging today's infectious animalcules.* Current Opinion in Microbiology, 2006. **9**(3): p. 297-306.

135. Schmid, T., et al., *Towards chemical analysis of nanostructures in biofilms I: imaging of biological nanostructures.* Analytical and Bioanalytical Chemistry, 2008. **391**(5): p. 1899-1905.

136. Pawley, J., *The 39 steps: a cautionary tale of quantitative 3-D fluorescence microscopy.* BioTechniques, 2000. **28**(5): p. 884,886,888.

137. North, A.J., *Seeing is believing? A beginners' guide to practical pitfalls in image acquisition.* Journal of Cell Biology, 2006. **172**(1): p. 9-18.

138. Leis, A.P., et al., *Optically transparent porous medium for nondestructive studies of microbial biofilm architecture and transport dynamics.* Applied and Environmental Microbiology, 2005. **71**(8): p. 4801-4808.

139. Tam, A.C., *Applications of photoacoustic sensing techniques.* Reviews of Modern Physics, 1986. **58**(2): p. 381-431.

140. Schmid, T., *Photoacoustic spectroscopy for process analysis.* Analytical and Bioanalytical Chemistry, 2006. **384**(5): p. 1071-1086.

141. Schmid, T., et al., *On-line monitoring of opaque liquids by photoacoustic spectroscopy.* Analytical and Bioanalytical Chemistry, 2003. **375**(8): p. 1130-1135.

142. Schmid, T., et al., *Photoacoustic absorption spectra of biofilms.* Review of Scientific Instruments, 2003. **74**(1): p. 755-757.

143. Kopp, C. and R. Niessner, *Depth-resolved determination of the absorption coefficient by photoacoustic spectroscopy within a hydrogel.* Analytical Chemistry, 1999. **71**(20): p. 4663-4668.

144. Schmid, T., et al., *Depth-resolved analysis of biofilms by photoacoustic spectroscopy.* Analytical Sciences, 2001. **17**: p. S574-S577.

145. Xi, C.W., et al., *High-resolution three-dimensional imaging of biofilm development using optical coherence tomography.* Journal of Biomedical Optics, 2006. **11**(3): p. -.

146. Ivleva, N.P., et al., *In situ surface-enhanced Raman scattering analysis of biofilm.* Analytical Chemistry, 2008. **80**(22): p. 8538-8544.

147. Krause, M., et al., *Localizing and identifying living bacteria in an abiotic environment by a combination of Raman and fluorescence microscopy.* Analytical Chemistry, 2008. **80**(22): p. 8568-8575.

148. Hell, S.W. and J. Wichmann, *Breaking the diffraction resolution limit by stimulated-emission - stimulated-emission-depletion fluorescence microscopy.* Optics Letters, 1994. **19**(11): p. 780-782.

149. Willig, K.I., et al., *STED microscopy reveals that synaptotagmin remains clustered after synaptic vesicle exocytosis.* Nature, 2006. **440**(7086): p. 935-939.

150. Milferstedt, K., M.N. Pons, and E. Morgenroth, *Optical method for long-term and large-scale monitoring of spatial biofilm development.* Biotechnology and Bioengineering, 2006. **94**(4): p. 773-782.

151. Toner, B., et al., *Zinc sorption by a bacterial biofilm.* Environmental Science and Technology, 2005. **39**(21): p. 8288-8294.

152. Sheng, G.-P. and H.-Q. Yu, *Characterization of extracellular polymeric substances of aerobic and anaerobic sludge using three-dimensional excitation and emission matrix fluorescence spectroscopy.* Water Research, 2006. **40**(6): p. 1233-1239.

153. Jenkins, A.T.A., et al., *Study of the attachment of Pseudomonas aeruginosa on gold and modified gold surfaces using surface plasmon resonance.* Biotechnology Progress, 2004. **20**(4): p. 1233-1236.

154. Berg, H.C., *How to track bacteria.* The Review of Scientific Instruments, 1971. **42**(6): p. 868-71.

155. Leitz, M., et al., *Monitoring of biofilm growth using ATR-leaky mode spectroscopy.* Journal of Physics D-Applied Physics, 2002. **35**(1): p. 55-60.

156. Richter, L., et al., *Development of a microfluidic biochip for online monitoring of fungal biofilm dynamics.* Lab on a Chip, 2007. **7**(12): p. 1723-1731.

157. Lerchner, J., et al., *Miniaturized calorimetry - A new method for real-time biofilm activity analysis.* Journal of Microbiological Methods, 2008. **74**(2-3): p. 74-81.

158. Bolton, J., et al., *Procedure to quantify biofilm activity on carriers used in wastewater treatment systems.* Journal of Environmental Engineering-Asce, 2006. **132**(11): p. 1422-1430.

159. Aota, A., et al., *Flow velocity profile of micro counter-current flows.* Analytical Sciences, 2007. **23**(2): p. 131-133.

160. Aota, A., et al., *Countercurrent laminar microflow for highly efficient solvent extraction.* Angewandte Chemie-International Edition, 2007. **46**(6): p. 878-880.

161. Ghaleb, K.A., et al., *Investigation of the mixing efficiency of a chaotic micromixer using thermal lens spectrometry.* Applied Spectroscopy, 2006. **60**(5): p. 564-567.

162. Dittrich, P.S., K. Tachikawa, and A. Manz, *Micro total analysis systems. Latest advancements and trends.* Analytical Chemistry, 2006. **78**(12): p. 3887-3907.

163. Morishima, K., et al., *Demonstration of a bio-microactuator powered by cultured cardiomyocytes coupled to hydrogel micropillars.* Sensors and Actuators B-Chemical, 2006. **119**(1): p. 345-350.

164. Chan, K.L.A. and S.G. Kazarian, *ATR-FTIR spectroscopic imaging with expanded field of view to study formulations and dissolution.* Lab on a Chip, 2006. **6**(7): p. 864-870.

165. Yamauchi, M., et al., *Miniaturized thermal lens and fluorescence detection system for microchemical chips.* Journal of Chromatography A, 2006. **1106**(1-2): p. 89-93.

166. Weibel, D.B., W.R. DiLuzio, and G.M. Whitesides, *Microfabrication meets microbiology.* Nature Reviews Microbiology, 2007. **5**(3): p. 209-218.

167. Lu, H., et al., *Microfluidic shear devices for quantitative analysis of cell adhesion.* Analytical Chemistry, 2004. **76**(18): p. 5257-5264.

168. Tanaka, Y., et al., *Culture and leukocyte adhesion assay of human arterial endothelial cells in a glass microchip.* Analytical Sciences, 2007. **23**(3): p. 261-266.

169. Balaban, N.Q., et al., *Bacterial persistence as a phenotypic switch.* Science, 2004. **305**(5690): p. 1622-1625.

170. Park, S., et al., *Influence of topology on bacterial social interaction.* Proceedings of the National Academy of Sciences of the United States of America, 2003. **100**(24): p. 13910-13915.

171. DiLuzio, W.R., et al., *Escherichia coli swim on the right-hand side.* Nature, 2005. **435**(7046): p. 1271-1274.

172. Saito, T., et al., *Oxygen consumption of cell suspension in a poly(dimethylsiloxane) (PDMS) microchannel estimated by scanning electrochemical microscopy.* Analyst, 2006. **131**(9): p. 1006-1011.

173. Zhang, Q., et al., *Microbial detection in microfluidic devices through dual staining of quantum dots-labeled immunoassay and RNA hybridization.* Analytica Chimica Acta, 2006. **556**(1): p. 171-177.

174. Wolter, A., R. Niessner, and M. Seidel, *Detection of Escherichia coli O157 : H7, Salmonella typhimurium, and Legionella pneumophila in water using a flow-through chemiluminescence microarray readout system.* Analytical Chemistry, 2008. **80**(15): p. 5854-5863.

175. Keymer, J.E., et al., *Bacterial metapopulations in nanofabricated landscapes.* Proceedings of the National Academy of Sciences of the United States of America, 2006. **103**(46): p. 17290-17295.

176. Bos, R., et al., *Retention of bacteria on a substratum surface with micro-patterned hydrophobicity.* Fems Microbiology Letters, 2000. **189**(2): p. 311-315.

177. Tamaki, E., et al., *Single-cell analysis by a scanning thermal lens microscope with a microchip: Direct monitoring of cytochrome c distribution during apoptosis process.* Analytical Chemistry, 2002. **74**(7): p. 1560-1564.

178. Tamaki, E., et al., *Microchannel-assisted thermal-lens spectrometry for microchip analysis.* Journal of Chromatography A, 2003. **987**(1-2): p. 197-204.

179. Bialkowski, S.E., *Photothermal spectroscopy methods for chemical analysis*. Chemical Analysis. Vol. 134. 1996, New York: John Wiley & Sons, Inc.

180. Shen, J. and R.D. Snook, *Thermal lens measurement of absolute quantum yields using quenched fluorescent samples as references.* Chemical Physics Letters, 1989. **155**(6): p. 583-586.

181. Winston, H. and R.A. Gudmundsen, *Refractive gradient effects in proposed liquid lasers.* Applied Optics, 1964. **3**(1): p. 143-&.

182. Gomez, S.L., et al., *Thermal lens effect of low-density lipoprotein lyotropic-like aggregates investigated by using the Z-scan technique.* Liquid Crystals Today, 2006. **15**(1): p. 1-3.

183. Tokeshi, M., et al., *Determination of subyoctomole amounts of nonfluorescent molecules using a thermal lens microscope: Subsingle molecule determination.* Analytical Chemistry, 2001. **73**(9): p. 2112-2116.

184. Shimosaka, T., et al., *Spatial resolution improvement of scanning microscopy based on thermal lens spectroscopy with a total-internal-reflection arrangement.* Analytical Sciences, 2005. **21**(4): p. 469-472.

185. Shimosaka, T., et al., *Development of a scanning microscopy by total internal reflection coupled with thermal lens spectroscopy.* Micron, 2004. **35**(4): p. 297-302.

186. Fujinami, M., K. Toya, and T. Sawada, *Development of photothermal near-field scanning optical microscope photothermal near-field scanning optical microscope.* Review of Scientific Instruments, 2003. **74**(1): p. 621-623.

187. Uchiyama, K., et al., *Thermal lens microscope.* Japanese Journal of Applied Physics, Part 1: Regular Papers, Short Notes & Review Papers, 2000. **39**(9A): p. 5316-5322.

188. Kimura, H., et al., *Quantitation of drug concentration by photo-thermal microscopy in a renal tubule of fixed kidney.* Analytical Sciences, 1997. **13**(5): p. 729-734.

189. Kimura, H., et al., *Assay of spherical cell surface molecules by thermal lens microscopy and its application to blood cell substances.* Analytical Chemistry, 2001. **73**(17): p. 4333-4337.

190. Kimura, H., et al., *Detection and measurement of a single blood cell surface antigen by thermal lens microscopy.* Analytical Biochemistry, 2000. **283**(1): p. 27-32.

191. Burgi, D.S. and N.J. Dovichi, *Submicrometer resolution images of absorbance and thermal diffusivity with the photothermal microscope.* Applied Optics, 1987. **26**(21): p. 4665-9.

192. Kimura, H., et al., *Analysis of serum proteins adsorbed to a hemodialysis membrane of hollowfiber type by thermal lens microscopy.* Analytical Sciences, 1999. **15**(11): p. 1101-1107.

193. Harata, A., T. Matuda, and S. Hirashima, *Ultraviolet-laser excitation microscopic photothermal lens Imaging for observing biological cells.* Japanese Journal of Applied Physics Part 1-Regular Papers Brief Communications & Review Papers, 2007. **46**(7B): p. 4561-4563.

194. Moreau, J. and V. Loriette, *Confocal thermal-lens microscope.* Optics Letters, 2004. **29**(13): p. 1488-1490.

195. Boyer, D., et al., *Imaging single metal nanoparticles in scattering media by photothermal interference contrast.* Physica E-Low-Dimensional Systems & Nanostructures, 2003. **17**(1-4): p. 537-540.

196. Boyer, D., et al., *Photothermal imaging of nanometer-sized metal particles among scatterers.* Science, 2002. **297**(5584): p. 1160-1163.

197. Cognet, L., et al., *Single metallic nanoparticle imaging for protein detection in cells.* Proceedings of the National Academy of Sciences of the United States of America, 2003. **100**(20): p. 11350-11355.

198. Berciaud, S., et al., *Photothermal heterodyne imaging of individual nonfluorescent nanoclusters and nanocrystals.* Physical Review Letters, 2004. **93**(25): p. -.

199. Lasne, D., et al., *Label-free optical imaging of mitochondria in live cells.* Optics Express, 2007. **15**(21): p. 14184-14193.

200. Berciaud, S., et al., *Photothermal heterodyne imaging of individual metallic nanoparticles: Theory versus experiment.* Physical Review B, 2006. **73**(4): p. -.

201. Hao, P.-F., et al., *Experimental investigation of water flow in smooth and rough silicon microchannels.* Journal of Micromechanics and Microengineering, 2006. **16**(7): p. 1397-1402.

202. Pfund, D., et al., *Pressure drop measurements in a microchannel.* Aiche Journal, 2000. **46**(8): p. 1496-1507.

203. Li, H. and M.G. Olsen, *MicroPIV measurements of turbulent flow in square microchannels with hydraulic diameters from 200 mm to 640 mm.* International Journal of Heat and Fluid Flow, 2006. **27**(1): p. 123-134.

204. Aota, A., A. Hibara, and T. Kitamori, *Pressure balance at the liquid-liquid interface of micro countercurrent flows in microchips.* Analytical Chemistry, 2007. **79**(10): p. 3919-3924.

205. Jun, S., R.D. Lowe, and R.D. Snook, *A model for cw laser-induced mode-mismatched dual-beam thermal lens spectrometry.* Chemical Physics, 1992. **165**(2-3): p. 385-396.

206. Dovichi, N.J., *Thermo-optical spectrophotometries in analytical chemistry.* CRC Critical Reviews in Analytical Chemistry, 1987. **17**(4): p. 357-423.

207. Gordon, J.P., et al., *Long-transient effects in lasers with inserted liquid samples.* Journal of Applied Physics, 1965. **36**(1): p. 3-8.

208. Whinnery, J.R., *Laser measurement of optical-absorption in alquids.* Accounts of Chemical Research, 1974. **7**(7): p. 225-231.

209. Sheldon, S.J., L.V. Knight, and J.M. Thorne, *Laser-induced thermal lens effect - a new theoretical model.* Applied Optics, 1982. **21**(9): p. 1663-1669.

210. Anraku, R., et al., *Numerical analysis of thermal lens effect for sensitive detection on microchips.* Electrophoresis, 2008. **29**(9): p. 1895-1901.

211. Thorne, J.B. and D.R. Bobbitt, *Comparison of Beer law and thermal lens techniques for absorption-measurements under conditions of high scattering backgrounds.* Applied Spectroscopy, 1993. **47**(3): p. 360-363.

212. Aamodt, L.C. and J.C. Murphy, *Effect of 3-D heat-flow near edges in photothermal measurements.* Applied Optics, 1982. **21**(1): p. 111-115.

213. Friedrich, K. and H.G. Walther, *The effect of edges on photothermal imaging.* Journal of Applied Physics, 1991. **70**(9): p. 4697-4701.

214. Hsueh, P.-R., et al., *Nosomical infections caused by Sphingomonas paucimobilis: Clinical features and microbiological characteristics.* Clinical Infectious Diseases, 1998. **26**(March): p. 676-81.

215. Kilic, A., et al., *Nosomical outbreak of Sphingomonas paucimobilis bacteremia in a hemato/oncology unit.* Japanese Journal of Infectious Diseases, 2007. **60**(6): p. 394-96.

216. Ishihara, K., T. Ueda, and N. Nakabayashi, *Preparation of phospholipid polymers and their properties as polymer hydrogel membranes.* Polymer Journal, 1990. **22**(5): p. 355-360.

217. Ishihara, K., et al., *Reduced thrombogenicity of polymers having phospholipid polar groups.* Journal of Biomedical Materials Research, 1990. **24**(8): p. 1069-1077.

218. Iwasaki, Y. and K. Ishihara, *Phosphorylcholine-containing polymers for biomedical applications.* Analytical and Bioanalytical Chemistry, 2005. **381**(3): p. 534-546.

219. Shin, D.S., et al., *Protein patterning by maskless photolithography on hydrophilic polymer-grafted surface.* Biosensors & Bioelectronics, 2003. **19**(5): p. 485-494.

220. Wang, E., C.M. Babbey, and K.W. Dunn, *Performance comparison between the high-speed Yokogawa spinning disc confocal system and single-point scanning confocal systems.* Journal of Microscopy-Oxford, 2005. **218**: p. 148-159.

221. Hyde, F.W., M. Alberg, and K. Smith, *Comparison of fluorinated polymers against stainless steel, glass and polypropylene in microbial biofilm adherence and removal.* Journal of Industrial Microbiology & Biotechnology, 1997. **19**(2): p. 142-149.

222. Webster, D.C., B.J. Chisholm, and S.J. Stafslien, *Mini-review: Combinatorial approaches for the design of novel coating systems.* Biofouling, 2007. **23**(3): p. 179-192.

223. Moreau, J. and V. Loriette, *Confocal dual-beam thermal-lens microscope: Model and experimental results.* Japanese Journal of Applied Physics Part 1-Regular Papers Brief Communications & Review Papers, 2006. **45**(9A): p. 7141-7151.

224. Briggs, M.W. and G.R. Long, *Thermal lens spectrophotometry in agarose gels.* Applied Spectroscopy, 1996. **50**(2): p. 241-244.

225. Kong, J.Y., et al., *The intrinsic thermal conductivity of some wet proteins in relation to their hydrophobicity - analysis on gelatin gel.* Agricultural and Biological Chemistry, 1982. **46**(3): p. 783-788.

226. Hsu, C.L. and D.R. Heldman, *Prediction models for the thermal conductivity of aqueous starch.* International Journal of Food Science and Technology, 2004. **39**(7): p. 737-743.

227. Croxatto, A., et al., *VanT, a homologue of Vibrio harveyi LuxR, regulates serine, metalloprotease, pigment, and biofilm production in Vibrio anguillarum.* Journal of Bacteriology, 2002. **184**(6): p. 1617-1629.

228. Stahly, G.L., C.L. Sesler, and W.R. Brode, *A method for measuring bacterial pigments by the use of the spectrophotometer and the photoelectric colorimeter.* Journal of Bacteriology, 1942. **43**: p. 149-54.

229. Heinen, U.J., et al., *Comparative studies on the nature and distribution of pigments from two thermophilic bacteria.* Archiv fuer Mikrobiologie, 1971. **76**(1): p. 18-27.

230. Shidara, S., et al., *Purification and some properties of cytochrome C' from a strain of Achromobacter xylosoxidans.* Journal of Biochemistry, 1986. **99**(6): p. 1749-1752.

231. Yoshimura, T., et al., *Identification of heme axial ligands of cytochrome C' from Alcaligenes Sp Ncib 11015.* Biochimica Et Biophysica Acta, 1985. **831**(3): p. 267-274.

232. Suzuki, S., et al., *Spectral properties of carbon-monoxide or cyanide complexes of cytochromes C' from denitrifying bacteria.* Inorganica Chimica Acta-Bioinorganic Chemistry, 1988. **153**(4): p. 227-233.

233. Thompson, R.C., et al., *Problems in extraction and spectrophotometric determination of chlorophyll from epilithic microbial biofilms: towards a standard method.* Journal of the Marine Biological Association of the United Kingdom, 1999. **79**(3): p. 551-558.

234. Ellinghausen, H.C. and M.J. Pelczar, *Spectrophotometric characterization of Neisseria pigments.* Journal of Bacteriology, 1955. **70**(4): p. 448-453.

235. Nosoh, Y. and M. Itoh, *503 Mmu pigment in bacteria and yeast.* Plant and Cell Physiology, 1965. **6**(4): p. 771-&.

236. Marcano O., A., J. Ojeda, and N. Melikechi, *Absorption spectra of dye solutions measured using a white light thermal lens spectrophotometer.* Applied Spectroscopy, 2006. **60**(5): p. 560-563.